

SEGMENTAL CONCRETE BOX GIRDER BRIDGE THERMAL ANALYSIS  
BASED ON NEW TURKISH SOLAR ZONE MAP DEVELOPED TO ASSESS  
TEMPERATURE GRADIENT LOADING

A THESIS SUBMITTED TO  
THE GRADUATE SCHOOL OF NATURAL AND APPLIED SCIENCES  
OF  
MIDDLE EAST TECHNICAL UNIVERSITY

BY

ARZU İPEK YILMAZ

IN PARTIAL FULFILLMENT OF THE REQUIREMENTS  
FOR  
THE DEGREE OF MASTER OF SCIENCE  
IN  
CIVIL ENGINEERING

JANUARY 2015



Approval of the thesis:

**SEGMENTAL CONCRETE BOX GIRDER BRIDGE THERMAL ANALYSIS  
BASED ON NEW TURKISH SOLAR ZONE MAP DEVELOPED TO ASSESS  
TEMPERATURE GRADIENT LOADING**

submitted by **ARZU İPEK YILMAZ** in partial fulfillment of the requirements for  
the degree of **Master of Science in Civil Engineering Department, Middle East  
Technical University** by,

Prof. Dr.Gülbin Dural Ünver  
Dean, Graduate School of **Natural and Applied Sciences**

\_\_\_\_\_

Prof. Dr. Ahmet Cevdet Yalçiner  
Head of Department, **Civil Engineering**

\_\_\_\_\_

Assoc. Prof. Dr. Alp Caner  
Supervisor, **Civil Engineering Dept., METU**

\_\_\_\_\_

**Examining Committee Members:**

Assoc. Prof. Dr.Ayşegül Askan Gündoğan  
Civil Engineering Dept., METU

\_\_\_\_\_

Assoc. Prof. Dr. Alp Caner  
Civil Engineering Dept., METU

\_\_\_\_\_

Assoc. Prof. Dr.Eray Baran  
Civil Engineering Dept., METU

\_\_\_\_\_

Assoc. Prof. Dr. Yalın Arıcı  
Civil Engineering Dept., METU

\_\_\_\_\_

Assist. Prof. Dr. Burcu Güneş  
Civil Engineering Dept., İTÜ

\_\_\_\_\_

**Date:** 30.01.2015

**I hereby declare that all information in this document has been obtained and presented in accordance with academic rules and ethical conduct. I also declare that, as required by these rules and conduct, I have fully cited and referenced all material and results that are not original to this work.**

Name, Last Name : Arzu İpek Yılmaz

Signature :

## ABSTRACT

### SEGMENTAL CONCRETE BOX GIRDER BRIDGE THERMAL ANALYSIS BASED ON NEW TURKISH SOLAR ZONE MAP DEVELOPED TO ASSESS TEMPERATURE GRADIENT LOADING

Yılmaz, Arzu İpek

M.S., Department of Civil Engineering

Supervisor: Assoc. Prof. Dr. Alp Caner

January 2015, 128 pages

Solar radiation and daily temperature fluctuation originated non-linear temperature distribution through the depth of the box girder bridge structures cause significant stress development in addition to the ones caused by other load effects such as dead, live and uniform temperature loading on concrete superstructure. Unfortunately, the significance of hourly temperature gradient changes on segmental bridge design had not been addressed in detail for Turkish bridge design mainly due to the lack of a Turkish solar zone map and limited awareness of engineers on computation methods. The aim of this study is to construct a new solar zone map for Turkey to assess the magnitude of non-linear temperature gradient to be used in thermal analysis of segmental concrete bridges and outline a comprehensive analysis method. In this scope, temperature and solar radiation changes at sixteen Turkish cities representing different geographies are evaluated to form the boundaries of solar zone regions on

Turkish country map and obtain corresponding temperature gradient loading. It has been found out that the solar zones defined for the bridges of United States of America and Turkey results in slightly different thermal gradient loading. The new findings on region based temperature gradient loading have been used in analysis of a selected segmental concrete box girder bridge. The nonlinear temperature distribution developed through the depth of the sample box girder type bridge caused stresses as high as the ones generated by dead and live loads; that, especially for negative gradient condition, the high tensile stresses imposes the requirement of additional prestressing, in order to satisfy tensile stress limitation requirements and avoid cracking of the section.

**Keywords:** thermal gradient, solar radiation, segmental bridges, box girder bridges, design codes

## ÖZ

### DİLİMSEL KUTU KESİTLİ ARD-ÇEKMELE KÖPRÜ SICAKLIK ANALİZİ İÇİN YENİ TÜRKİYE SOLAR IŞINIM BÖLGELERİ HARİTASI OLUŞTURULARAK DÜŞEY SICAKLIK DEĞİŞİMİ YÜKLEMESİNİN BELİRLENMESİ

Yılmaz, Arzu İpek

Yüksek Lisans, İnşaat Mühendisliği Bölümü

Tez Yöneticisi: Doç. Dr. Alp Caner

Ocak 2015, 128 sayfa

Kutu kesitli köprülerde; güneş ışınımı ve gün içinde hava sıcaklığında meydana gelen değişimlerden kaynaklı, köprü üstyapı derinliği doğrultusunda meydana gelen, doğrusal olmayan sıcaklık değişimi, üstyapıda köprü ölü yüklerinin, hareketli yüklerin ve uniform sıcaklık değişimlerinin yarattığı gerilmelere ek olarak kayda değer miktarda ilave gerilmelerin oluşmasına yol açmaktadır. Ne yazık ki, saatlik düşey sıcaklık değişimi Türkiye’de ard-çekmeli dilimsel köprü tasarımında; ülke için oluşturulmuş solar ışınım haritasının bulunmaması ve tasarımcıların hesap yöntemleri konusunda yeterince bilgi sahibi olmamasından dolayı yeterli ölçüde dikkate alınmamaktadır. Bu çalışmanın amacı, Türkiye için yeni bir solar ışınım haritasının oluşturulması ile düşey sıcaklık değişimi değerlerinin belirlenmesi ve tasarımcılara dilimsel kutu kesitli köprü tasarımı için hesap aşamaları hakkında bilgi verilmesidir. Bu doğrultuda Türkiye’den farklı coğrafi özelliklere sahip on altı temsili şehir seçilmiş ve bu şehirlere ait sıcaklık ile solar ışınım değerleri elde edilmiş; ve ardından, yapılan değerlendirmeler sonucunda solar ışınım bölgesi

sınırları belirlenerek Türkiye iki ışınlm bölgesine ayrılmıştır. Amerika Birleşik Devletleri ve Türkiye'nin düşey sıcaklık değışimi yüklemeleri büyük oranda benzeşmektedir. Elde edilen yükleme değeri, temsili bir dilimsel kutu kesitli köprünün analizinde kullanılmıştır ve doğrusal olmayan bu sıcaklık değışimi dağılımlarının köprü derinliğı boyunca oluşturduğu gerilmelerin, ölü yükler ve hareketli yükler sebebiyle ortaya çıkan gerilmeler kadar yüksek olduğu görölmüştür. Özellikle negatif düşey sıcaklık değışimi sebebiyle ortaya çıkan çekme gerilmelerinin; şartnamelerin tasarımlarda izin verdikleri gerilme limitlerini aşmaması ve betonda çatlamaya sebep olmaması istenildiğinden ekstra ard-çekme ihtiyacı doğuracak mertebelerde olduğu görölmüştür.

**Anahtar Kelimeler:** düşey sıcaklık değışimi, solar ışınlm, dilimsel köprüler, kutu kesitli köprüler, tasarım kodları

To my beloved grandmothers İpek Şahin and Arzu Yılmaz

## ACKNOWLEDGEMENTS

I would like to thank my supervisor, Assoc. Prof. Dr. Alp Caner for his support, guidance and opportunities he provided me. Receiving appreciation from him in every step, gave me encouragement and energy to do better things throughout the research.

I would also like to express my thanks to Assoc. Prof. Dr. Ayşegül Askan Gündoğan, Assoc. Prof. Dr. Eray Baran, Assoc. Prof. Dr. Yalın Arıcı, and Assist. Prof. Dr. Burcu Güneş for their comments, criticism, suggestions and contributions on this study. I am also grateful to my all other instructors from both my graduate and undergraduate years who helped me to get this place. Mr. Bülent Aksoy from Turkish State Meteorological Service is also acknowledged for his guidance at the beginning of this study.

I owe thanks to Yüksel Domaniç Engineering, and every member of the company; especially to Dr. Arman Domaniç for being so cheerful and motivating, and Fatih Polat for his guidance. I am thankful to Dr. Bengi Atak, who not only taught me how to design a bridge when I was newly graduated, but also is a real friend, and Nalan Darende Şafak for always being thoughtful and caring. I thank my colleagues Ahmet Fatih Koç and Berat Ertekin for both being very good friends, and providing me consultancy whenever I need any help, and Gencay Küçük for making our working room a happier place. I am indebted so much to Menekşe Canatan Yalçın for being far beyond than just a workmate but a real angel accompanying me in every part of my life.

Gizem Mestav Sarıca and Müge Özgenođlu, my beyond lovely thesis-sisters, made everything easier and possible for me. It was a pleasure to study with them in any place and any time. Besides academic support, their existence was just enough for me to be inspired.

Doubtlessly, I thank Ceren Usalan and Naz Topkara Özcan for being with me whenever I need and making me feel safe, comforted and cheerful. I feel very lucky to have them in my life. If a friendship lasts longer than 7 years, it will last a lifetime.

I would like to thank Melis Aysun Ekici for being with me with her kind personality and moral supports. I am thankful to my friends Özlem Temel, Feyza Soysal, Janset Görgü Yaman, Ava Bagherpoor, Merve Aktaş, Pelin Ergen, Emine Altay, Sebil Çetinkaya, Pınar Şirek, Dr. Ahmet Kuşyılmaz, Dr. Mustafa Can Yücel, Dr. Kaan Kaatsız and Alper Özge Gür for their valuable friendship, being with me for my undergraduate and graduate times, sharing good memories and adding happy moments to my life.

I would like to express my sincere thanks for Utku Albostan and Cihat Çađın Yakar for their valuable cooperation and helps during this thesis. Very special thanks to Ali Bulut Üçüncü for coming up with solutions, being a rescuer and making me secure every time.

Finally, I would like to express gratitude to my family, Şenel Yılmaz, Civan Ali Yılmaz and Cansu Yılmaz who always supported, believed, loved, and encouraged me.

## TABLE OF CONTENTS

ABSTRACT .....	v
ÖZ.....	vii
ACKNOWLEDGEMENTS .....	x
TABLE OF CONTENTS .....	xii
LIST OF TABLES .....	xv
LIST OF FIGURES.....	xvii
LIST OF ABBREVIATIONS .....	xxii
CHAPTERS	
1. INTRODUCTION.....	1
1.1 General .....	1
1.2 Aim and Scope .....	2
2. LITERATURE REVIEW.....	5
2.1 Information about Box Girder Bridges .....	5
2.2 Information about Segmental Bridge Construction .....	7
2.3 Segmental Box Girder Bridges in Turkey.....	9

2.4	Theoretical Background about Temperature Effects on Bridge Structures .....	11
2.4.1	Uniform Temperature Changes.....	13
2.4.2	Thermal Gradients.....	14
2.5	Major Factors Effecting Vertical Temperature Differences in the Depth of Girder: .....	18
2.6	Structural Response of Bridges to Temperature Variations.....	19
2.7	Previous Studies and Historical Development of Design Thermal Gradients in Design Codes.....	28
2.8	Review of Formulas to Predict the Temperature Gradient in the Literature .....	33
2.9	Current Design Practice .....	34
2.9.1	Brief Information about AASHTO Codes .....	34
2.9.2	Corresponding Load Combinations of AASHTO Codes.....	36
2.9.3	BS EN 1991-1-5:2003 Requirements .....	45
2.9.4	Technical Specifications for Highway Bridges of Turkey (Yol Köprüleri için Teknik Şartname) (1982) Requirements: .....	46
3.	SOLAR ZONE MAP TO BE USED FOR THERMAL GRADIENT LOADING OF TURKISH BRIDGES .....	47
3.1.	Information about the Project.....	47
3.2.	Collection of Data .....	48
3.3.	Statistical Comparison of Suggested and Measured Values .....	54
4.	ANALYSIS FOR THERMAL GRADIENT .....	59
4.1.	Information about Analyzed Bridge Model .....	59
4.2.	Analysis to Obtain Design Gradient .....	61
4.3.	Analysis to Obtain Stresses and Forces and the Results .....	74
4.4.	Comparison of the Thermal Gradient Originated Resultant Forces and Stresses with the Resultants of the Other Load Types.....	86

5.	CONCLUSIONS AND FUTURE WORK .....	97
	REFERENCES.....	101
APPENDICES		
A.	NUMERICAL HAND CALCULATION DESIGN EXAMPLE.....	105
B.	THE TEMPERATURE AND SOLAR RADIATION DATA FOR THE ANALYZED CITIES.....	113

## LIST OF TABLES

### TABLES

Table 2.1 Uniform Temperature Ranges According to AASHTO 2012 (in degrees Celsius).....	13
Table 2.2 Uniform Temperature Ranges according to Technical Specifications for Highway Bridges of Turkey (in degrees Celsius) .....	14
Table 2.3 Positive Temperature Differentials (after AASHTO, 1999).....	32
Table 2.4 Load Combinations and Load Factors (Adopted from the AASHTO LRFD Specification(2012), Table 3.4.1-1) .....	39
Table 2.5 Load Factors for Permanent Loads $\gamma_p$ (AASHTO 2012).....	41
Table 2.6 Load Factors for Permanent Loads Due to Superimposed Deformations, $\gamma_p$ (AASHTO 2012).....	41
Table 3.1 The 22 Year Annual Monthly Averaged Normal Radiation (Kwh/m <sup>2</sup> /day) Values for Grid Cells of Turkey .....	55
Table 3.2 Comparison of Monthly Averaged Radiation Values.....	57
Table 4.1 Material Properties for the Analytical Computations .....	61
Table 4.2. Properties Of The Computer Used In Heat Transfer Analysis .....	63
Table 4.4 Positive and Negative Temperature Gradient Values for the Analyzed Cities .....	71
Table 4.5 Recommended Thermal Gradient Values for Positive and Negative Gradients .....	72
Table 4.6 Allowable compression and tension stresses for C35 concrete for thermal gradient analysis of a segmental bridge top section according to AASHTO (2012). 85	
Table A.A.1 Positive Temperature Gradient Primary Force Calculations for Zone 1 .....	108
Table A.A.2 Negative Temperature Gradient Primary Force Calculations for Zone 1 .....	108
Table A.A.3 Necessary Positive Temperature Gradient, Primary and Secondary Axial Load and Temperature Values to Calculate Secondary Thermal Effects .....	111

Table A. A.4 Necessary Negative Temperature Gradient, Primary and Secondary  
Axial Load and Temperature Values to Calculate Secondary Thermal Effects ..... 111

## LIST OF FIGURES

### FIGURES

Figure 1.1 Flowchart for the outline of the study.....	4
Figure 2.1 Evolvment of box girder cross-section (Schlaich, 1982).....	6
Figure 2.2 Common construction methods for segmental bridges (Schlaich, 1982)...	8
Figure 2.3 Classification of segmental box girder bridges according to bridge and span lengths and construction time (Schlaich, 1982).....	9
Figure 2.4 Nibelungen Bridge, Germany (adopted from Honorio, 2007) .....	9
Figure 2.5 K�m�rhan Bridge, Malatya-Elazığ Turkey .....	10
Figure 2.6 Imrahor Viaduct, Ankara Turkey .....	10
Figure 2.7 G�lburnu Bridge, Giresun, Turkey .....	11
Figure 2.8 Ortak�y Viaduct, Artvin, Turkey .....	11
Figure 2.9 Thermal cracks in a bridge deck (adopted from <a href="http://www.cement.org">http://www.cement.org</a> )	12
Figure 2.10 Replacement of Newmarket Viaduct with a more sustainable new structure.....	16
Figure 2.11 Conditions for the development of positive (a) and negative (b) thermal gradients (Hamilton et al., 2009).....	16
Figure 2.12 Factors affecting thermal gradient (Zhou et al., 2013).....	18
Figure 2.13 Determinate beam subjected to linear gradient. (Roberts et al., 1993)...	19
Figure 2.14 Directions showing the depth (y) and the width (z) of the structure .....	20
Figure 2.15 Beams subjected to non-linear gradient (Roberts, 1993).....	22
Figure 2.16. Indeterminate beam subjected to non-linear gradient (Roberts, 1993)..	24
Figure 2.17 Stress components for indeterminate structures caused by vertical thermal gradient .....	26
Figure 2.18 Positive vertical temperature gradient in concrete and steel superstructures (after AASHTO 1999). .....	29
Figure 2.19 Solar radiation zones for the United States, AASHTO (the same from 1989 to 2012) .....	30

Figure 2.20 Evolvement of positive and negative thermal gradients for Zone 3 (for superstructure depths greater than 2ft, AASHTO 1989, 1994, 1999).....	31
Figure 2.21 Temperature difference values for various concrete bridge deck types.	45
Figure 3.1. 16 representative cities selected for the thermal gradient analysis.....	48
Figure 3.2 Annual Monthly Averaged Direct Normal Radiation of Turkey (kWh/m <sup>2</sup> /day) .....	50
Figure 3.3 Annual Monthly Averaged Direct Normal Radiation of the U.S.A (kWh/m <sup>2</sup> /day) .....	51
Figure 3.4 Map of Turkey with latitude and longitudes and proposed solar radiation zones.....	51
Figure 3.5 Map of the USA with latitude and longitudes and AASHTO solar radiation zone map (AASHTO 1989a~AASHTO LRFD2010 Figure 3.12.3-1) .....	51
Figure 3.6 Solar Radiation data for Ankara between Jan.2012-Dec.2012.....	52
Figure 3.7 Temperature data for Ankara between 01.01.2012-31.12.2012 .....	52
Figure 3.8 Solar Radiation data for Istanbul between Jan.2012-Dec.2012.....	53
Figure 3.9 Temperature data for Istanbul between 01.01.2012-31.12.2012 .....	53
Figure 4.1 Bridge girder cross section used in the analysis with its dimensions in mm .....	60
Figure 4.2 Elevation view of the bridge (Adopted from Theryo, 2005) .....	60
Figure 4.3 Finite element model of the girder and the line along which the readings are taken .....	64
Figure 4.4 An example Panthalassa output visualization for 23.03.12, 2p.m.(GMT+2) .....	64
Figure 4.5 Maximum measured positive gradients (a) and negative gradients (b) in Ankara compared to recommended AASHTO Zone 1 and Turkey Zone 1.....	66
Figure 4.6 Maximum measured positive gradients (a) and negative gradients (b) in İstanbul compared to recommended AASHTO Zone 2 and Turkey Zone 2. ....	67
Figure 4.7 Maximum measured positive gradients for 16 city analyzed for Zone 1 (a) and Zone 2 (b) compared to recommended AASHTO and Turkey Zone 1 and 2. ....	68

Figure 4.8 T <sub>1</sub> value for Ankara from Zone 1 for the day with highest positive gradient 05.06.2012 (a) and for the day which the most severe negative gradient occurs, 15.08.2012 (b).....	69
Figure 4.9 T <sub>1</sub> value for İstanbul from Zone 2 for the day with highest positive gradient 14.07.2012 (a) and for the day which the lowest negative gradient occurs, 04.12.2012 (b).....	70
Figure 4.10 Recommended thermal gradient shapes and values for positive and negative gradient.....	73
Figure 4.11 3D model of the analyzed bridge, constructed in LARSA 4D.....	74
Figure 4.12 Segment labels of the analyzed bridge model, (a) plan view, (b) elevation view.....	75
Figure 4.13 Comparison of LRFD Design Example restraining moment values with the analysis values for AASHTO Zone 3 positive gradient condition.....	76
Figure 4.14 Comparison of LRFD Design Example top stress and bottom stress values with the analysis values for AASHTO Zone 3.....	77
Figure 4.15 Non-linear positive temperature gradient restraining moments for Zone 1.....	78
Figure 4.16 Non-linear negative temperature gradient restraining moments for Zone 1.....	78
Figure 4.17 Non-linear positive temperature gradient restraining moments for Zone 2.....	79
Figure 4.18 Non-linear negative temperature gradient restraining moments for Zone 2.....	79
Figure 4.19 Maximum stresses at support under positive gradient for Zone 1.....	80
Figure 4.20 Maximum stresses at support under negative gradient for Zone 1.....	80
Figure 4.21 Maximum stresses at support under positive gradient for Zone 2.....	80
Figure 4.22 Maximum stresses at support under negative gradient for Zone 2.....	81
Figure 4.23 Positive thermal gradient total stresses for proposed Zone 1.....	81
Figure 4.24 Negative thermal gradient total stresses for proposed Zone 1.....	82
Figure 4.25 Positive thermal gradient total stresses for proposed Zone 2.....	82
Figure 4.26 Negative thermal gradient total stresses for proposed Zone 2.....	83

Figure 4.27 Top stress values for different concrete grades caused by positive gradient of Zone 1 .....	84
Figure 4.28 Bottom stress values for different concrete grades caused by positive gradient of Zone 1 .....	84
Figure 4.29 Positive and negative moment values for various truck loads.....	87
Figure 4.30 Maximum and minimum truck stresses for mid-span .....	87
Figure 4.31 Maximum and minimum truck stresses for support .....	88
Figure 4.32 Zone 1 maximum compression and tension stresses for mid-span.....	89
Figure 4.33 Zone 1 maximum compression and tension stresses for support.....	89
Figure 4.34 Zone 2 maximum compression and tension stresses for mid-span.....	90
Figure 4.35 Zone 2 maximum compression and tension stresses for support.....	90
Figure 4.36 Compression stress proportions on the thermal gradient case included load combinations for Zone 1.....	91
Figure 4.37 Tension stress proportions on the thermal gradient case included load combinations for Zone 1 .....	92
Figure 4.38 Compression stress proportions on the thermal gradient case included load combinations for Zone 2.....	93
Figure 4.39 Tension stress proportions on the thermal gradient case included load combinations for Zone 2 .....	94
Figure A.1 Equivalent force and stress diagram for positive and negative gradient	106
Figure A.2 Equivalent I-section for the example box girder section .....	106
Figure A.3 Equivalent section dimensions and the applied gradient .....	107
Figure B.1 Solar radiation data for Adana between Jan.2012-Dec.2012.....	113
Figure B.2 Temperature data for Adana between Jan.2012-Dec.2012 .....	113
Figure B.3 Solar radiation data for Ankara between Jan.2012-Dec.2012.....	114
Figure B.4 Temperature data for Ankara between Jan.2012-Dec.2012.....	114
Figure B.5 Solar radiation data for Antalya between Jan.2012-Dec.2012.....	115
Figure B.6 Temperature data for Antalya between Jan.2012-Dec.2012.....	115
Figure B.7 Solar radiation data for Bingöl between Jan.2012-Dec.2012 .....	116
Figure B.8 Temperature data for Bingöl between Jan.2012-Dec.2012.....	116
Figure B.9 Solar radiation data for Bursa between Jan.2012-Dec.2012 .....	117

Figure B.10 Temperature data for Bursa between Jan.2012-Dec.2012 .....	117
Figure B.11 Solar radiation data for Çanakkale between Jan.2012-Dec.2012 .....	118
Figure B.12 Temperature data for Çanakkale between Jan.2012-Dec.2012.....	118
Figure B.13 Solar radiation data for Edirne between Jan.2012-Dec.2012.....	119
Figure B.14 Temperature data for Edirne between Jan.2012-Dec.2012.....	119
Figure B.15 Solar radiation data for Erzurum between Jan.2012-Dec.2012 .....	120
Figure B.16 Temperature data for Erzurum between Jan.2012-Dec.2012 .....	120
Figure B.17 Solar radiation data for Gaziantep between Jan.2012-Dec.2012 .....	121
Figure B.18 Temperature data for Gaziantep between Jan.2012-Dec.2012 .....	121
Figure B.19 Solar radiation data for İstanbul between Jan.2012-Dec.2012 .....	122
Figure B.20 Temperature data for İstanbul between Jan.2012-Dec.2012 .....	122
Figure B.21 Solar radiation data for İzmir between Jan.2012-Dec.2012.....	123
Figure B.22 Temperature data for İzmir between Jan.2012-Dec.2012.....	123
Figure B.23 Solar radiation data for Kars between Jan.2012-Dec.2012.....	124
Figure B.24 Temperature data for Kars between Jan.2012-Dec.2012.....	124
Figure B.25 Solar radiation data for Muğla between Jan.2012-Dec.2012.....	125
Figure B.26 Temperature data for Muğla between Jan.2012-Dec.2012 .....	125
Figure B.27 Solar radiation data for Samsun between Jan.2012-Dec.2012.....	126
Figure B.28 Temperature data for Samsun between Jan.2012-Dec.2012.....	126
Figure B.29 Solar radiation data for Trabzon between Jan.2012-Dec.2012 .....	127
Figure B.30 Temperature data for Trabzon between Jan.2012-Dec.2012 .....	127
Figure B.31 Solar radiation data for Van between Jan.2012-Dec.2012.....	128
Figure B.32 Temperature data for Van between Jan.2012-Dec.2012.....	128

## LIST OF ABBREVIATIONS

AASHTO	American Association of State Highway and Transportation Officials
AE	Absolute error
ASBI	American Segmental Bridge Institute
ASD	Allowable stress design
ASHRAE	American Society of Heating, Refrigerating and Air-Conditioning Engineers
B	Buoyancy
BL	Blast loading
BR	Vehicular braking force
CE	Vehicular centrifugal force
CR	Force effects due to creep
CT	Vehicular collision force
CV	Vessel collision force
DC	Dead load of structural components and nonstructural attachments
DD	Downdrag force
DL	Structure dead load
DT	Gradient Loading
DW	Dead load of wearing surfaces and utilities
EE	Earth Pressure
EH	Horizontal earth pressure load
EL	Miscellaneous locked-in force effects resulting from the construction process, including jacking apart of cantilevers in segmental construction
EQ	Earthquake load

ES	Earth surcharge load
EV	Vertical pressure from dead load of earth fill
FHWA	Federal Highway Administration
FR	Friction load
GDH	General Directorate of Highways
GMPE	Ground Motion Prediction Equation
IC	Ice load
IM	Vehicular dynamic load allowance
KAMAG	Support Program for Research and Development Projects of Public Institutions (in Turkish)
LFD	Load Factor Design
LL	Vehicular live load
LRFD	Load and Resistance Factor Design
LS	Live load surcharge
METU	Middle East Technical University
MBE	Mean bias error
MPE	Mean percentage error
NASA	National Aeronautics and Space Administration
NCHRP	National Cooperative Highway Research Program
NOAA	National Oceanic and Atmospheric Administration
PCI	Prestressed Concrete Institute
PL	Pedestrian live load
PTI	Post Tensioning Institute
PS	Secondary forces from post-tensioning
R	Rib shortening
RMSE	Root mean square error
RPE	Relative percentage error
S	Shrinkage
SDL	Superimposed dead load

SE	Standard error
SE	Force effect due to settlement
SF	Stream flow pressure
SH	Force effects due to shrinkage
SSE	Surface Meteorology and Solar Energy
T	Temperature loading in AASHTO Standard Specifications
T'	Temperature loading in AASHTO Guide Specifications for Design and Construction of Segmental Concrete Bridges
T <sub>1</sub>	Temperature at the top of the section
T <sub>2</sub>	Temperature at 10 cm below the top of the section
T <sub>3</sub>	Temperature at the bottom of the section
TG	Force effect due to temperature gradient
TU	Force effect due to uniform temperature
TSMS	Turkish State Meteorological Service
TÜBİTAK	Scientific and Technological Research Council of Turkey (in Turkish)
WA	Water load and stream pressure
WL	Wind on live load
WS	Wind load on structure
WSD	Working stress design

## CHAPTER 1

### INTRODUCTION

#### 1.1 General

Segmental concrete box bridges are subject to not only the annual uniform temperature changes -which can be accommodated by providing expansion joints, flexible bearings or low lateral stiffness substructures-, but also a second type of thermal variation which occurs throughout a cross section, named, thermal gradient (or temperature gradient). Solar radiation induced temperature differences along the depth of bridge cross section are mainly due to convection from surroundings. Also, conduction of heat cause non-uniform expansion and contraction of a bridge. The thermal change through the depth may affect bridge section in two ways. Under positive thermal gradient; which is the condition of deck is warmer than webs, the top surface of the structure expands more than the bottom surface, causing the structure to deflect upward, and under negative thermal gradient, the case of the top of girder is colder than web, the tendency to contraction causes tensile stresses to develop at deck which cause cracking type of problems.

Positive gradient gets higher when several days of cool weather is followed by unclouded warm days with intense solar radiation and light winds. A maximum negative gradient takes place when several days of warm weather is followed by a severe cold weather and rain cooling the deck occurs. The cause of large gradients is a result of low conductivity of concrete that the heat gain cannot be transferred quickly to other parts of the cross section.

In Germany, Austria, New Zealand, State of Colorado, and State of Florida significant cracks are reported which are attributed to the thermal gradients.

In addition to the cracking and serviceability problems; since the thermal gradient profile is nonlinear, compatibility stresses are also generated to satisfy plane sections remain plane assumption of Bernoulli. Furthermore; boundary conditional restrains cause axial and bending stresses to develop in the cross section. According to Wood (2007), in a continuous structure thermal gradient stresses caused by longitudinal moments can equal those of live loads.

The non-linear temperature difference through the depth of section causes huge thermal stresses that additional prestressing requirement arises besides the ones for dead and live load of box girder in order not to exceed mainly the allowable tensile stress limitations.

## **1.2 Aim and Scope**

The main objective of this study is to construct a comprehensive solar radiation map for Turkey using hourly solar radiation and temperature data to recommend vertical design gradient values, especially for box girder bridges, which are subjected to high compressive and tensile stress values that may result in exceedance of allowable limits for concrete.

Since the nonlinear thermal gradients are considered only in serviceability checks; do not affect the ultimate strength condition controls of a bridge, and after the condition of crack development, the stress causing forces are relieved; it is argued by some researchers that, designing for thermal stresses as high as those determined analytically can produce overly-conservative and costly structures. In this study, it is intended to investigate the role of thermal gradient loads on the overall load resultants of a bridge.

After the current Introduction Chapter, In Chapter 2, brief information about box girder bridges, segmental bridge design in the world and Turkey is given. After that, the theoretical background about temperature effects including uniform temperature and thermal gradient caused differences is given. The major causes of thermal gradients and their effects on the structure, especially bridge superstructure are examined. State of art of temperature gradient subject; historical development and previous studies of other researchers across the world on this issue are summarized, and suggested formulas in the literature to predict temperature gradients are reviewed. Then, the provisions regarding to the thermal gradients in design codes of the U.S., Europe and Turkey are summarized.

In Chapter 3, solar zone mapping of Turkey is done. AASHTO bridge specifications recommends the use of thermal gradient loads in design since 1989 and in this specification; the U.S. is divided into four zones per the country's solar radiation zones and some gradient values are given to be applied through the depth of the girder. In this study, a similar map for Turkey is constructed to be used in design of segmental bridges. In order to do this, temperature and solar radiation data of sixteen cities from two recommended solar radiation zones of Turkey are collected and processed to be applied to a box girder bridge section which is constructed in a finite element analysis program to see the thermal differences through the depth of the girder. Then, thermal gradient shapes and design gradient values are constituted accordingly.

In chapter 4, suggested positive and negative thermal gradients are applied a bridge model. The compressive and tensile stresses and bending moments developed in the analyzed bridge superstructure are obtained to see the amount of additional prestressing requirement. In the final step, the results are tabulated to be compared with the loads caused by other design load cases to see the effect of vertical gradients on the box girder bridge design. In the following figure, a flowchart of the study is given.

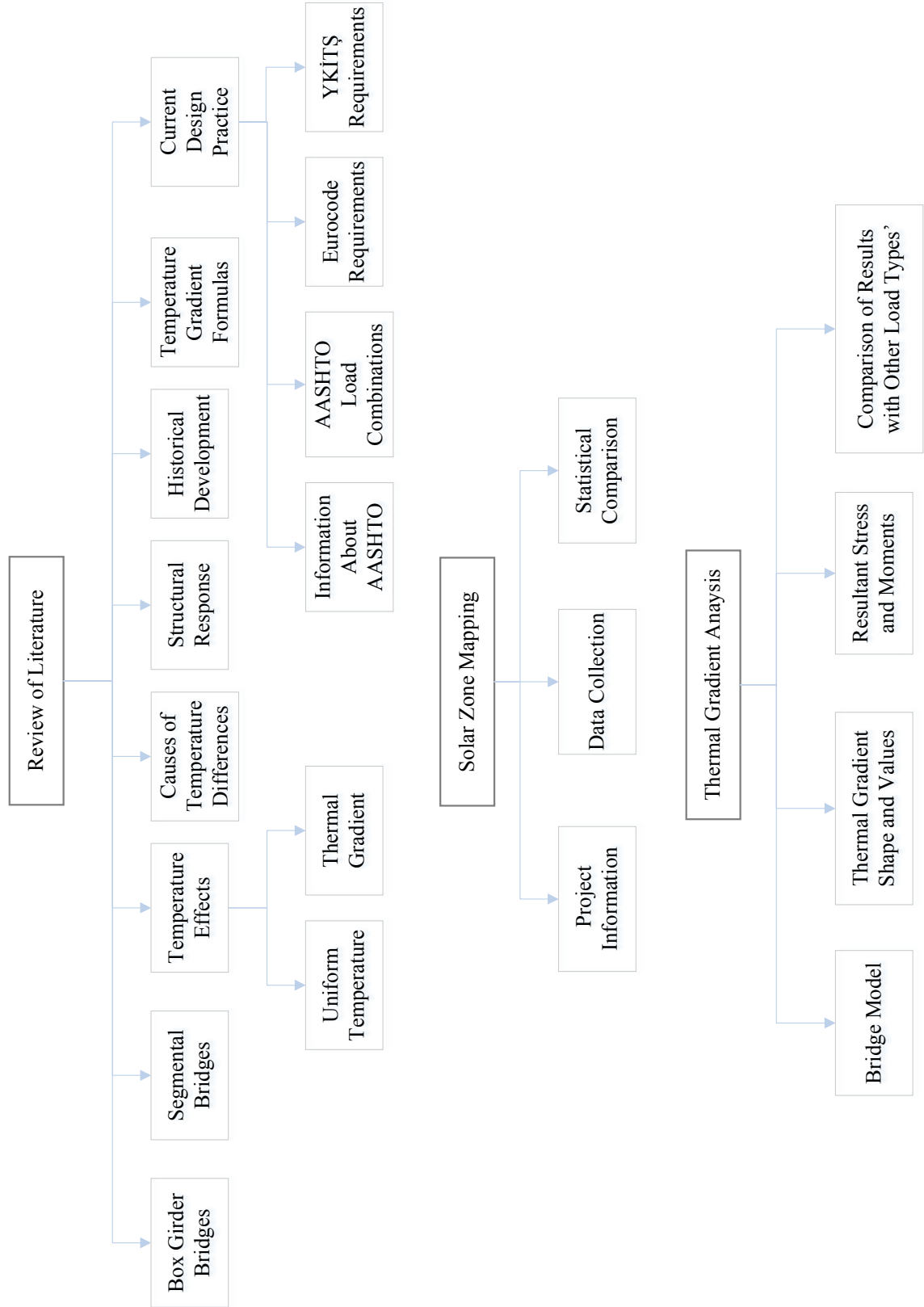


Figure 1.1 Flowchart for the outline of the study

## CHAPTER 2

### LITERATURE REVIEW

#### 2.1 Information about Box Girder Bridges

*“When the history of our time is written, posterity will know us not by a cathedral or temple, but by a bridge”*

- Montgomery Shuyler (1877), writing about John Roebling’s Brooklyn Bridge

Dated from the ancient times, mankind has a general desire to make an astonishing impact among the observers about the illustriousness and enormousness when speaking about large scale constructions. Due to their size and importance, these types of structures unequivocally create an impact and, in addition to their function to serve securely and safely connection, the structures turn into a representative monument of the place they were built.

The basic function of a bridge is to assist human by being to pass over geographical obstacles, and as these obstacles kept getting bigger, distances get longer, man had not only do find new ways of reaching the other side but also improved the aesthetics and design of bridges.

For larger span lengths, dead load of the structure gains importance and in order to reduce the dead load, removal of the not fully utilized parts of the section (material near center of gravity contributes very little for flexure and hence can be removed) led to cellular or box girder structures.

Concrete box girder bridges permit man to build longer and better bridges since they can be used in longer spans comparing to I-beam or T-beam girder bridges. Longer spans also have the advantage of reducing the number of piers for the same valley which lead to more economical and aesthetical structures. Earlier box girder sections were composed of slightly cantilevered slabs ( Figure 2.1, a-e). With the development of prestressing concrete technology, cantilever length is increased. Longer construction times and higher formwork cost resulted in the reduction in the number of cells ( Figure 2.1, f-g).

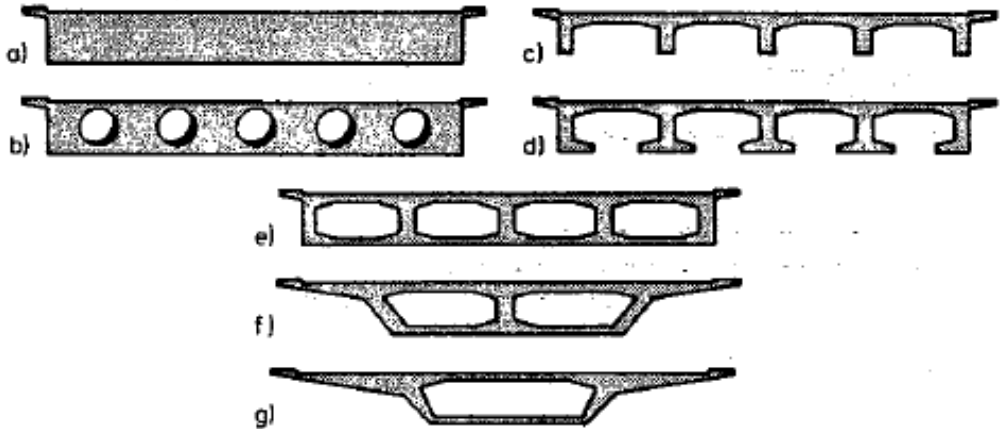


Figure 2.1 Evolvment of box girder cross-section (Schlaich, 1982)

The first box girder shaped concrete bridge sections are used for arc bridges by Boussiron in France (1899) and Maillart in Switzerland (1901). With the development of prestressed concrete technology, box girder superstructure selection is prevailed all over the world.

## **2.2 Information about Segmental Bridge Construction**

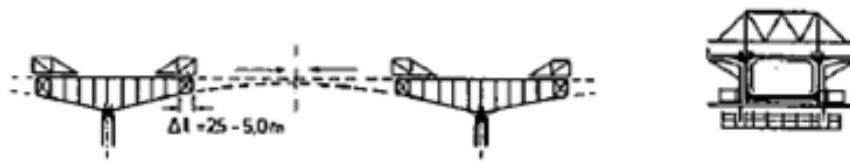
Segmental bridges are concrete box girder bridges whose adjacent deck sections are constructed using repetitive elements that are progressively connected to form a completed structure. Segmental construction was first used in China in the seventh century for arch bridges. The technique was used in Europe much later, in the twelfth century (Roberts, 1993).

For segmental bridges the typical construction material is concrete. The common methods that are used in segmental bridge construction and one example bridge that has been built by that method are given schematically in Figure 2.2.

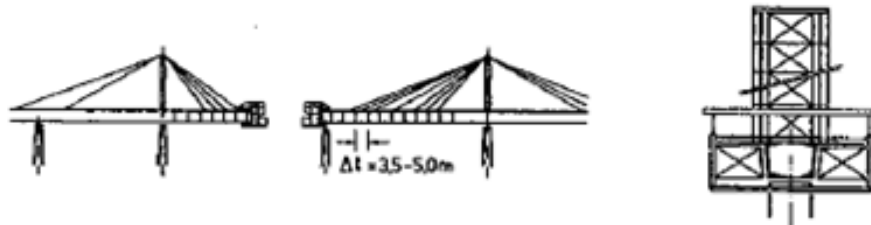
The span length, bridge length and construction process according to the selected construction method for box girder bridge construction is tabulated by Schlaich et al. (1982) is given in Figure 2.3. As seen in that chart, segmental, balanced cantilever bridge construction is a fast way to build longer spans and the method is preferred for a wide range of bridge length from 200 m to 1000 m.

In general, box girder bridges are constructed over stationary scaffolding. The most common construction methods are the segmental balanced cantilever construction and incremental launching method or cantilever method with launching gantry.

It was in the beginning of the 1950s that the cantilever method was realized to be extremely useful for prestressed concrete bridge construction by a German engineer, Ulrich Finsterwalder (1897 – 1988). His first construction was the Lahn Bridge, 1951; with a span of 62 m, but his knowledge in this particular subject resulted in the construction of Nibelungen Bridge (Figure 2.4). This structure, with considerably longer span lengths of 101.65 m, 114.2 m and 104.2 m captured worldwide attention and became a mark for long span bridges, in prestressed concrete.



a) classical balanced cantilever construction (Rhine Bridge)



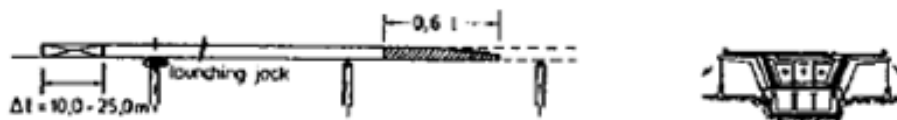
b) cantilever construction with auxiliary cables (Lahntal Bridge)



c) cantilever construction with launching gantry (Siegtal Bridge)



d) launching girder (Krannenberg Bridge)



e) incremental launching method (Taubertal Bridge)

Figure 2.2 Common construction methods for segmental bridges (Schlaich, 1982)

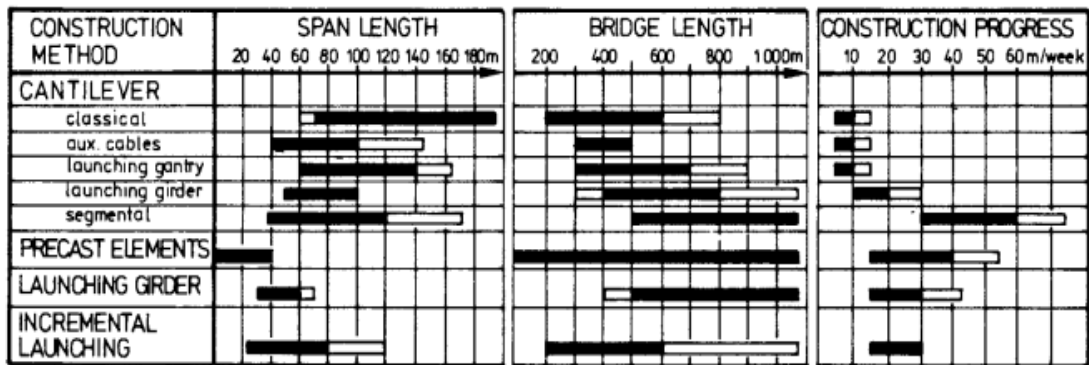


Figure 2.3 Classification of segmental box girder bridges according to bridge and span lengths and construction time (Schlaich, 1982)



Figure 2.4 Nibelungen Bridge, Germany (adopted from Honorio, 2007)

### 2.3 Segmental Box Girder Bridges in Turkey

Because of aforementioned reasons in the previous section, prestressed/post-tensioned box girder bridge type is getting more and more common in the world and in Turkey. Some example segmental box girder bridges constructed in Turkey are as follows:

- Malatya, Kömürhan Bridge (the one opened to service in 1986) with 76.5 m-135 m- 76.5 m span lengths (Figure 2.5)
- Ankara, İmrahor Viaduct with 72 m - 4 x 115 m - 72 m. spans (Figure 2.6)
- Giresun, Gülburnu Bridge with 82.5 m-165 m. -82.5 m spans (Figure 2.7)
- Artvin, Ortaköy Viaduct with 78 m - 78 m spans (Figure 2.8)



Figure 2.5 Kömürhan Bridge, Malatya-Elazığ, Turkey

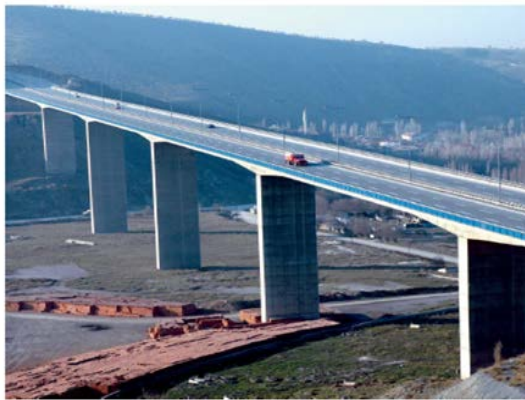


Figure 2.6 İmrahor Viaduct, Ankara, Turkey



Figure 2.7 Gülburnu Bridge, Giresun, Turkey



Figure 2.8 Ortaköy Viaduct, Artvin, Turkey

#### **2.4 Theoretical Background about Temperature Effects on Bridge Structures**

Thermal stresses occur as a result of constraints to deformations sourced by temperature changes. Seasonal and daily variations in temperature from the temperature at which it was constructed are usually the causes of temperature differences for all or part of the structure.

Variations in temperature distribution of a structure and particularly in a bridge member can be described in terms of a uniform change component which only causes axial elongation and shortening of the member, and a temperature gradient, that causes bending deformations. These bending deformations may lead to thermal cracks which affect the durability of concrete deck as given in Figure 2.9.



Figure 2.9 Thermal cracks in a bridge deck (adopted from <http://www.cement.org>)

The American Association of State Highway and Transportation Officials (AASHTO) Bridge Design Specifications has required the consideration of the stresses due to thermal gradients in the design of continuous segmental concrete bridges for nearly 25 years. The Guide Specifications for Design and Construction of Segmental Concrete Bridges (1989 edition and later versions), AASHTO Standard Specifications for Highway Bridges (2002 and the preceding), and the Load and Resistance Factor Design (LRFD) Specifications (2012 and the former LRFD versions) necessitate the consideration of nonlinear thermal gradient load cases for serviceability analysis of the segmental bridges.

### 2.4.1 Uniform Temperature Changes

The uniform temperature changes along the length of the bridge cause uniform expansion or contraction of the unrestrained superstructure, which leads to the development of axial forces if the structure is restrained against this deformation.

AASHTO (2012) considers the deformations due to uniform temperature change in design of concrete deck bridges having concrete or steel girders. The temperature range should be taken according to climate type of the location and the material used according to Table 2.1 or selected according to the  $T_{\max}$  design  $T_{\min}$  design of the contour maps of the country.

Table 2.1 Uniform Temperature Ranges According to AASHTO 2012 (in degrees Celsius)

Climate	Steel or Aluminum	Concrete	Wood
Moderate	-17 to 49	-12 to 27	-12 to 24
Cold	-34 to 49	-17 to 27	-17 to 24

Here, the number of freezing days is the main factor determining the climate type. If the number of freezing days is less than 14 the climate is considered to be moderate and freezing days are the days on which average temperature is less than 32°F (0°C).

According to Technical Specifications for Highway Bridges of Turkey (Yol Köprüleri için Teknik Şartname in Turkish, 1973) thermal stresses and deformations because of uniform temperature changes should be considered in design of highway bridges. The decrease and increase amounts of surrounding air temperature is taken into account according to predecided quantities during the construction of the structure according to the region it will be build (Table 2.2).

In the design of structural elements, the unidirectional thermal movement,  $\delta_{\tau}$  is calculated with the equation,

$$\delta_{\tau} = \alpha L \Delta T \tag{2.1}$$

where;

$\alpha$  = thermal expansion coefficient of the material. (can be taken as  $12 \times 10^{-6}/^{\circ}\text{C}$  for steel, and  $10^{-5}/^{\circ}\text{C}$  for concrete members) L is the length of the member and  $\Delta T$  is the relative temperature difference.

Unless stated otherwise, the specification indicates that; uniform temperature differences can be taken into account as the following values; or, alternatively, the difference between the maximum and minimum extreme values in last centennial period for that location can also be used. These values found from relevant institutions like State Meteorological Service.

Table 2.2 Uniform Temperature Ranges according to Technical Specifications for Highway Bridges of Turkey (in degrees Celsius)

Concrete Structures	Temperature Increase	Temperature Decrease
Mild Climate	15	20
Cold Climate	20	25

**2.4.2 Thermal Gradients**

Segmental bridges are subject to not only the annual uniform temperature changes which can be accommodated by providing expansion joints of flexible bearings and substructures, but also a second type of thermal variation which occurs throughout a cross section named thermal gradient.

Temperature differences along a bridge cross section depth because of solar radiation, convection from surroundings and conduction cause non-uniform expansion and contraction of the bridge.

According to AASHTO (2012), open girder construction and multiple steel box girders have traditionally, but perhaps not necessarily correctly, been designed without consideration of temperature gradient. However, for concrete box girders, since the heat flow in concrete is very low, differential temperatures occur throughout the cross section. The main cause of the gradient development is the low thermal conductivity of concrete.

Ignoring thermal gradients in design may cause the concrete cracking for bridges and viaducts, especially for the superstructure. The number of the bridges that experienced cracking which is attributed to thermal gradients in history cannot be underestimated. The Fourth Danube Bridge in Vienna, the Newmarket Viaduct in New Zealand (Figure 2.10), and four cast-in-place segmental prestressed concrete box girder bridges in Colorado were subjected to cracking in the webs and bottom deck soffits which was imputed to thermal gradients (Imbsen et al., 1985). Csagoly and Bollman observed significant opening of segmental bridge dry joints due to thermal gradients in a variety of bridges studied in the Florida Keys (Roberts, 1993). Leonhardt et al. (1965) reported 5 mm cracks in the Jagst Bridge in Germany which mainly attributed to differential temperatures. According to Wood (2007), in a continuous structure thermal gradient stresses caused by longitudinal moments can equal those of live loads.

Depending on the surrounding environmental conditions; these thermal differences along the depth may affect bridge section in two ways (Figure 2.11(a) (b)). Under positive thermal gradient; which is the condition of deck warmer than webs, the top surface of the structure expands more than the bottom surface, causing the structure to deflect upward. Under negative thermal gradient, the case of the top of girder is colder than web; the tendency to contraction causes high tensile stresses to develop at deck. Due to the limitations on the allowable tensile stresses in segmental bridges specified in design codes (and to avoid cracking type of durability problems) large prestressing force is required to counteract the tension originated from negative gradient.



Figure 2.10 Replacement of Newmarket Viaduct with a more sustainable new structure

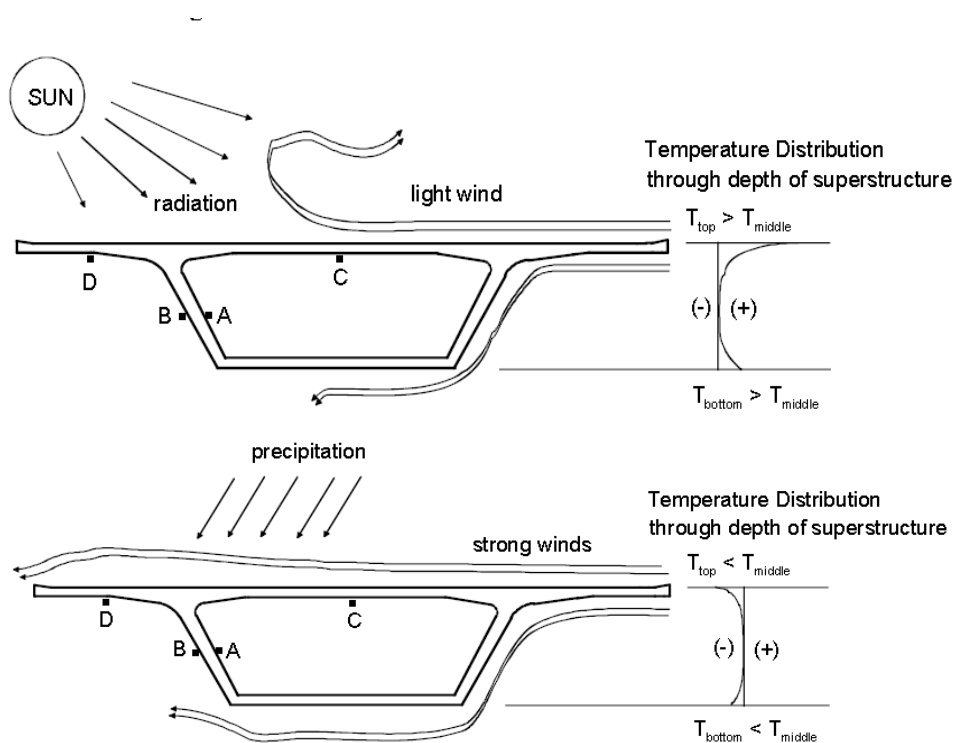


Figure 2.11 Conditions for the development of positive (a) and negative (b) thermal gradients (Hamilton et al., 2009)

A linear temperature gradient causes uniform curvature in an unrestrained superstructure. If the structure is restrained against curvature (for instance restraints from vertical supports, bridge piers); then secondary moments develop as the result of the linear gradient. Since the thermal gradient profile is accepted as nonlinear, compatibility stresses are generated to satisfy the assumption of Bernoulli beam theory that plane sections remain plane. Furthermore, boundary condition restraints cause axial and bending stresses to develop in the cross section.

Positive gradient gets higher when several days of cool weather is followed by unclouded warm days with intense solar radiation and light winds and conversely; negative gradient takes place when several days of warm weather is followed by severe cold weather and rain which cools the deck. The cause of large gradients is a result of low conductivity of concrete that the heat gain cannot be transferred quickly to other parts of the cross section.

Temperature gradients are calculated by finding the average web temperature (the temperature that does not remarkably change through the depth) and using it as baseline temperature and by subtracting it from the top and bottom temperatures.

The geometry of box-girder sections may also lead to the development of transverse thermal gradients because of a similar reason with vertical gradients; temperature differentials occur between parts of the section that are inside and outside the box. In AASHTO (1999); analysis for the effects of transverse thermal gradients is generally considered unnecessary except for relatively shallow bridges with thick webs and the usage of a plus or minus 5.5 °C transverse temperature differential in such cases is recommended in the specification.

The detailed literature review and code provisions about temperature gradients will be given in the coming sections.

## 2.5 Major Factors Effecting Vertical Temperature Differences in the Depth of Girder:

The principal causes of vertical temperature differences in a girder can be summarized into 3 titles: Climatological factors, geometrical and material properties. Primary climatological factors; solar radiation, air temperature, and wind speed depends on geographical parameters such as latitude, longitude, altitude and also time. Geometric factors are the differences in cross-sectional geometry, overlay thickness, and orientation of bridge. Finally the material properties are the thermal conductivity, color, density, specific heat, and absorptivity of bridge deck components. The most effective of the aforementioned factors for bridge decks are the solar radiation and air temperature (Figure 2.12). Solar radiation is the combination of the direct radiation which is the radiation traveling on a straight line from the sun to the earth surface, and the diffuse radiation is the sunlight that has been scattered by molecules and particles in the atmosphere and returns down to the surface.

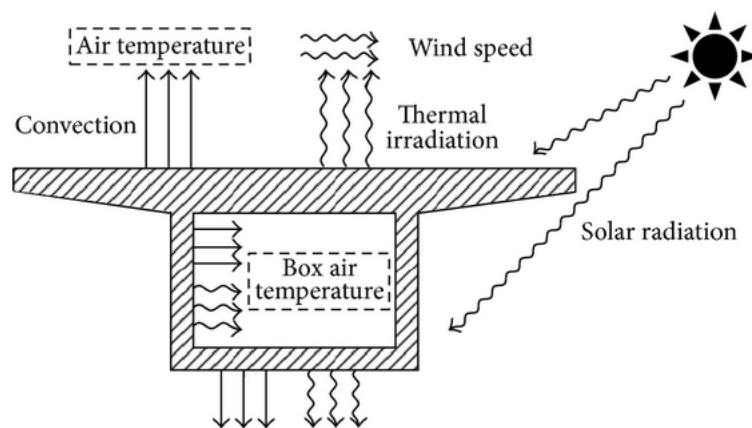


Figure 2.12 Factors affecting thermal gradient (Zhou et al., 2013)

Thermal gradients affect the structure in many hazardous ways. In the construction stage, the bowing of match cast segments caused by the temperature gradient during hydration of concrete leads to the development of gaps between two adjacent elements and that may significantly reduce the durability and the load bearing capacity of the structure.

## 2.6 Structural Response of Bridges to Temperature Variations

In structures that are externally statically determinate, for which all of the external reaction component forces can be calculated using only static equilibrium like simple-span bridges, there will be no temperature induced stresses. For instance, if the structure is subjected to positive linear temperature gradient, it will elongate and camber with an upward curve and these deformations occur without leading to the external forces or resultant stresses (Figure 2.13), and these deformations can be accommodated by providing bearings with adequate displacement and rotation capacities. In some skew bridges, longitudinal expansion also causes lateral displacement.

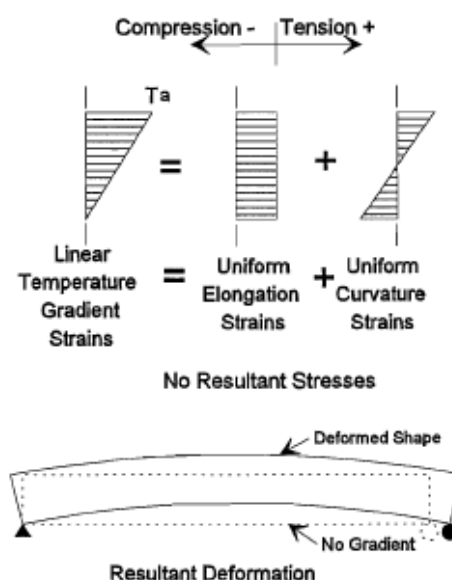


Figure 2.13 Determinate beam subjected to linear gradient. (Roberts et al., 1993)

If the statically determinant structure is subjected to a non-linear temperature gradient; the main Euler-Bernoulli beam theory of “plane sections remain plane” assumption is valid and the gradient causes self-equilibrating stress (Eigen stress) development. Since there will be no shear deformation, stresses will develop because of different strains over the section should be overcome to keep the planed form. To determine the magnitude of self-equilibrating stresses, the following steps may be carried.

First, the member should be assumed as a fixed member at both ends with a full restraint of elongation and rotation like Figure 2.15 (a) and the compressive or tensile temperature gradient stress,  $f_{RT}$ , throughout the depth, “y” of the structure (Figure 2.14) should be found by Equation (2.2) assuming fully restrained structure:

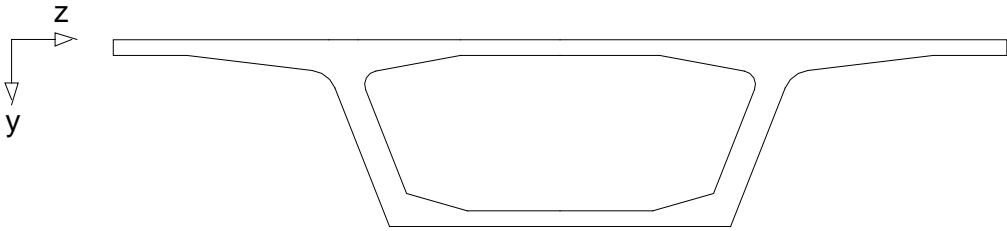


Figure 2.14 Directions showing the depth (y) and the width (z) of the structure

$$f_{TR(y)} = E \alpha TG(y) \tag{2.2}$$

Then the restraining force  $P_R$ , and the restraining moment about the z axis  $M_{ZR}$  can be found from the following formulas (noting that the restraining force is compressive if the temperature gradient is positive and will be explained in detail in following sections):

Axial force developed from the restraint:

$$P_R = \int_y f_{RT} b(y) dy = \int_y E \alpha TG(y) b(y) dy \quad (2.3)$$

Moment developed from the restraint conditions:

$$M_{ZR} = \int_y P_R y dy = \int_y E \alpha TG(y) b(y) y dy \quad (2.4)$$

where:

$y$  = distance from the center of gravity of the cross-section

$TG(y)$  = temperature at depth  $y$

$b(y)$  = section width at depth  $y$

$E$  and  $\alpha$  are the modulus of elasticity and coefficient of thermal expansion of the structure material, respectively.

If the axial and rotational restrains  $P$  and  $M$  in Figure 2.15 (a) are removed for the case of determinate beams as in Figure 2.15(b), the remaining stress (complete internal stress state in statically determinate structures),  $f_{SE}$  is the self-equilibrating stresses, the strain distribution  $\varepsilon(y)$  and curvature ( $\phi$ ) of the structure can be calculated by equations:

The self-equilibrating thermal stresses:

$$f_{SE}(y) = f_{RT}(y) - \frac{P_R}{A} - \frac{M_{ZR} y}{I_z} = E \alpha TG(y) - \frac{P_R}{A} - \frac{M_{ZR} y}{I_z} \quad (2.5)$$

The strain distribution  $\varepsilon(y)$ :

$$\varepsilon(y) = \frac{1}{E} \left( \frac{P_R}{A} - \frac{M_{ZR} y}{I_z} \right) \quad (2.6)$$

The curvature ( $\phi$ ):

$$\phi(y) = \frac{-Mz_R y}{EI_z} \quad (2.7)$$

where:

A = cross-section area

$I_z$  = moment of inertia of the section about the concerned axis

Noting that the net force on section originated from self-equilibrating stresses is zero.

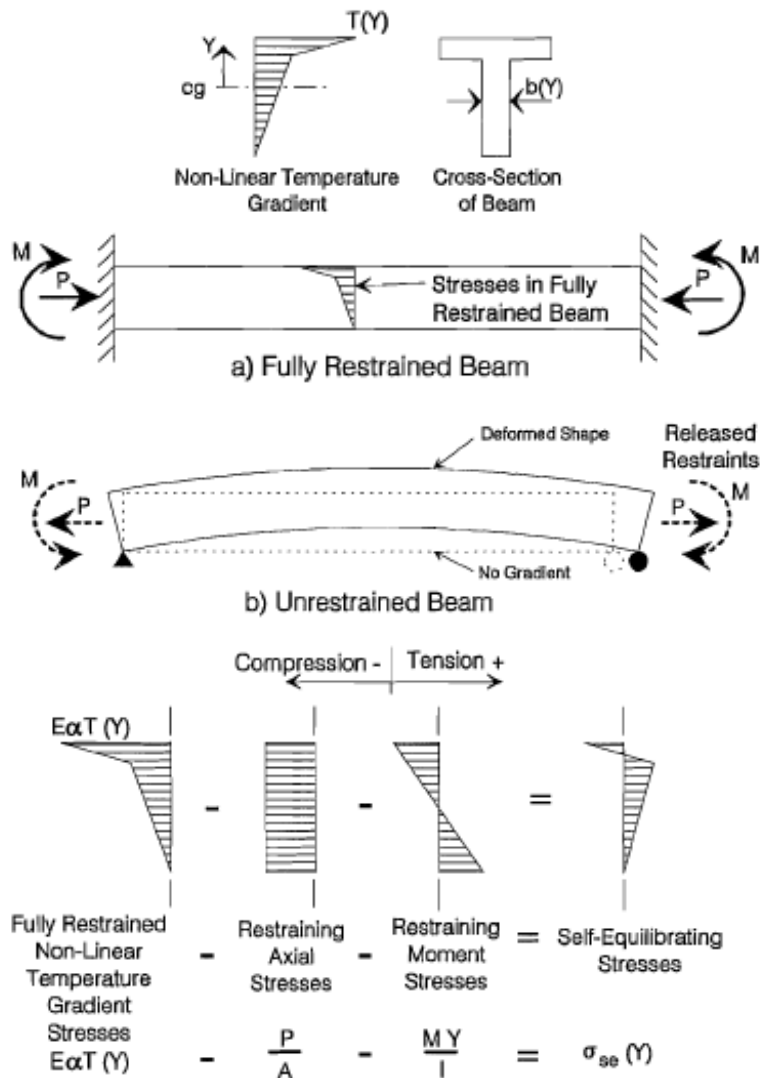


Figure 2.15 Beams subjected to non-linear gradient (Roberts, 1993)

The strain corresponding to self-equilibrating thermal stresses;  $\varepsilon_{se}(y)$  can be calculated from equation:

$$\varepsilon_{se}(y) = \varepsilon(y) - \alpha TG(y) \quad (2.8)$$

Noting that, in fact, this self-equilibrating stresses (in other words Eigen stresses), that are developed from nonlinear part of temperature gradient does not cause any deformation the structure because the forces are self-equilibrating.

In externally statically indeterminate structures, forces that are restraining these temperature-induced deformations are developed. For continuous bridge girders, restraining bending moments are induced at the intermediate supports (Figure 2.16). For example, under the positive gradient case, the top fibers of the deck will undergo greater elongation than the middle and bottom fibers. Since the cross section of the beam is able to resist out-of-plane flexural distortion (uniform bending), the fibers of the beam will undergo a uniform curvature in addition to the elongation. Self-equilibrating stresses are compressive in the top and bottom fibers and tensile in the middle fibers of the cross section. These bending moments which caused because of temperature gradient are similar in concept to the secondary moments caused by prestressing.

Thermal stress solution for indeterminate structures is a more complex problem. After the decision for the design gradient and acquirement of cross-sectional properties of the structure, the curvature ( $\phi$ ), axial deformation and self-equilibrating stresses can be determined. To find the restraining stresses, the unrestrained moment  $M_{ur}$  which is equal to  $(\phi EI)$  should be applied to the ends of the indeterminate girder and the resulting restraining moments and stresses can then be calculated.

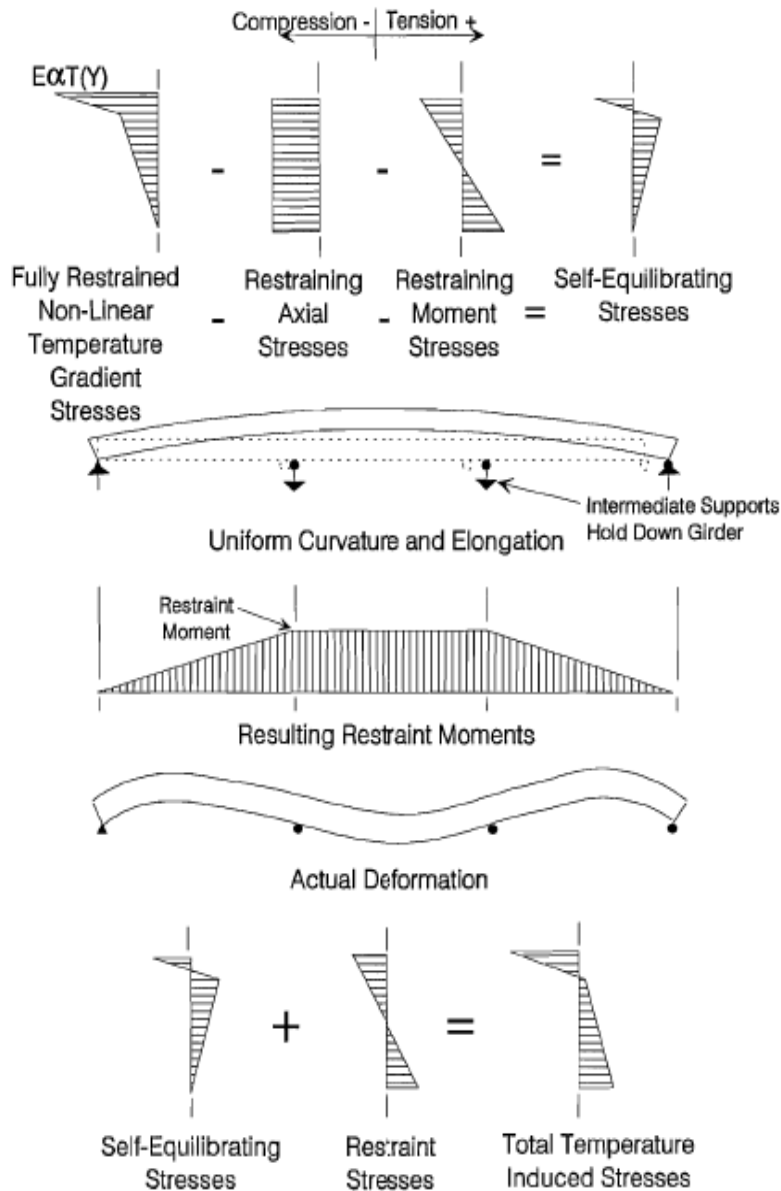


Figure 2.16. Indeterminate beam subjected to non-linear gradient (Roberts, 1993)

The additional continuity stresses shall be found by performing a structural analysis using the negative of the restraining axial force  $P$  and bending moment  $M$  given in the Equations 2.3 and 2.4 given before.

The loads at the ends of the continuous structure are calculated by using structural analysis software programs. Stresses computed from this structural analysis are then superimposed on stresses due to the primary restraining axial force and bending moment to give continuity stresses. In an alternate way, the indeterminate structure can be allowed to undergo continuity deformations due to the nonlinear gradient (that can be obtained from Equation 2.8 given before).

By removing enough number of redundant supports to make the structure statically determinate and the necessary reactions to implement that compatibility and accompanying continuity stresses can then be determined by using relevant methods (e.g. the flexibility method) afterwards. The total stress state in the continuous structure due to the nonlinear thermal gradient is the sum of the self-equilibrating stresses (determined previously with sectional analysis) and the continuity stresses (Figure 2.17).

If the thermal differences are assumed to take place through the width as well as the depth of the cross section (as mentioned before, this case could be critical in the cases for relatively shallow bridges with thick webs), self-equilibrating thermal stresses can be determined using Equation 2.9 through Equation 2.13, which are two-dimensional versions of Equations 2.2 through where the directions of which y and z axis represents were shown in Figure 2.14, previously.

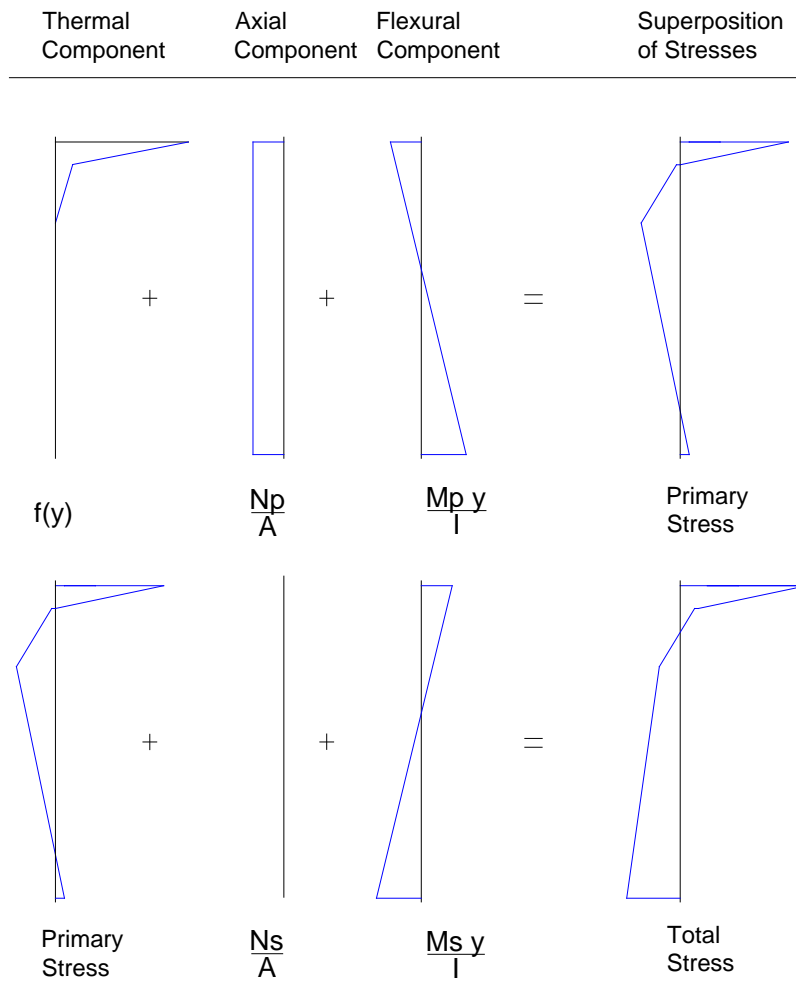


Figure 2.17 Stress components for indeterminate structures caused by vertical thermal gradient

The vertical thermal stress assuming fully restrained structure:

$$f_{RT}(z, y) = (E \alpha TG(z, y)) \quad (2.9)$$

Restraining axial force:

$$P_R = \iint_{zy} \sigma_{RT}(y, z) dz dy \quad (2.10)$$

Restraining moment in z direction:

$$Mz_R = \iint_{zy} f_{RT}(y, z) y dz dy \quad (2.11)$$

Restraining moment in y direction:

$$My_R = \iint_{zy} f_{RT}(y, z) z dz dy \quad (2.12)$$

Self-equilibrating stress distribution:

$$f_{SE}(z, y) = f_{RT}(z, y) - \frac{P_R}{A} - \frac{Mz_R y}{I_z} - \frac{My_R z}{I_y} \quad (2.13)$$

where;  $I_z$  is the moment of inertia of section about the z axis,  $I_y$  is the moment of inertia of the section about the y axis.

In addition to the aforementioned cases, another type of indeterminacy, internal indeterminacy, which is the ability to calculate all of the external reaction component forces and internal forces using only static equilibrium, also may occur over the cross section. Because of nonlinear temperature distribution over the height of the girder, thermally induced stresses will develop during curing and in service. However, stresses due to external indeterminacy are unlikely to occur in curing phase because the members are simply supported while curing.

A hand calculation is give in Appendix A. exemplifying the calculating procedure for primary force and stresses for all of the interested solar radiation zones.

## **2.7 Previous Studies and Historical Development of Design Thermal Gradients in Design Codes**

In 1967; German Code DIN 1072 (1967) was the first code to mention a differential linear temperature distribution in the design of bridges by recommending a temperature decreasing  $5^{\circ}\text{C}$  from upper surface to the soffit. New Zealand Code's recommendation (1970) considering a constant temperature in the top slab is replaced by a highly nonlinear-sixth order curve in 1973; and once again changed into the requirement to use a fifth order parabola for first 1200mm depth of girder with a  $57.6^{\circ}\text{F}$  ( $32^{\circ}\text{C}$ ) temperature gradient in (Priestley, 1987). The first recommendation to consider thermal gradient in segmental bridge design in the United States was done by PCI-PTI (Prestressed Concrete Institute-Post Tensioning Institute) in 1977 as a constant gradient in top slab with  $18^{\circ}\text{F}$  ( $10^{\circ}\text{C}$ ) temperature differential (PTI, 1977). After that Hoffman et al. (1980) made an experimental study in Pennsylvania and proposed to use  $36^{\circ}\text{F}$  ( $20^{\circ}\text{C}$ ) differential, instead of PCI-PTI's  $18^{\circ}\text{F}$  ( $10^{\circ}\text{C}$ ) and; after them Elbadry et al. (1983) developed a finite element computer program and in 1984 Cooke et al. did a similar study with prestressed concrete bridges and reasonable agreement was found as cited by Shushkewich (1998). In 1983 Potgieter et al. conducted a detailed study on nonlinear thermal gradients in 26 locations of the United States and developed a finite difference computer model which does heat flow analysis and predicted gradients for that locations and they verified their results by comparing the data got from Kishwaukee Bridge in Illinois. After that, Imbsen et al. (1985) improved Potgieter et al. (1983)'s work and presented a comprehensive state-of-art report; "National Cooperative Highway Research Program (NCHRP) Report 276" on thermal effects in concrete bridges, which later formed the basis for AASHTO guide specifications regarding thermal gradients.

Prior to AASHTO (1989c) former AASHTO Standard Specifications for Highway Bridges were considering stresses, axial expansion and contraction only because of uniform temperature changes and ignoring the probable stress distributions

throughout the depth of girder. In 1989 A ASHTO published their Guide Specification, Thermal Effects in Concrete Bridge Superstructures (AASHTO 1989a), which was based on NCHRP Report 276. The AASHTO Guide Specification for Design and Construction of Segmental Concrete Bridges (AASHTO 1989b) required the consideration of thermal gradients in the design of all segmental bridges.

The United States is divided into four solar radiation zones and a design gradient distribution across the depth of girder is specified for both positive and negative gradient, in different magnitudes for each zone. Internal stresses and structure deformations due to temperature gradients should be calculated by imposing the thermal gradient values  $T_1$ ,  $T_2$  and  $T_3$  in appropriate locations through the depth of the girder (which are shown in Figure 2.18), selected according to solar radiation map of the USA (Figure 2.19). The shape and the values of the positive and the negative gradients evolved though the years.

Here dimension factor “A” is 300 mm (12 in.) for superstructure depths greater than 400mm (16 in) and, 100 mm (4 in.) less than the depth of the superstructure and temperature  $T_3$  shall be taken as  $0^{\circ}\text{F}$  ( $0^{\circ}\text{C}$ ) unless a unless a site-specific study is made to determine an appropriate value, but it shall not exceed  $5^{\circ}\text{F}$  ( $2.8^{\circ}\text{C}$ ) and  $2.5^{\circ}\text{F}$  ( $-1.4^{\circ}\text{C}$ ) for negative gradients.

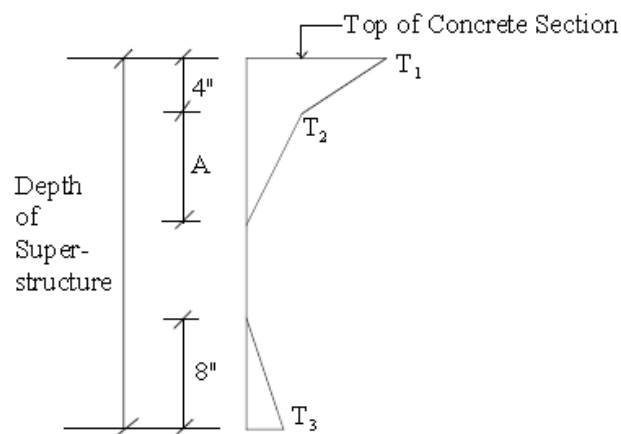


Figure 2.18 Positive vertical temperature gradient in concrete and steel superstructures (after AASHTO 1999).

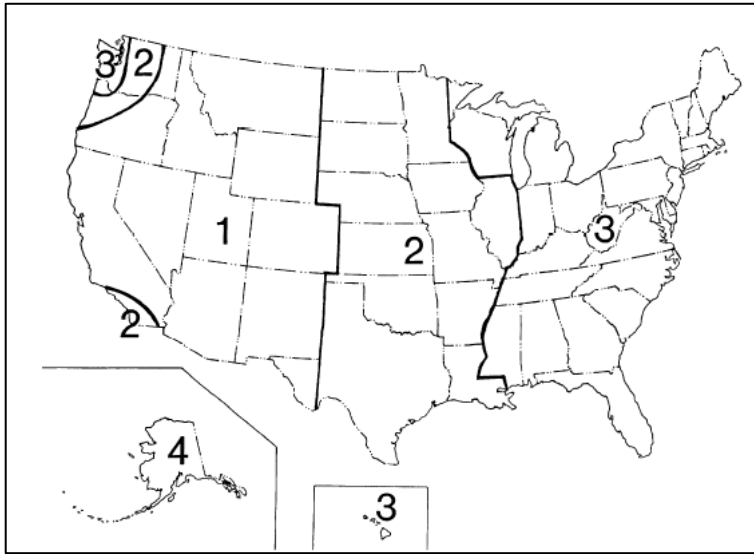


Figure 2.19 Solar radiation zones for the United States, AASHTO (the same from 1989 to 2012)

After that, several field studies conducted by researchers that are generally verifying the positive gradient design values. The negative gradients in the AASHTO (1989a) were based on the British Standard BS 5400 (1978). The shape of negative thermal gradients has since been modified over time depending on new analysis and experimental studies. In AASHTO (1994b), the magnitude of negative gradient is reduced to both simplify the design process and reduce the high tensile stresses occurring over the top few inches of the cross section, since the amount of prestressing required for that much tension found to be quite large and resulted in requirement to place tendons that otherwise would not require none. Then AASHTO LRFD Bridge Design Specifications (AASHTO, 1998a) and AASHTO Guide Specifications for Design and Construction of Segmental Concrete Bridges (AASHTO, 1999) simplified the positive gradient and reduced negative gradient by 40 percent. Prior to 1998, negative gradient was taken as -0.50 times the positive gradient. Also, in that codes surface conditions had been involved in design for negative gradient as -0.30 times of positive for plain concrete surfaces and -0.20 times for surfaces with 2 in. (5cm) asphalt topping because of the insulating nature of the asphalt by reducing the loss of heat from the surface of the flange, therefore the

magnitude of thermal gradient. Moreover, prior to 1994, thermal gradient shapes were applicable only to superstructure depths greater than 2ft but from that on, different superstructure depths are taken into account in design. Nonlinear thermal gradient values which are given in Table 2.3 and the shapes of the gradients (Figure 2.18) are remained the identical after 1999 in other intermediary specifications and also the same in latest 2012 LRFD Specifications (AASHTO, 2012).

Here in Figure 2.20, the evolution of design gradients in AASHTO for Zone 3 through the years is given as an example.

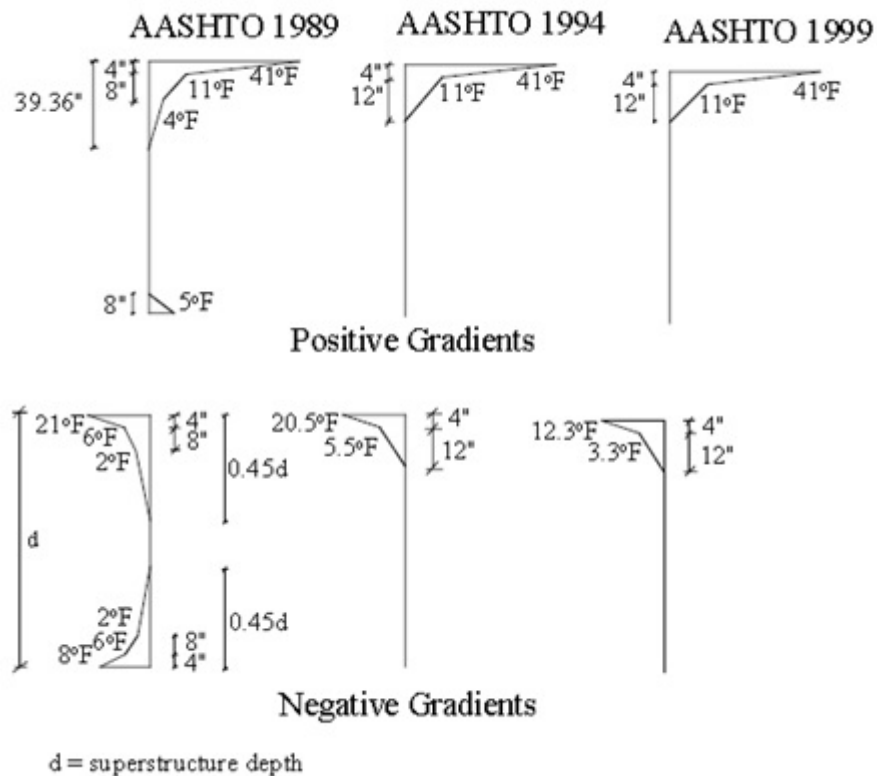


Figure 2.20 Evolution of positive and negative thermal gradients for Zone 3 (for superstructure depths greater than 2ft, AASHTO 1989, 1994, 1999)

It is important to note that, in AASHTO LRFD (2012), it is stated that, the data in Table 2.3 does not make a distinction with regard to presence or lack of asphalt overlay for positive gradient; because, the field measurement studies of Spring (1997) were not in conformity with each other regarding to the insulating or contributing effect of asphalt on deck. Moreover, Roberts et al. (1993) observed the average monitored maximum positive gradient for the no topping case is 30% less than the value with the 2 inch (5 cm) asphalt topping for San Antonio “Y” project; in contrast to the original analysis by Potgieter et al. (1983)’s confirmations (which form the basis for AASHTO thermal gradients) with data from the Kishwaukee Bridge which had an asphalt topping. Roberts et al. (1993)’s explanation to this is that; the absorptive constant for bare concrete used in the analysis has a great impact on the calculated gradient. Potgieter et al.’s used a high value for the absorptive which assumed the concrete was smooth and dirty and dark colored from passing traffic and pollution. Conversely, the concrete in the San Antonio “Y” project’ was very light in color due to the white crushed limestone aggregate, and the surface is roughened. Because of such possible differences in wearing coats, effect of insulating materials above deck is ignored in AASHTO for design for positive gradient.

Table 2.3 Positive Temperature Differentials (after AASHTO, 1999)

<b>Zone</b>	<b>T<sub>1</sub> °C (°F)</b>	<b>T<sub>2</sub> °C (°F)</b>
1	30 (54)	8 (14)
2	25 (46)	7 (12)
3	23 (41)	6 (11)
4	21 (38)	5 (9)

The negative gradient values are found by multiplying the values shown in Table 2.3 by -0.2 with the same shape as positive gradient for the decks with asphalt topping.

On the subject of thermal gradient design for segmental concrete bridges; AASHTO LRFD (2012) is still allied to the some of the publications such as; Thermal Effects in Concrete Bridge Superstructures (AASHTO, 1989a) and the Guide Specifications for Design and Construction of Segmental Concrete Bridges (AASHTO, 1999), which will be detailed in the following sections.

## 2.8 Review of Formulas to Predict the Temperature Gradient in the Literature

There are some formulas developed to predict temperature gradient along the depth of the girder depending on daily air temperature, solar radiation or both.

Potgieter et al. (1983) developed following formula to predict temperature variation along the depth of a girder section as:

$$\Delta T_v = 28.2 \left( \frac{H \cdot \alpha_s}{29.089} - 0.7 \right) + 0.342(TV - 11.1) + [32.3 - 4.84v + 0.771v^2 - 0.008v^3 + 0.00463v^3] \quad (2.14)$$

in which TV is the air temperature variation (or the difference between the daily maximum and minimum air temperatures), and  $\alpha_s$  is the solar absorptivity of concrete, range from 0.5 to 0.8 depending on the color and v is the wind speed.

Roberts-Wollman et al. (2002) proposed a simpler equation which calculates the differential based on a different variable in terms of,  $T_{\max}$ , maximum air temperature,  $T_{3-avg}$ , the three-day average air temperature and H, solar radiation as:

$$\Delta T_v = 0.9(T_{\max} - T_{3-avg}) + 0.56(H - 12) \quad (2.15)$$

Later; Lee et al. (2102) proposed an equation to calculate the maximum vertical temperature differential,  $\Delta T_v$ , on a prestressed girder as:

$$\Delta T_v = \frac{3}{4}H + \frac{1}{15}(T_{\max} - 2T_{\min}) - [0.37 + 2.93v - 0.25v^2 + 0.008v^3] \quad (2.16)$$

where H is the total daily solar radiation ( $\text{MJ}/\text{m}^2$ ),  $T_{\max}$  and  $T_{\min}$  are the daily maximum and minimum air temperatures ( $^{\circ}\text{C}$ ), and v is the daily average wind speed (m/sec).

## **2.9 Current Design Practice**

### ***2.9.1 Brief Information about AASHTO Codes***

The first national standard for bridges in the United States was published in 1931 by American Association of State Highway Officials (AASHO, a former organization of AASHTO), which is called “Standard Specifications for Highway Bridges and Incidental Structures” which depends on working stress design (WSD), based on allowable stresses. Since the theory and practice of bridge design and computer analysis technology developed so much more accurate analysis is possible. Also, regarding to the advances in material strength and durability properties, structural behavior is improved. Moreover, experiences from pre-build large number of huge number of different bridge types, in other words bridge engineering knowledge the resulted in the enhancement of the code through the years.

With renaming it as “Standard Specifications for Highway Bridges” and reissuing in approximately four year interval editions, the Standard Specifications (also will be called as AASHTO LFD) which based on allowable stress design (ASD) reached its final form as 17th edition, in 2002.

Extending to the recent times, the ASD specification started not to reverberate or comprise the recently developing design philosophy, load-and-resistance factor design (LRFD), which has been gaining importance and countenance in other areas of structural engineering as well in the USA and in other parts of the world like Canada and Europe.

In 1986, the Subcommittee submitted a request to the AASHTO Standing Committee on Research to undertake an assessment of U.S. bridge design specifications, and this task is done under the National Cooperative Highway Research Program (NCHRP), an applied research program which is completed in 1987 aiming to review foreign design specifications and codes, and to render recommendations based on these investigations.

The main report which was a milestone of the acknowledgement of thermal gradient in AASHTO Design Codes was the NCHRP Report 276 and the 1<sup>st</sup> edition of AASHTO LRFD Specifications was published in 1994, the 2<sup>nd</sup> in 1998, the next in 2004, then 2007, 2010, 2012 and 2014.

After the publication of LRFD specifications; bridge design can be done according to either of two standards to guide their designs; the long-time familiar AASHTO Standard Specifications for Highway Bridges, and newly adopted AASHTO LRFD Bridge Design Specifications, with its accompanying guidelines, AASHTO LRFD Bridge Construction Specifications and AASHTO LRFD Movable Highway Bridge Design Specifications. After 2007, the Federal Highway Administration (FHWA) and the states have established a goal to integrate LRFD standards in all new bridge designs.

Interim Specifications are usually published in the middle of the year, and revised edition of this the specifications are generally published in at most every four years. The Interim Specifications have the same status as AASHTO standards, and tentative revisions are approved by at least two-thirds of the Subcommittee.

In Turkey, highway bridges are designed according to modified version of the Standard Specifications for Highway Bridges (AASHTO LFD).

### ***2.9.2 Corresponding Load Combinations of AASHTO Codes***

Both uniform temperature and temperature gradient should be included in service limit state load combinations. Temperature gradient may be reduced by 50% if live load is present in service load combinations. Designers should be cautious in that for uniform temperature load factor of 1.0 should be used when checking stresses, and 1.2 for structural deformations.

Temperature gradient may not be included in strength limit state load combinations, while uniform temperature should. Two load factors are assigned to uniform temperature in strength limit states like service limit states. A factor of 0.5 shall be used for strength capacity calculations and 1.2 for structural deformations in strength limit state calculations. Besides, it is not recommended to combine thermal gradient with high wind forces.

In the subsequent topics, the AASHTO codes which are temperature gradient load case will be briefly scrutinized.

### **2.9.2.1 AASHTO Standard Specifications for Highway Bridges Requirements:**

AASHTO Standard Specification (2002) and prior Standard Specifications which is widely used in bridge design does not consider thermal gradient loading for design of bridges. Only uniform temperature changes are included in design load combinations symbolized with T.

### **2.9.2.2 AASHTO Guide Specification for Highway Bridges (1989) Requirements**

This specification also only requires the consideration of thermal effects in any bridge design by recommending to consider the stresses and movements caused by only uniform temperature changes.

### **2.9.2.3 AASHTO Guide Specifications for Design and Construction of Segmental Concrete Bridges (1989) Requirements:**

The temperature loading, T in the standard specification is redefined (symbolized by T' here) in the segmental specification as the sum of the original temperature loading in Standard Specification, T, and thermal gradient loading (DT).

$$T' = T + DT$$

The AASHTO Guide Specifications for Design and Construction of Segmental Concrete Bridges (1989) ameliorates the AASHTO Guide Specifications for Highway Bridges (1989) load cases by adding the following service load condition which takes thermal gradient into consideration (The loads in below equations shown in parentheses are the loads required by the AASHTO Segmental Specification and the others are defined and required by the AASHTO Standard Specification):

$$(DL + SDL + EL) + EE + B + SF + R + S + (DT)$$

where

DL = structure dead load

B = buoyancy

SDL = superimposed dead load

SF = stream flow pressure

EL = Miscellaneous locked-in force effects resulting from the construction process, including jacking apart of cantilevers in segmental construction

R = rib shortening

EE = earth pressure

S = shrinkage

Moreover, in this specification it is stated that, for load combinations that include full live load with impact, DT can be reduced by 50 percent.

#### **2.9.2.4 AASHTO LRFD Specification Requirements: (1994)**

The AASHTO LRFD divides load combinations into main categories according to the limit state considered as Strength, Extreme Event, Service and Fatigue limit states as shown in Table 2.4.

The temperature gradient effects of the 2012 edition of the AASHTO LRFD Bridge Design Specifications are analyzed under the load combinations Strength I, Strength II, Strength III, Strength V, Service I and Service III.

Table 2.4 Load Combinations and Load Factors (Adopted from the AASHTO LRFD Specification(2012), Table 3.4.1-1)

Load Combination Limit State	DC DD DW EH EV ES EL PS CR SH	LL IM CE BR PL LS	WA	WS	WL	FR	TU	TG	SE	Use One of These at a Time				
										EQ	BL	IC	CT	CV
Strength I (unless noted)	$\gamma_F$	1.75	1.00	—	—	1.00	0.50/1.20	$\gamma_{TG}$	$\gamma_{SE}$	—	—	—	—	—
Strength II	$\gamma_F$	1.35	1.00	—	—	1.00	0.50/1.20	$\gamma_{TG}$	$\gamma_{SE}$	—	—	—	—	—
Strength III	$\gamma_F$	—	1.00	1.4 0	—	1.00	0.50/1.20	$\gamma_{TG}$	$\gamma_{SE}$	—	—	—	—	—
Strength IV	$\gamma_F$	—	1.00	—	—	1.00	0.50/1.20	—	—	—	—	—	—	—
Strength V	$\gamma_F$	1.35	1.00	0.4 0	1.0	1.00	0.50/1.20	$\gamma_{TG}$	$\gamma_{SE}$	—	—	—	—	—
Extreme Event I	$\gamma_F$	$\gamma_{EQ}$	1.00	—	—	1.00	—	—	—	1.00	—	—	—	—
Extreme Event II	$\gamma_F$	0.50	1.00	—	—	1.00	—	—	—	—	1.00	1.00	1.00	1.00
Service I	1.00	1.00	1.00	0.3 0	1.0	1.00	1.00/1.20	$\gamma_{TG}$	$\gamma_{SE}$	—	—	—	—	—
Service II	1.00	1.30	1.00	—	—	1.00	1.00/1.20	—	—	—	—	—	—	—
Service III	1.00	0.80	1.00	—	—	1.00	1.00/1.20	$\gamma_{TG}$	$\gamma_{SE}$	—	—	—	—	—
Service IV	1.00	—	1.00	0.7 0	—	1.00	1.00/1.20	—	1.0	—	—	—	—	—
Fatigue I— LL, IM & CE only	—	1.50	—	—	—	—	—	—	—	—	—	—	—	—
Fatigue II— LL, IM & CE only	—	0.75	—	—	—	—	—	—	—	—	—	—	—	—

All permanent and transient load and force abbreviations which are stated in the table are;

- Permanent Loads

*CR* = force effects due to creep

*DD* = downdrag force

*DC* = dead load of structural components and nonstructural attachments

*DW* = dead load of wearing surfaces and utilities

*EH* = horizontal earth pressure load

*EL* = miscellaneous locked-in force effects resulting from the construction process, including jacking apart of cantilevers in segmental construction

*ES* = earth surcharge load

*EV* = vertical pressure from dead load of earth fill

*PS* = secondary forces from post-tensioning

*SH* = force effects due to shrinkage

Transient Loads

*BL* = blast loading

*BR* = vehicular braking force

*CE* = vehicular centrifugal force

*CT* = vehicular collision force

*CV* = vessel collision force

*EQ* = earthquake load

*FR* = friction load

*IC* = ice load

*IM* = vehicular dynamic load allowance

*LL* = vehicular live load

*LS* = live load surcharge

*PL* = pedestrian live load

*SE* = force effect due to settlement

*TG* = force effect due to temperature gradient

*TU* = force effect due to uniform temperature

*WA* = water load and stream pressure

*WL* = wind on live load

*WS* = wind load on structure

The load factors for the permanent loads and the ones caused because of superimposed deformations are given in Table 2.5 and Table 2.6.

Table 2.5 Load Factors for Permanent Loads  $\gamma_p$  (AASHTO 2012)

Type of Load, Foundation Type, and Method Used to Calculate Downdrag		Load Factor	
		Maximum	Minimum
<i>DC</i> : Component and Attachments		1.25	0.90
<i>DC</i> : Strength IV only		1.50	0.90
<i>DD</i> : Downdrag	Piles, $\alpha$ Tomlinson Method	1.4	0.25
	Piles, $\lambda$ Method	1.05	0.30
	Drilled shafts, O'Neill and Reese (1999) Method	1.25	0.35
<i>DW</i> : Wearing Surfaces and Utilities		1.50	0.65
<i>EH</i> : Horizontal Earth Pressure			
• Active		1.50	0.90
• At-Rest		1.35	0.90
• <i>AEP</i> for anchored walls		1.35	N/A
<i>EL</i> : Locked-in Construction Stresses		1.00	1.00
<i>EV</i> : Vertical Earth Pressure			
• Overall Stability		1.00	N/A
• Retaining Walls and Abutments		1.35	1.00
• Rigid Buried Structure		1.30	0.90
• Rigid Frames		1.35	0.90
• Flexible Buried Structures			
o Metal Box Culverts and Structural Plate Culverts with Deep Corrugations		1.5	0.9
o Thermoplastic culverts		1.3	0.9
o All others		1.95	0.9
<i>ES</i> : Earth Surcharge		1.50	0.75

Table 2.6 Load Factors for Permanent Loads Due to Superimposed Deformations,  $\gamma_p$  (AASHTO 2012)

Bridge Component	<i>PS</i>	<i>CR, SH</i>
Superstructures—Segmental Concrete Substructures supporting Segmental Superstructures (see 3.12.4, 3.12.5)	1.0	See $\gamma_p$ for <i>DC</i> , Table 3.4.1-2
Concrete Superstructures—non-segmental	1.0	1.0
Substructures supporting non-segmental Superstructures		
• using $I_g$	0.5	0.5
• using $I_{effective}$	1.0	1.0
Steel Substructures	1.0	1.0

The load factor  $\gamma_{TG}$  should be chosen project based taking into consideration the type of structure being designed and also the limit state being investigated.

In the commentary it is indicated that, in lieu of project specific information,  $\gamma_{TG}$  may be taken as:

- 0.0 at the strength and extreme event limit states,
- 1.0 at the service limit state when live load is not considered, and
- 0.50 at the service limit state when live load is considered.

In addition to the Table 2.4, for only segmentally constructed bridges, the following combination also shall be investigated at the service limit state:

$$DC + DW + EH + EV + ES + WA + CR + SH + TG + EL + PS$$

This load combination has no live load; hence, 100% of the temperature gradient shall be included. In general, this load combination is the controlling equation for segmental concrete bridge design where live load force effects are small in areas such as the ones near the closure pours in the top of the box.

To sum up, in the scope of this study; thermal gradient included the load combinations for segmental bridges considering the maximum load factors for permanent loads and taking dead loads, live loads and thermal gradient load as main variables are:

- Service I (with live load):  $1.00DC + 1.00DW + 1.00(LL + IM) + 0.50TG$
- Service III (with live load):  $1.00DC + 1.00DW + 0.80(LL + IM) + 0.50TG$
- Service I and III (without live load) and Service Comb. for Segmental Bridges:  $1.00DC + 1.00DW + 1.00TG$

### **The stress limits for Concrete**

According to AASHTO LRFD (2012) Chapter 5.9.4, the stress limits for concrete should be checked for both before the losses due to creep and shrinkage and for the service loads after losses have occurred.

Temporary Stresses Before the Losses Due To Creep and Shrinkage (at the time where prestress is applied):

- Compression Stresses:

AASHTO LRFD (2012) limits the compressive stresses including segmentally constructed bridges, shall be  $0.60 f'_{ci}$  for all prestressed concrete components, whereas AASHTO (2002) recommends the value  $0.60 f'_{ci}$  for pretensioned and  $0.55 f'_{ci}$  (MPa) for post-tensioned members, where  $f'_{ci}$  is the compressive strength of concrete at the time of initial prestress.

$$f'_{ci} = 0.75 \times f_c$$

where  $f'_c$ : compressive strength of concrete at 28 days

$$\sigma_{all,c} = 0.6 f'_{ci}$$

- Tension Stresses

-For segmentally constructed bridges; longitudinal stresses through joints in the precompressed tensile zone, for joints which does not have minimum necessary bonded auxiliary reinforcement, tension is not allowed.

-For joints with minimum bonded auxiliary reinforcement through the joints, that sufficiently carry the calculated tensile force at a stress of  $0.5 f_y$  (not to exceed 210 MPa); with internal tendons or external tendons, in longitudinal direction  $0.63 \sqrt{f'_{ci}}$  tension stress is allowed.

-For transverse stresses, any type of joint may carry  $0.25 \sqrt{f'_c}$  (MPa) tension stress.

Stresses at Service Limit State after Losses (for fully prestressed components):

- Compression Stresses:

Compression should be checked for Service-I Load Combination given in Table 2.4. In segmentally constructed bridges due to the sum of effective prestress and permanent loads, compressive stress must be less than  $0.45 f'_c$ .

$$\sigma_{all,t} = 0.45 f'_c$$

- Tension Stresses:

For longitudinal service load combinations that involve traffic loading tension stresses in members with bonded or unbonded prestressing tendons should be investigated using load combination Service III specified in Table 2.4. For transverse analyses of box girder bridges load combination Service I should be investigated which are involving traffic loadings.

For segmentally constructed bridges;

-Longitudinal stresses through joints in the pre-compressed tensile zone, for joints which does not have minimum necessary bonded auxiliary reinforcement, tension is not allowed. For joints with minimum bonded auxiliary reinforcement through the joints, that sufficiently carry the calculated tensile force at a stress of  $0.5 f_y$ ; with internal tendons or external tendons,  $0.25 \sqrt{f'_c}$  (MPa) tension stress is allowed.

-For transverse stresses, also the stress through joints may be  $0.25 \sqrt{f'_c}$  (MPa) .

-For the stresses at web, in the depth of neutral axis  $0.289 \sqrt{f'_c}$  (MPa)

-For the other areas with bonded reinforcement, assuming the section is not cracked,  $0.5 \sqrt{f'_c}$  (MPa) tension is allowed

### 2.9.3 BS EN 1991-1-5:2003 Requirements

Eurocode considers the nonlinear vertical temperature component and recommends two different approaches. The first one is vertical linear component approach that; an equivalent temperature difference component with  $\Delta T_{M,heat}$  and  $\Delta T_{M,cool}$  to be applied between top and bottom of the bridge deck. For concrete box girder deck bridges; if the top of the section is warmer than the bottom, 10 °C and for bottom warmer than top 5°C temperature difference should be applied. The values given are based on 5 cm surfacing depth and for other depths, these values should be multiplied by the factor  $k_{sur}$ . The  $k_{sur}$  values are ranging from 0.6 to 1.2 depending on the bridge type and also warmer area of the section (whether the top or the bottom) . The second approach considers the non-linear temperature difference component as given in Figure 2.21 In the code, it is also stated that the given values of vertical temperature differences for bridge decks to be used in a country may be found in the country's National annex.

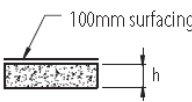
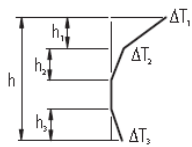
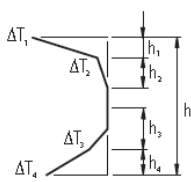
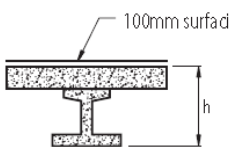
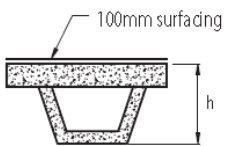
Type of Construction	Temperature Difference ( $\Delta T$ )																																																								
	(a) Heating	(b) Cooling																																																							
 3a. Concrete slab	 $h_1 = 0.3h$ but $\leq 0.15m$ $h_2 = 0.3h$ but $\geq 0.10m$ but $\leq 0.25m$ $h_3 = 0.3h$ but $\leq (0.10m + \text{surfacing depth in metres})$ (for thin slabs, $h_1$ is limited by $h - h_2 - h_3$ )	 $h_1 = h_4 = 0.20h$ but $\leq 0.25m$ $h_2 = h_3 = 0.25h$ but $\geq 0.20m$																																																							
 3b. Concrete beams																																																									
 3c. Concrete box girder																																																									
	<table border="1"> <thead> <tr> <th>h</th> <th><math>\Delta T_1</math></th> <th><math>\Delta T_2</math></th> <th><math>\Delta T_3</math></th> </tr> </thead> <tbody> <tr> <td><math>\leq 0.2</math></td> <td>8.5</td> <td>3.5</td> <td>0.5</td> </tr> <tr> <td>0.4</td> <td>12.0</td> <td>3.0</td> <td>1.5</td> </tr> <tr> <td>0.6</td> <td>13.0</td> <td>3.0</td> <td>2.0</td> </tr> <tr> <td><math>\geq 0.8</math></td> <td>13.0</td> <td>3.0</td> <td>2.5</td> </tr> </tbody> </table>	h	$\Delta T_1$	$\Delta T_2$	$\Delta T_3$	$\leq 0.2$	8.5	3.5	0.5	0.4	12.0	3.0	1.5	0.6	13.0	3.0	2.0	$\geq 0.8$	13.0	3.0	2.5	<table border="1"> <thead> <tr> <th>h</th> <th><math>\Delta T_1</math></th> <th><math>\Delta T_2</math></th> <th><math>\Delta T_3</math></th> <th><math>\Delta T_4</math></th> </tr> </thead> <tbody> <tr> <td><math>\leq 0.2</math></td> <td>-2.0</td> <td>-0.5</td> <td>-0.5</td> <td>-1.5</td> </tr> <tr> <td>0.4</td> <td>-4.5</td> <td>-1.4</td> <td>-1.0</td> <td>-3.5</td> </tr> <tr> <td>0.6</td> <td>-6.5</td> <td>-1.8</td> <td>-1.5</td> <td>-5.0</td> </tr> <tr> <td>0.8</td> <td>-7.6</td> <td>-1.7</td> <td>-1.5</td> <td>-6.0</td> </tr> <tr> <td>1.0</td> <td>-8.0</td> <td>-1.5</td> <td>-1.5</td> <td>-6.3</td> </tr> <tr> <td><math>\geq 1.5</math></td> <td>-8.4</td> <td>-0.5</td> <td>-1.0</td> <td>-6.5</td> </tr> </tbody> </table>	h	$\Delta T_1$	$\Delta T_2$	$\Delta T_3$	$\Delta T_4$	$\leq 0.2$	-2.0	-0.5	-0.5	-1.5	0.4	-4.5	-1.4	-1.0	-3.5	0.6	-6.5	-1.8	-1.5	-5.0	0.8	-7.6	-1.7	-1.5	-6.0	1.0	-8.0	-1.5	-1.5	-6.3	$\geq 1.5$	-8.4	-0.5	-1.0	-6.5
h	$\Delta T_1$	$\Delta T_2$	$\Delta T_3$																																																						
$\leq 0.2$	8.5	3.5	0.5																																																						
0.4	12.0	3.0	1.5																																																						
0.6	13.0	3.0	2.0																																																						
$\geq 0.8$	13.0	3.0	2.5																																																						
h	$\Delta T_1$	$\Delta T_2$	$\Delta T_3$	$\Delta T_4$																																																					
$\leq 0.2$	-2.0	-0.5	-0.5	-1.5																																																					
0.4	-4.5	-1.4	-1.0	-3.5																																																					
0.6	-6.5	-1.8	-1.5	-5.0																																																					
0.8	-7.6	-1.7	-1.5	-6.0																																																					
1.0	-8.0	-1.5	-1.5	-6.3																																																					
$\geq 1.5$	-8.4	-0.5	-1.0	-6.5																																																					

Figure 2.21 Temperature difference values for various concrete bridge deck types.

As seen in heating (top surface is warmer than web) condition, for bridge decks deeper than 0.8m, the  $\Delta T_1$  value is 13°C at most and for cooling condition; for sections deeper than 1.5m, this value is minimum -8.4°C.

The values of Eurocode are found too small considering the analysis results of the cities of Turkey, thus, the comparisons will be made with AASHTO instead of Eurocode.

#### ***2.9.4 Technical Specifications for Highway Bridges of Turkey (Yol Köprüleri için Teknik Şartname) (1982) Requirements:***

No requirement for thermal gradient through the depth of the structure. Only uniform temperature effects are included (given in detail in Chapter 2.4.1)

Within the scope of a national project (TUBITAK, 110G093) a new bridge design code for Turkey is being prepared by a large team of civil and earthquake engineers. In this code, the use of a positive and negative thermal gradient is proposed.

## CHAPTER 3

### **SOLAR ZONE MAP TO BE USED FOR THERMAL GRADIENT LOADING OF TURKISH BRIDGES**

#### **3.1. Information about the Project**

Since the specification which is prepared by General Directorate of Highways (GDH) in 1973 is not covering all the necessary cases for bridge design and there have been changes and improvements on the bridge design technology since 1973, the highway bridges are designed according to an adapted version of AASHTO Standard Specifications for Highway Bridges (AASHTO LFD) in Turkey. As a client organization GDH is conducting a project to update the current practice in Turkey, named; “Development of Design and Construction Technologies for Bridge Engineering in Turkey” coordinated by Middle East Technical University (METU) and funded by The Scientific & Technological Research Council of Turkey (TÜBİTAK) with Project-No: 110G093. The results of this study is also used to construct a solar radiation zone map for Turkey, similar to the map of AASHTO, recommend thermal gradient values to engineers designing especially segmental box girder bridges which are much susceptible for nonlinear temperature differences along the cross section and to see the effect of the gradient to the level of stresses and forces on the structure.

In this study; 16 cities from different regions of Turkey; Ankara, Adana, Antalya, Bingöl, Bursa, Çanakkale, Edirne, Erzurum, Gaziantep, İstanbul, İzmir, Kars, Muğla, Samsun, Trabzon and Van are selected as representative cities of contiguous areas (Figure 3.1) and the primary environmental data affecting the thermal gradient for these cities are collected.



Figure 3.1. 16 representative cities selected for the thermal gradient analysis

### 3.2. Collection of Data

Since the first step to construct a temperature map is to get irradiance values for geographic regions in desired proximity, the solar radiation data for Turkey had to be found. Solar radiation is obtained by ground measurement or satellite data.

In Turkey, Turkish State Meteorological Service (Meteoroloji Genel Müdürlüğü, TSMS) is responsible for the measurement, collection, recording, qualifying and the assessment of meteorological parameters. The institution is doing this by using meteorological observations, numerical weather prediction models and remote sensing products; and, does land, air and sea related meteorological forecasts to give early warnings for severe meteorological events (which are temperature, precipitation wind, pressure, snow amounts, waviness of seas, cloudiness and solar radiation data).

Solar radiation observations have been made by TSMS to determine irradiance in Turkey for a long period of time using ground measurements. These observations mainly consist of solar insolation and sunshine duration type of data. Bright sunshine duration data have been taken from Frans, Siap, or Muller sunshine recorders at 192 stations and the solar insolation data is also taken from Siap, Muller and Fuess actinographs installed at 163 stations all over the country. The data, especially solar insolation data, obtained from those instruments are not reliable due to the thermal sensitivity of the mechanical components of the sensors. Aksoy (1997) evaluated 14964 daily solar insolation data in total, obtained from actinographs and find a high error rate as 14.7% annual and 42.1% monthly averages.

In order to measure global and direct solar irradiation with fairly reliable, modernized pyrhelimeter and pyranometer network became operational in 5 stations in 1993 and this number is increased to 20 by 2003. However, the locations of these instruments were not uniformly distributed to cover all climate types of the country, and some of them were installed at unsuitable locations like the places which cannot get direct sunlight. Moreover, some stations had software and communication problems in data recording, and consequently, their data were not available. A quality-control check to see the correlation of the solar irradiation and bright sunshine hours was applied to the remaining eight stations and it has been found that the results of three of these stations had completely different trends from the general distribution. Therefore, after the elimination of these data, there are only five ground stations' data left for reliability analysis, taken for two years period, from January 2004 to December 2005. Because of these drawbacks, and lack of necessary amount of reliable data amount, Aksoy (2011) suggested to use satellite data taken from the Surface Meteorology and Solar Energy (SSE) dataset which are taken by the National Aeronautics and Space Administration (NASA) website. The global meteorological data is accessible on a 1 degree longitude by 1 degree latitude equal-angle grid covering the entire globe (64,800 regions) from July 1983 to December 2005. Turkey is covered with 85 grid cells of the SSE (26-45 east latitudes and 36-42 north longitudes). In order to confirm the reliable use of NASA/SSE data

for the country, Aksoy (2011) compared the SSE data for the geographical coordinates of Turkey with the data which is taken by ground stations. Aksoy found a good correlation between pyranometer and pyrhelimeter measured values and SSE data with a mean relative error 4%.

In the scope of this study, comparing solar Radiation map of the USA and Turkey constituted using the SSE data set, it is intended to subdivide Turkey into radiation zones. 22-year solar radiation values for Turkey and the USA is taken for every 1 latitude and 1 longitude grid cell from the website (140 grid cell for Turkey and 1207 grid cell for the USA) and comparing the irradiation values of the USA zones with the values for Turkey (Figure 3.2 and Figure 3.3) a solar radiation zone map is suggested for Turkey comprising the Zone 1 and Zone 2 of the USA (Figure 3.4 (a), (b) and Figure 3.5 (a), (b)). In this division; Aegean Region, Central Anatolia Region, Mediterranean Region, Eastern Anatolia Region and Southeastern Anatolia Region belong to Zone 1 and Marmara Region and Black Sea Region belong to Zone 2.

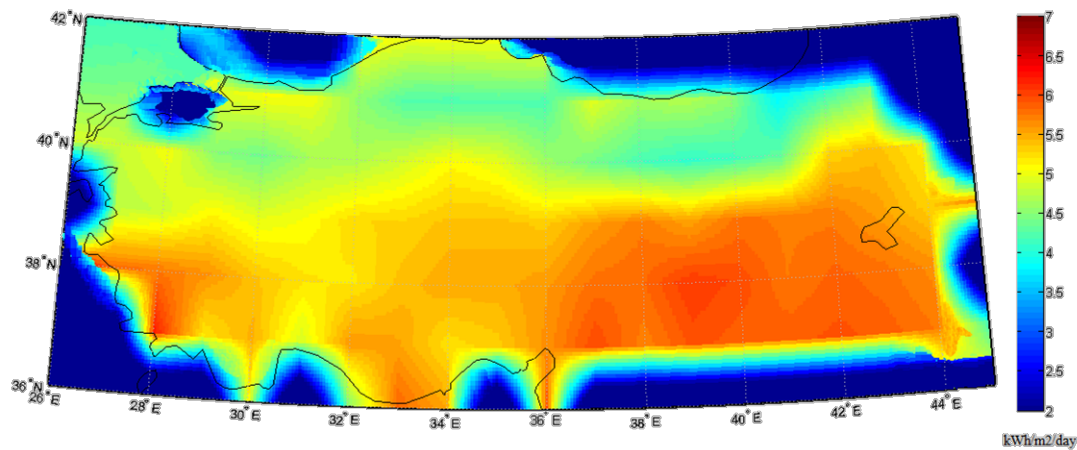


Figure 3.2 Annual Monthly Averaged Direct Normal Radiation of Turkey (kWh/m<sup>2</sup>/day)

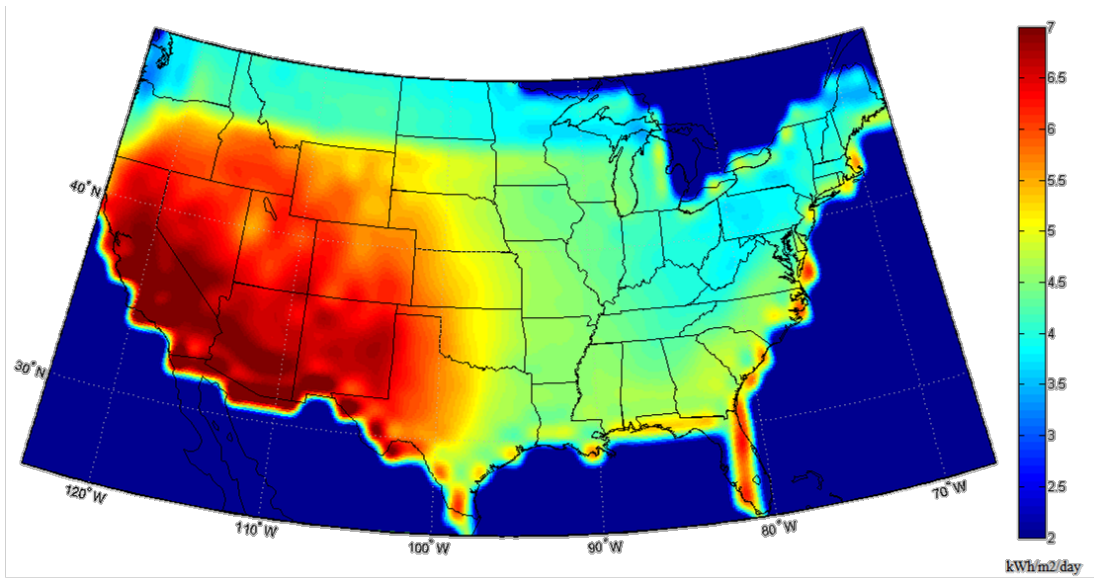


Figure 3.3 Annual Monthly Averaged Direct Normal Radiation of the U.S.A (kWh/m<sup>2</sup>/day)

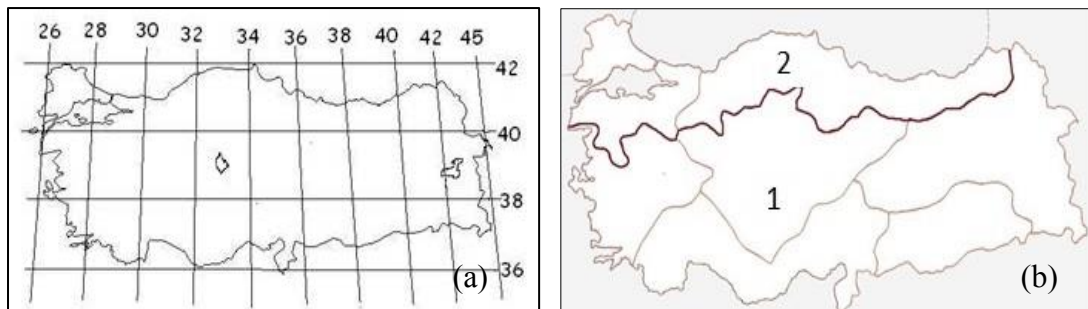


Figure 3.4 Map of Turkey with latitude and longitudes and proposed solar radiation zones

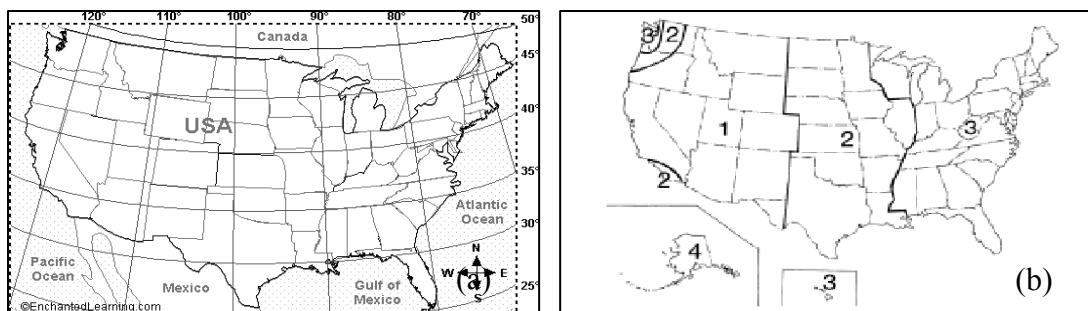


Figure 3.5 Map of the USA with latitude and longitudes and AASHTO solar radiation zone map (AASHTO 1989a~AASHTO LRFD2010 Figure 3.12.3-1)

Radiation data for Turkey is taken from monthly averaged solar insolation incident on a horizontal surface at 3-hourly intervals (in kW/m<sup>2</sup>) from the Surface Meteorology and Solar Energy (SSE) satellite dataset of National Aeronautics and Space Administration (NASA) (NASA, 2014). Hourly air temperature observation data was available in National Climatic Data Center of National Oceanic and Atmospheric Administration (NOAA) website. These data is than converted in an appropriate form in order to be used as input in the analysis program. In Figures 3.6, 3.7, 3.8, and Figure 3.9, the year 2012’s solar radiation and temperature change graph is given for two representative cities from different radiation zones, Ankara and Istanbul. The data graphs for all analyzed cities are given in the Appendix B.

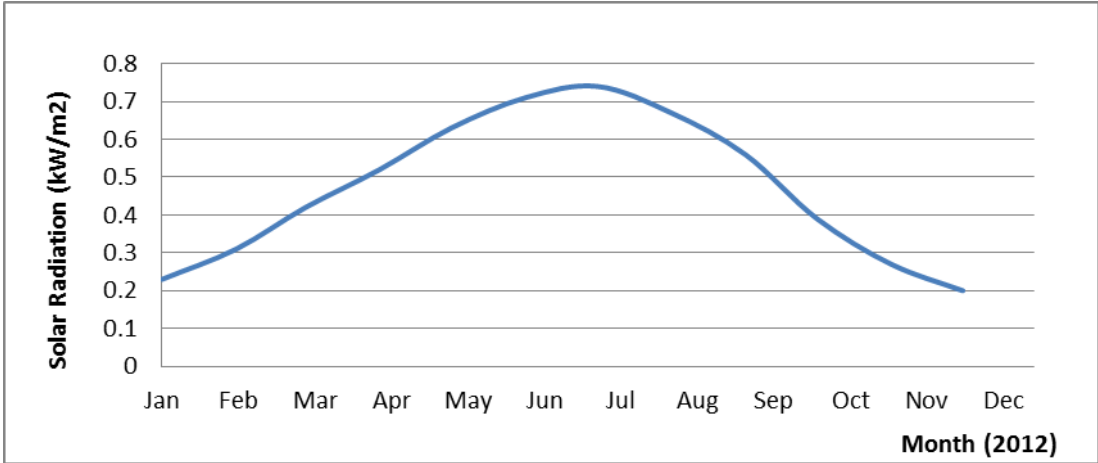


Figure 3.6 Solar Radiation data for Ankara between Jan.2012-Dec.2012

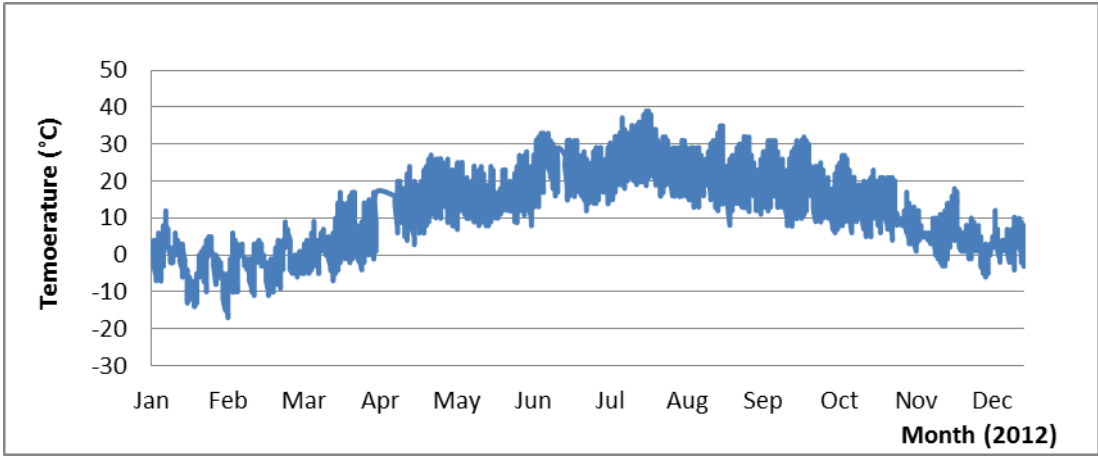


Figure 3.7 Temperature data for Ankara between 01.01.2012-31.12.2012

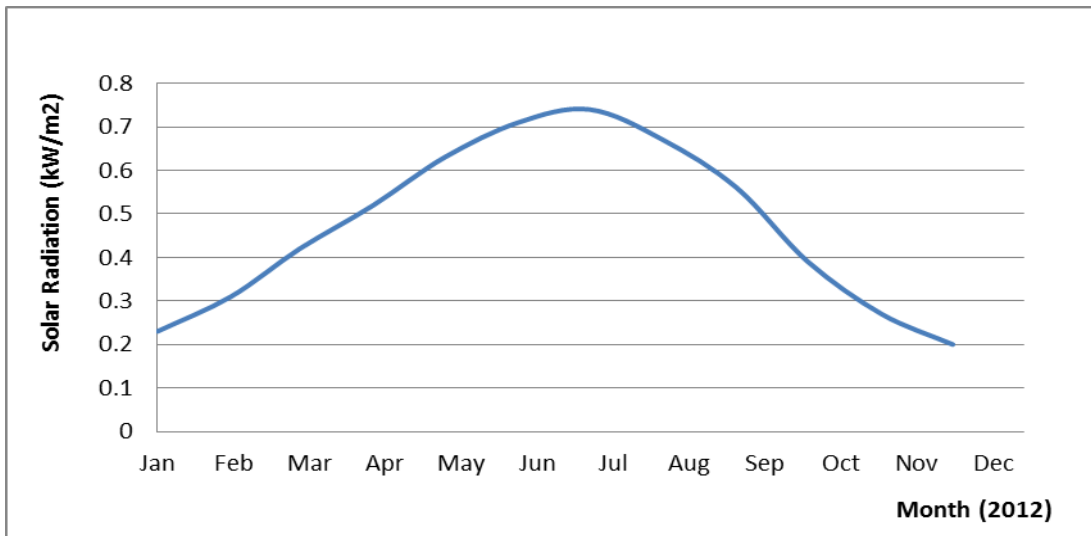


Figure 3.8 Solar Radiation data for Istanbul between Jan.2012-Dec.2012

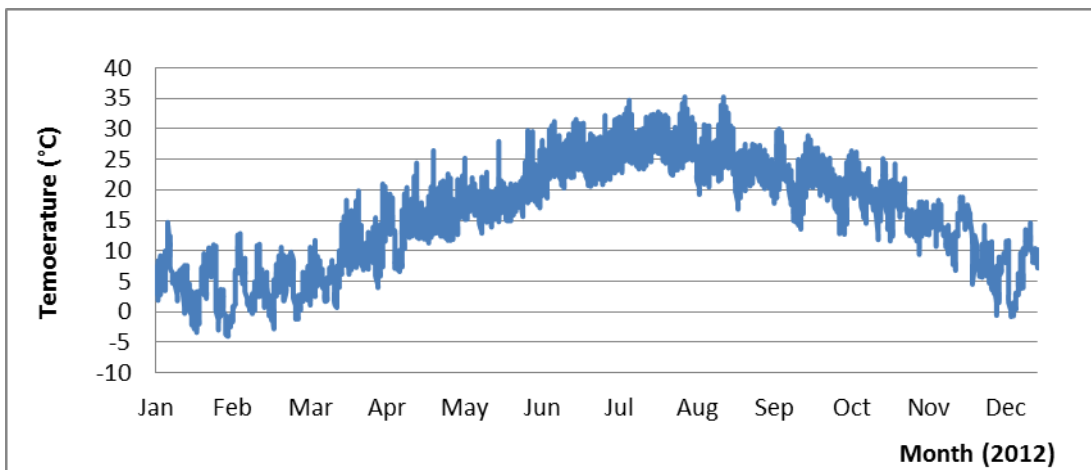


Figure 3.9 Temperature data for Istanbul between 01.01.2012-31.12.2012

### **3.3. Statistical Comparison of Suggested and Measured Values**

The 22 year Annual Monthly Averaged Normal Radiation (kWh/m<sup>2</sup>/day) values for each grid cell, which are explained in detail in the previous chapter, are shown in following table, Table 3.1

The suggested for values for each proposed solar radiation zones are named as the “predicted value” and the satellite originated data taken from related sources as the “observed value”

Table 3.1 The 22 Year Annual Monthly Averaged Normal Radiation (KWh/m<sup>2</sup>/day) Values for Grid Cells of Turkey

	26°	27°	28°	29°	30°	31°	32°	33°	34°	35°	36°	37°	38°	39°	40°	41°	42°	43°	44°	45°
42°	4.16	4.19	4.88	5.11	5.11	5.09	5.01	4.98	4.99	5.01	5.06	5.11	5.11	5.06	4.95	4.33	4.1	4.12	4.35	4.29
41°	4.39	4.43	4.42	4.93	5.06	5.02	4.54	4.24	4.21	4.25	4.21	4.93	4.63	4.72	4.56	3.8	4.1	4.46	4.27	4.68
40°	4.89	4.83	5.03	4.5	4.39	4.66	4.69	4.88	5.1	4.98	4.63	4.41	4.2	4.09	4.16	4.32	5.28	5.4	5.17	4.52
39°	5.72	4.74	4.84	5.12	4.95	5.06	5.27	5.3	5.39	5.41	5.33	5.57	5.73	5.54	5.77	5.73	5.72	5.55	5.31	5.65
38°	6.7	5.77	5.74	5.61	5.37	5.22	5.18	5.39	5.5	5.48	5.58	5.79	5.82	6.06	5.96	5.75	5.85	5.78	5.64	5.95
37°	6.78	6.64	6.19	5.84	5.47	5.7	5.59	5.53	5.23	5.33	5.62	5.98	5.7	5.94	5.86	5.88	5.93	5.86	5.74	6.14
36°	6.92	7.22	6.91	6.5	5.22	6.62	5.42	5.83	5.73	6.38	5.62	5.91	5.93	6.12	6.05	5.97	5.94	6.03	5.97	5.59

(Zone 2 values are highlighted and Zone 1 values are left in white background)

The observed values are the averages of the SSE values for each zone, shown above; and the predicted values are calculated as the average radiation amount in USA Solar Radiation maps corresponding to thermal gradient zones in AASHTO which are chosen as appropriate for the zones of Turkey.

The comparison of the averages of predicted radiation values of each zone with the observed values are presented as in Table 3.2

In the table,

Absolute error,  $AE = |H_{io} - H_{ip}|$

Standard error,  $SE = \frac{\sigma}{\sqrt{N}}$

Relative percentage error,  $RPE = \frac{H_o - H_p}{\bar{x}} * 100$

Mean percentage error,  $MPE = \frac{1}{N} \sum_{i=1}^N \left( \frac{H_{io} - H_{ip}}{H_{io}} * 100 \right)$

Mean bias error,  $MBE = \frac{1}{N} \sum_{i=1}^N (H_{io} - H_{ip})$

Root mean square error,  $RMSE = \sqrt{\frac{1}{N} \sum_{i=1}^N (H_{ip} - H_{io})^2}$

Here  $H_{io}$  is the  $i^{\text{th}}$  observed value,  $H_{ip}$  is the  $i^{\text{th}}$  predicted value,  $N$  is number of observations and  $\sigma^2$  is variance.

Mean percentage error can be defined as the deviation of anticipated monthly average irradiation values from the observed ones. The MBE, expressed as either a percentage or an absolute value, reveals whether a given model has a tendency to under- or over-predict. MBE values closest to zero are desirable. The RMSE indicates the level of dispersion that a model has, thus providing a term-by-term comparison and show the departure between the predicted and observed values. The lower RMSE values reflect a better model in terms of its absolute deviation. According to Lingamguna et al. (2004) relative percentage error, RPE smaller than 25% is desired for a model to be acceptable.

Table 3.2 Comparison of Monthly Averaged Radiation Values

	<b>Zone 1</b>	<b>Zone 2</b>
<i>Predicted Average Value</i>	5.930	4.770
<i>Observed Average Value</i>	5.511	4.673
Number Of Stations	102	38
Variance	0.426	0.153
Standard Deviation	0.653	0.391
Absolute Error	0.419	0.097
Standard Error	0.065	0.063
Relative Error	7.607	2.084
Mean Percentage Error	7.069	2.041
Mean Bias Error	0.419	0.097
Root Mean Square Error	0.773	0.398

The calculated error values and aforementioned commentaries show that error ratios are in acceptable limits and division of Turkey into two radiation zones as suggested is acceptable.



## CHAPTER 4

### ANALYSIS FOR THERMAL GRADIENT

#### 4.1. Information about Analyzed Bridge Model

A box girder bridge section AASHTO-PCI-ASBI Segmental Box Girder Standard Type 2700-2, a single cell concrete box girder 2.75 meters (9'-0") in depth which is a 5 span bridge with span configuration 46.65 + 3 x 61 + 46.65 m. producing a total length of 273.4 m and has span with 13.10 meters (43'-0") wide deck designed to accommodate two lanes of traffic is chosen for the analyses. This bridge is identical to the bridge in "Precast Balanced Cantilever Bridge Design using AASHTO LRFD Bridge Design Specifications, 2004" prepared by Theryo (2005) for American Segmental Bridge Institute (ASBI) (will be mentioned as 'LRFD Design Example' later on) given in Figure 4.1 for span section with 5cm asphalt topping was chosen as a representative section. The elevation of the bridge with the span configuration is also given in Figure 4.2 .

In that design example, the longitudinal analysis of the bridge was done using the TANGO Program and the effects of stage-by-stage construction and time dependent analyses were considered in design. Design according to all limit states of AASHTO LRFD (2004) Specifications (Strength, Extreme Event, Service, and Fatigue) were made. Since in that design example; bridge is analyzed not only permanent loads like and live load, but also for temperature effects, a comparison can be done considering the magnitudes of stresses and moments caused by thermal gradients between the LRFD Example and the bridge analyzed in this study.



The 28 day cylinder compressive strength of concrete is taken as 35 MPa, and material properties like conductivity, film convection, specific heat and emissivity for both the concrete and asphalt are taken according to The American Society of Heating, Refrigerating and Air-Conditioning Engineers (ASHRAE) Handbook (ASHRAE, 2001) and suggestions of Lee (2012). Also the air inside the box is modeled with corresponding parameters (Table 4.1)

Table 4.1 Material Properties for the Analytical Computations

	Concrete	Asphalt	Air
Modulus of Elasticity (kPa)	33000***	33	0.003
Density (kN m-3)	24*	21.1*	0.012*
Conductivity x,y,z (W m-1 °C-1)	1.5****	0.74*	0.024*
Film Convection (W m-2 °C-1)	23.92**	23.92**	5.6**
Specific Heat (kJ kg-1 °C-1)	1****	0.92*	1.005*
Thermal Expansion Coefficient (°C-1)	0.000001***	-	-
Emissivity Coefficient	0.85**	0.93*	0

The values with asterisk are retrieved from

- \* ASHRAE (2001)
- \*\* Lee (2012)
- \*\*\* TS500 (2000)
- \*\*\*\* Branco (1993)

#### 4.2. Analysis to Obtain Design Gradient

For the thermal gradient analysis of selected concrete girder section, it is assumed that temperature varies vertically with depth, but is constant at all points of equal depth.

The solar radiation and ambient temperature data of each city in a whole year of 2012 are taken as most influential parameters to the thermal changes throughout the depth of the structure.

In this study, extensible finite element analysis environment, Panthalassa is utilized for heat transfer analysis. It is developed by using C++ language with object oriented architecture. The platform let the users to add their own material, element or solution algorithms as plug-ins without changing the core library. Furthermore, the environment has capability of high performance computation due to its parallel solution algorithms (Albostan, 2013).

The bridge geometry is modeled with linear hexahedral elements. In order to reduce the computational cost, the cross section of the bridge is generated with linear hexahedral elements since no temperature gradient would be expected in the direction of the bridge span. In the analyzed model, 296 linear hexahedral elements and 674 nodal points are generated. The concrete girder is meshed in the direction of the thickness to observe the temperature gradient, clearly. 5 cm asphalt layer is added to the top surface. In addition to the concrete bridge superstructure and asphalt topping, the air inside the girder is modeled with linear hexahedral elements and connected to the innerside of the girder with one dimensional link elements. These link elements provide to transfer the heat energy between concrete and the air models. The general heat convection and heat radiation conditions require ambient temperature. In this model, however, the fluid temperature inside the girder changes according to the temperature values at the inner surface of the girder. Accordingly, these convection and radiation conditions are represented with the link elements. On the other hand, at each outer surface of the girder, heat convection condition with ambient temperature (acquired from the country's temperature observation data explained in detail in Section 3.2) is taken into account. Moreover, heat radiation due to sun (also explained in Section 3.2) is applied to the top surface (on asphalt layer).

Since heat radiation data obtained from the data source is as energy rate, it is defined as surface flux on the asphalt layer. On the other hand, heat radiation between outer air layer and outside surface of the girder is defined as heat radiation boundary condition.

Transient heat transfer analyses are performed by utilizing high performance computer. Analyses are made for the each city in order to give hourly temperature results for the whole year 2012 for each node of the section. A high performance computer that has the properties presented in Table 4.2 is used in the analyses, and with the provided computer, each analysis took approximately 8 hours (for the output frequency mentioned in the following paragraph).

Table 4.2. Properties Of The Computer Used In Heat Transfer Analysis

Processors	Intel Xenon E5630 2.53 GHz
Number of Cores	8
RAM	24 GB
Operating System	64 bit

Readings are obtained for a line along one of the webs in vertical direction from the topmost of the girder to the base (shown with the red line in Figure 4.3) and an example visualization of an output for a selected time is given in Figure 4.4. The initial temperature conditions are taken into account by starting the analysis with data of the prior month, i.e. December 2011. Results are acquired in hourly intervals in order not to omit the most critical gradient values. After the analysis the temperature of each node in cross section is used to calculate the thermal gradient. The highest positive gradient values tend to occur at 12 p.m. Greenwich Mean Time (2 p.m. for GMT +2 and 3 p.m. for GMT +3 time zones) in July while negative gradient values tend to occur at midnight times in December.

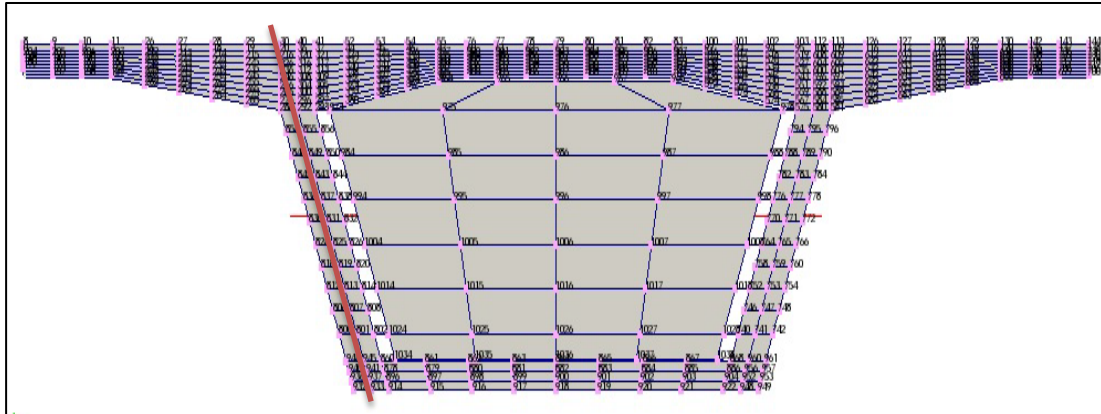


Figure 4.3 Finite element model of the girder and the line along which the readings are taken

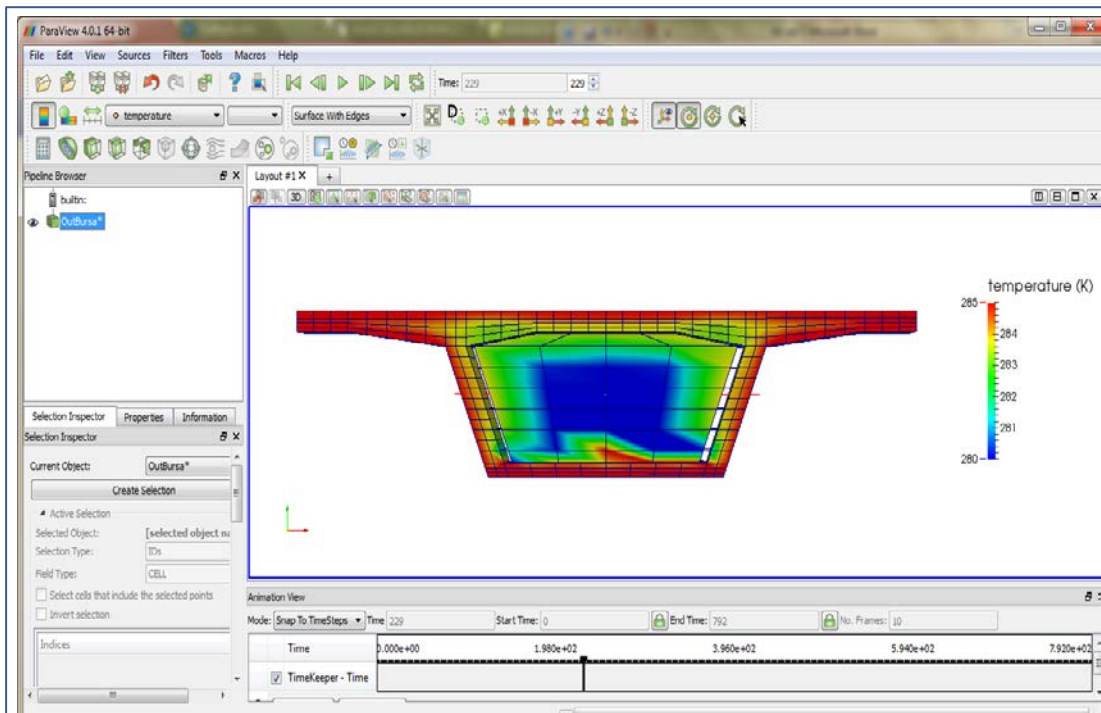


Figure 4.4 An example Panthalassa output visualization for 23.03.12, 2p.m.(GMT+2)

The 5 most critical positive gradient values are plotted along the depth of the girder for one example city from each proposed thermal zone, Ankara from Zone 1 and Istanbul from Zone 2 drawn together in Figures 4.5 and 4.6 with the relevant AASHTO Solar radiation zones and the zones which are recommended from their means. (The decision criteria for the selection of proposed gradient values for Turkey are explained in the following paragraphs). In the following graph, the highest positive gradient values for each city analyzed are also plotted (Figure 4.7). Generally  $T_3$  values, the temperature gradient values at the bottom of the section are so small that, they may be ignored in the design. AASHTO (1999 and subsequent) also allows omitting  $T_3$  in design unless a site-specific analysis is made.

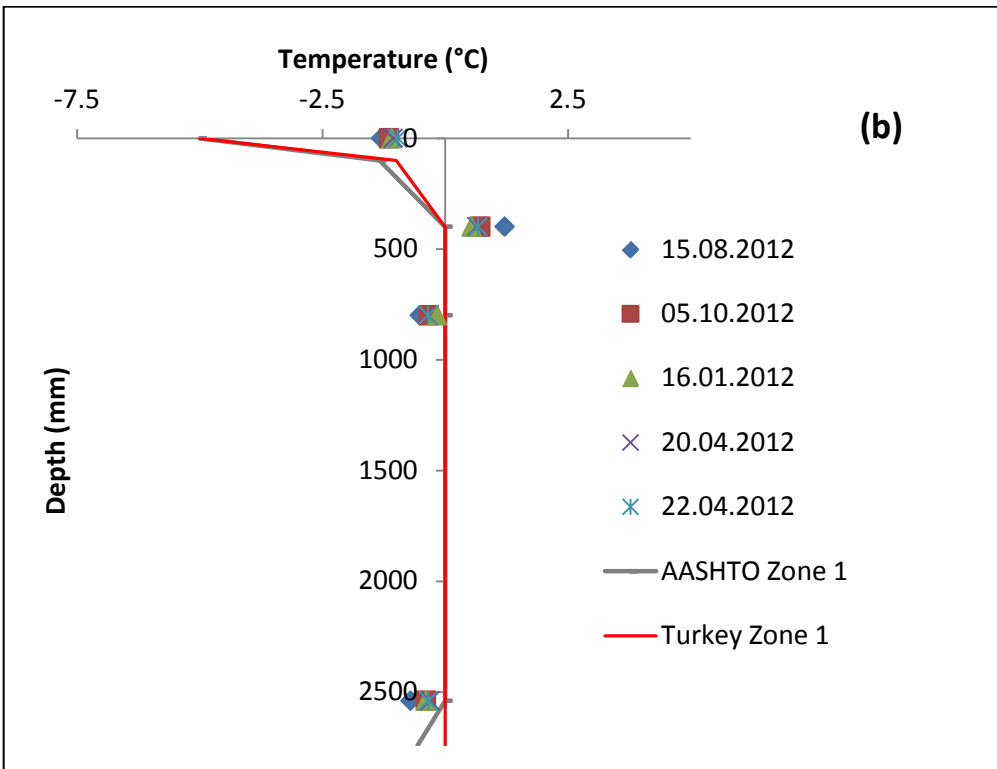
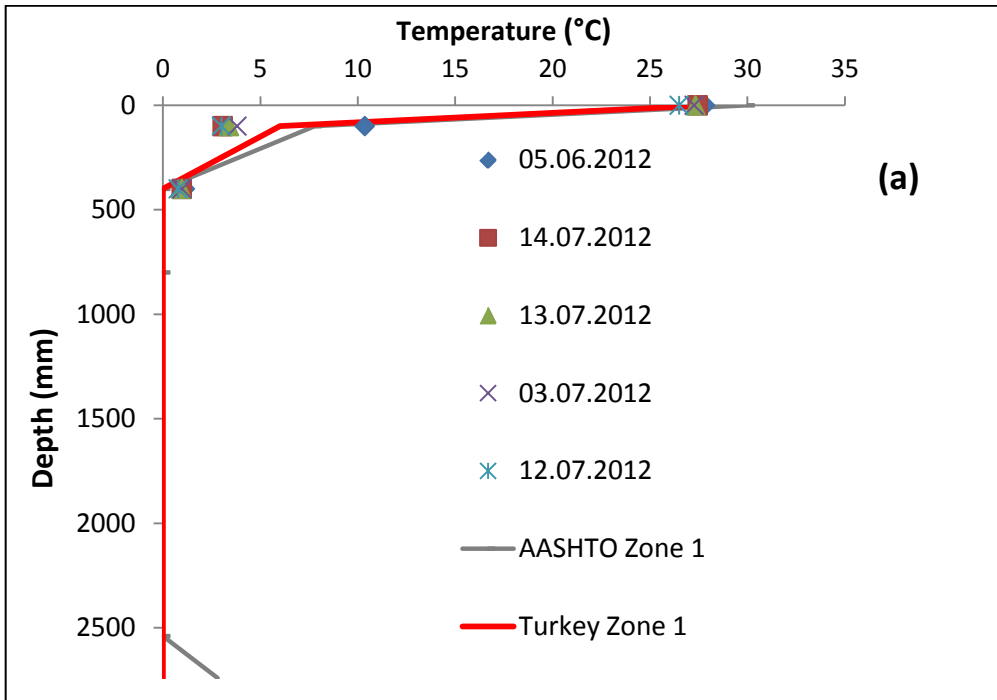


Figure 4.5 Maximum measured positive gradients (a) and negative gradients (b) in Ankara compared to recommended AASHTO Zone 1 and Turkey Zone 1.

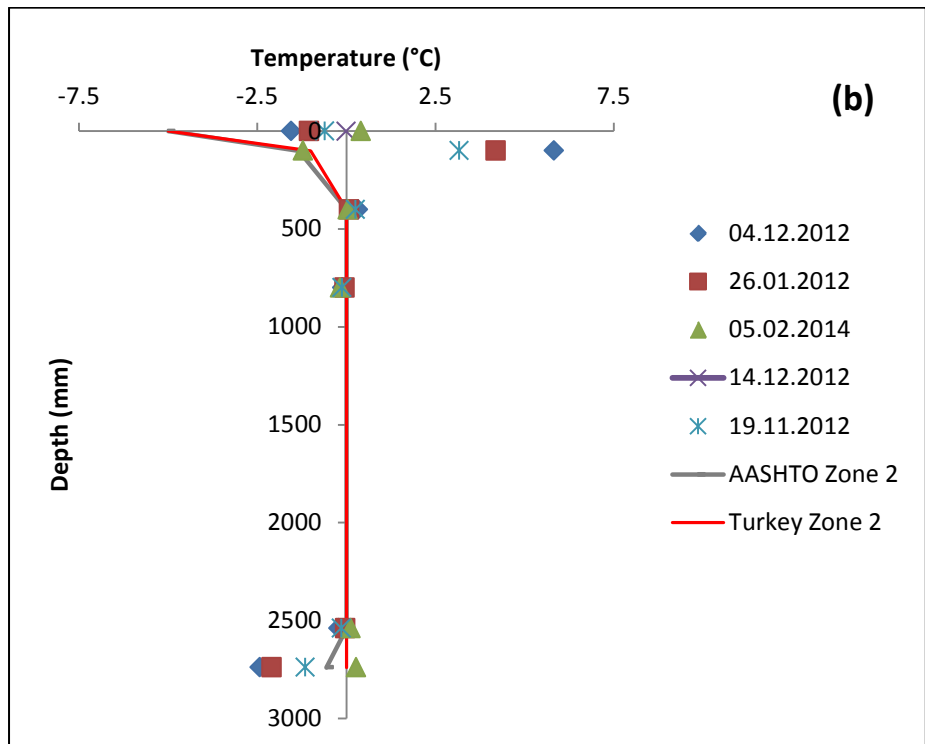
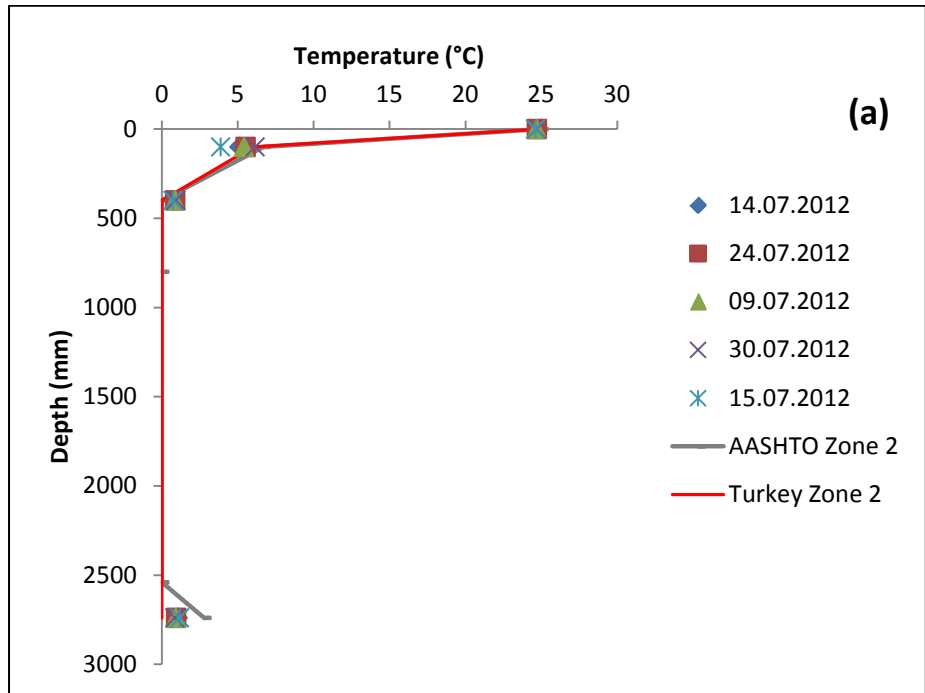


Figure 4.6 Maximum measured positive gradients (a) and negative gradients (b) in İstanbul compared to recommended AASHTO Zone 2 and Turkey Zone 2.

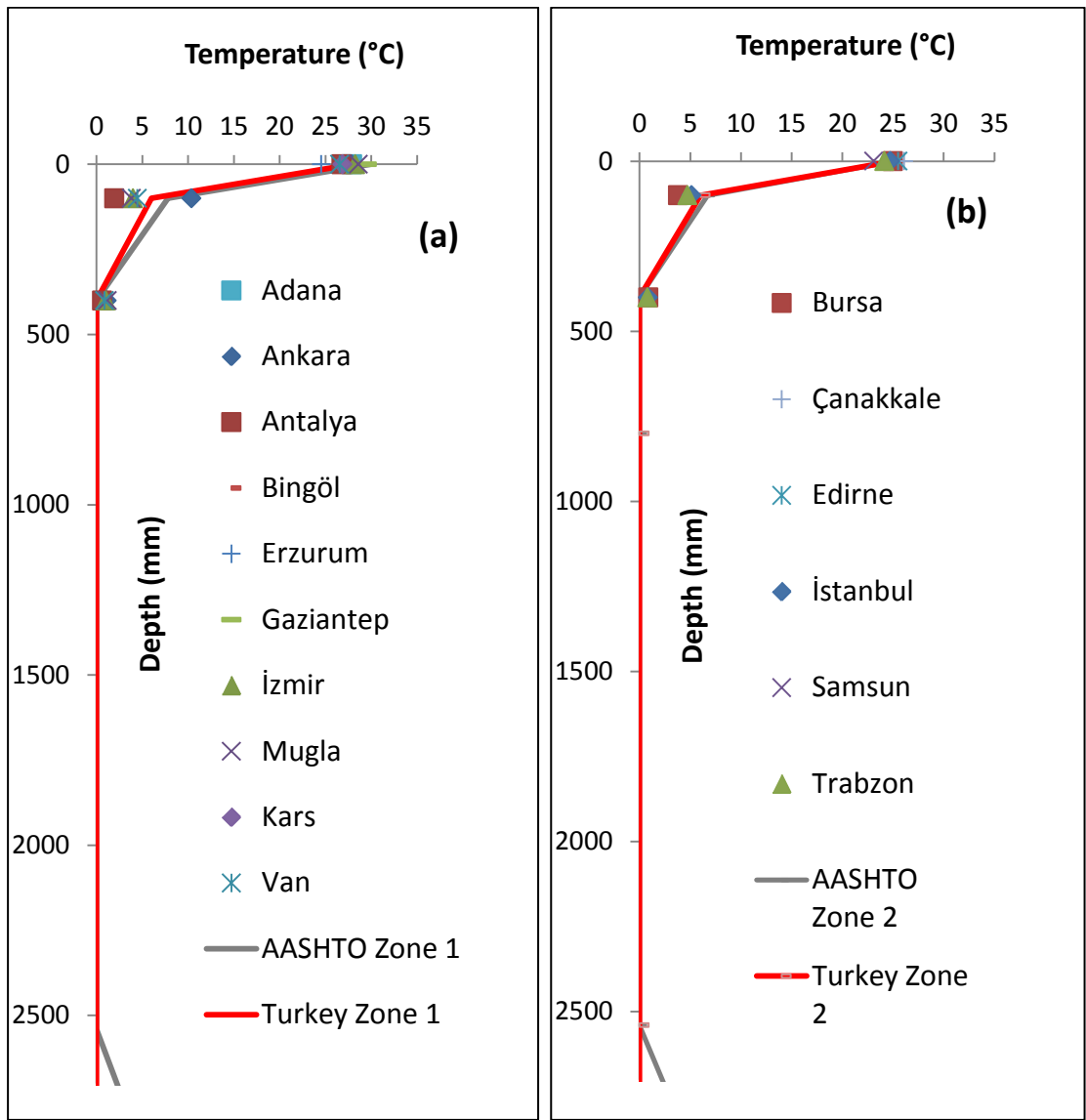


Figure 4.7 Maximum measured positive gradients for 16 city analyzed for Zone 1 (a) and Zone 2 (b) compared to recommended AASHTO and Turkey Zone 1 and 2.

The general tendency for the largest gradient values is similar for all of the analyzed cities. The highest positive gradients of the days correspond to 3 hours after mid-day 3p.m. as a result of the heat and radiation accumulation and the negative gradient values are the most severe at the 3 a.m. in most days, just before the rise of the sun. Figure 4.8 shows hourly changing gradient values for two example days for the most severe positive and negative gradient days of Ankara from Zone 1, Figure 4.9 shows the same daily changes for Istanbul from Zone 2.

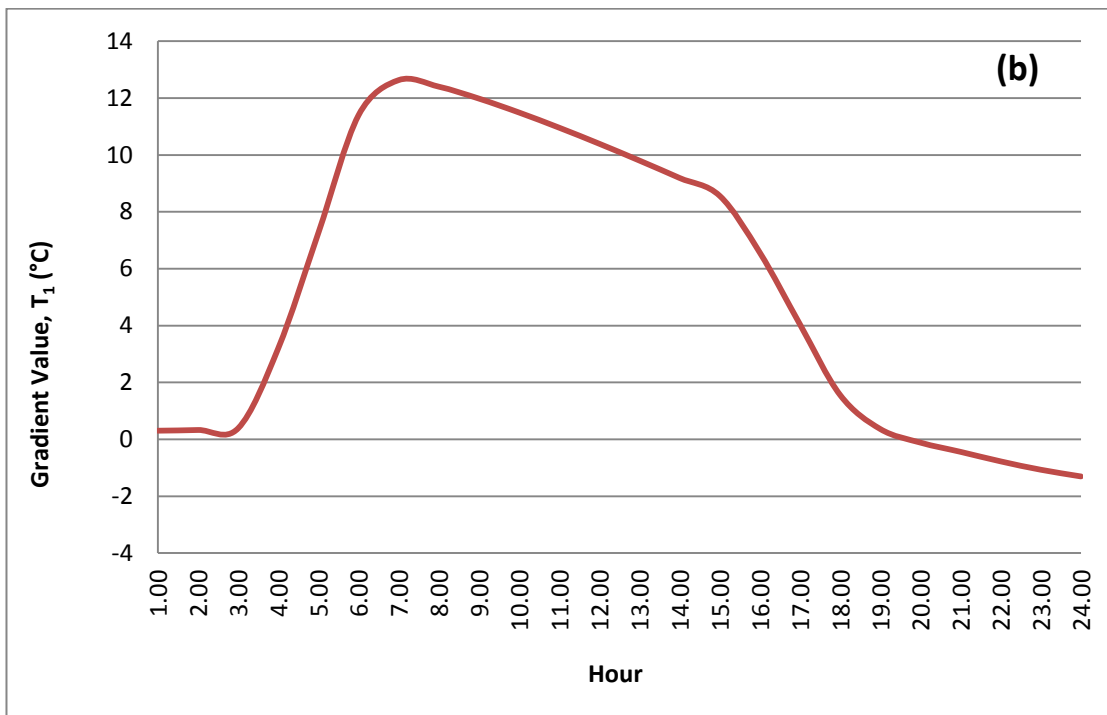
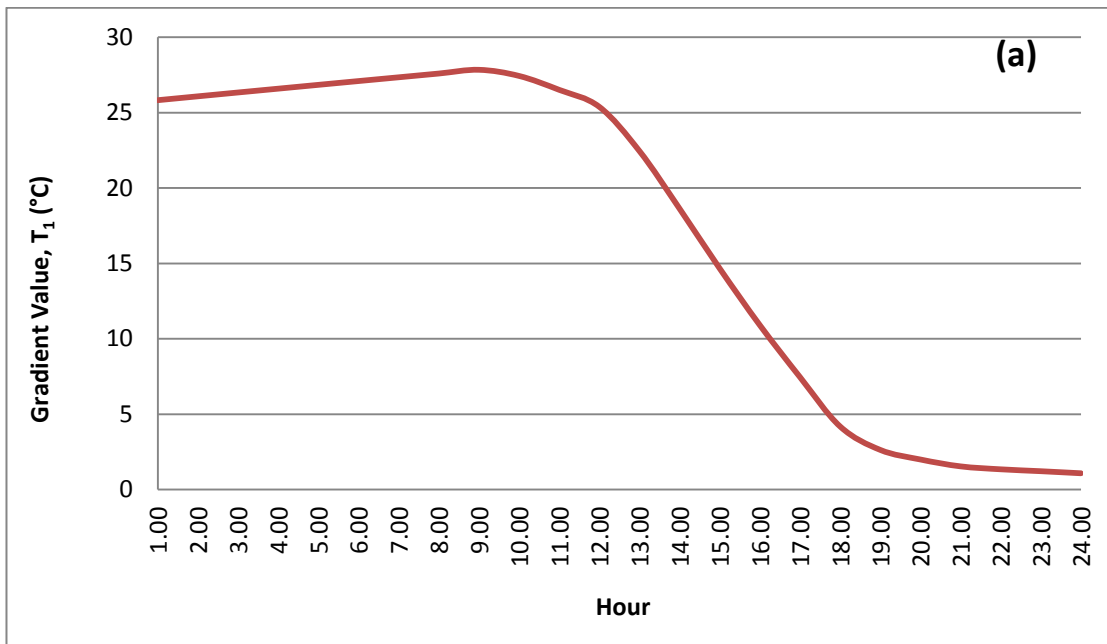


Figure 4.8  $T_1$  value for Ankara from Zone 1 for the day with highest positive gradient 05.06.2012 (a) and for the day which the most severe negative gradient occurs, 15.08.2012 (b)

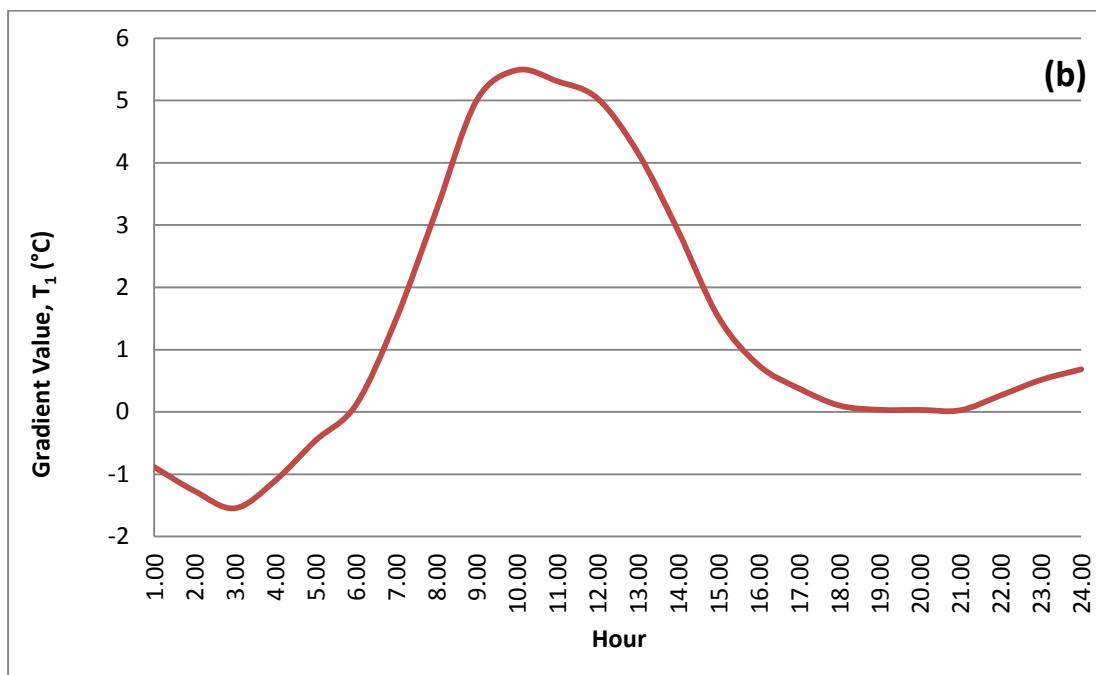
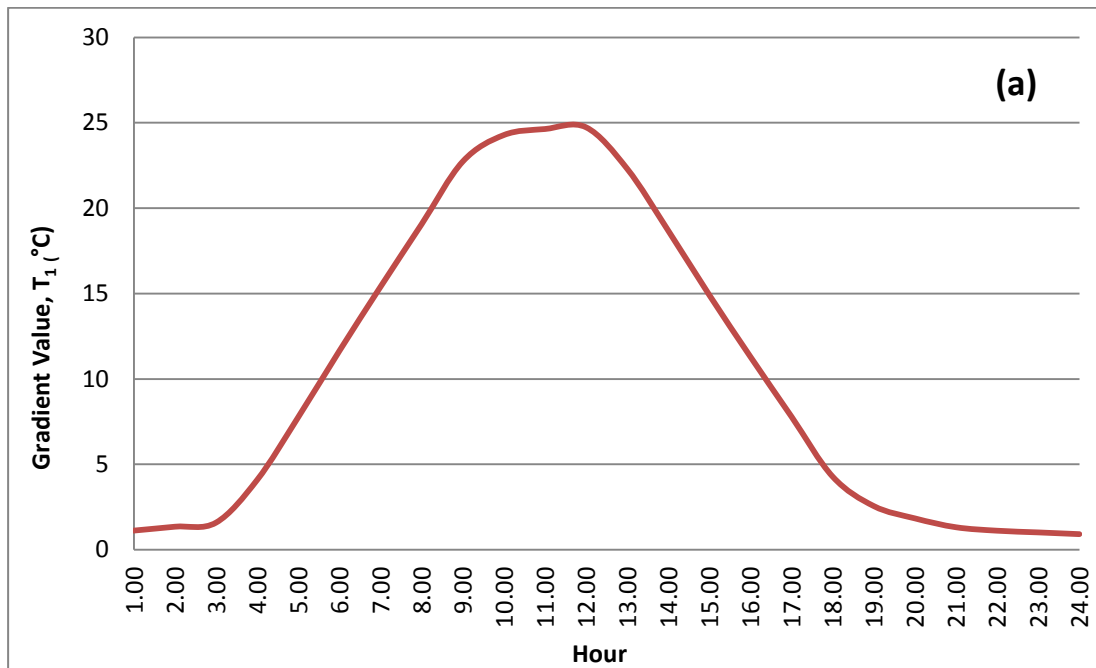


Figure 4.9  $T_1$  value for İstanbul from Zone 2 for the day with highest positive gradient 14.07.2012 (a) and for the day which the lowest negative gradient occurs, 04.12.2012 (b)

In Table 4.3, the analyses results showing the maximum temperature differential between top of concrete girder and average temperature of web for each city are given. Since the  $T_1$  gradient values actually show the temperature difference of top the deck from the average of webs,  $T_2$  as the difference between 10cm below the top surface and the average of web and,  $T_3$  is the difference of the bottom of the girder from the average of webs, to emphasize that these the values will be given with “delta” units, and will be referred with  $\Delta^\circ\text{C}$  instead of  $^\circ\text{C}$  units hereafter.

Table 4.3 Positive and Negative Temperature Gradient Values for the Analyzed Cities

Zone	City	Positive Temperature Gradient, $\Delta^\circ\text{C}$ ( $\Delta^\circ\text{F}$ )		Negative Temperature Gradient, $\Delta^\circ\text{C}$ ( $\Delta^\circ\text{F}$ )		Positive Temperature Gradient, $\Delta^\circ\text{C}$		Negative Temperature Gradient, $\Delta^\circ\text{C}$ ( $\Delta^\circ\text{F}$ )	
		T1(max)	T2(max)	T1(max)	T2(max)	T1(avg)	T2(avg)	T1(avg)	T2(avg)
Zone 1	Adana	27.0 (49.1)	4.5 (8.2)	-1.6 (-2.9)	-9.8 (-17.8)	4.2 (7.6)	3.2 (5.8)	-0.4 (-0.7)	-1.7 (-3.1)
	Ankara	27.1 (49.3)	5.5 (10)	-2.4 (-4.4)	-4.9 (-8.9)	7.2 (13.1)	5.2 (9.5)	-0.3 (-0.5)	-1.2 (-2.2)
	Antalya	26.4 (48.0)	4.3 (7.8)	-0.9 (-1.6)	-11.1 (-20.2)	6.8 (12.4)	5.1 (9.3)	-0.2 (-0.4)	-1.2 (-2.2)
	Bingöl	28.8 (52.4)	6.8 (12.4)	-0.8 (-1.5)	-3.2 (-5.8)	4.2 (7.6)	3.1 (5.6)	-0.2 (-0.4)	-1 (-1.8)
	Erzurum	24.5 (44.5)	4.6 (8.4)	-6.3 (-11.5)	-8.7 (-15.8)	3.8 (6.9)	5.2 (9.5)	-0.6 (-1.1)	-2.5 (-4.5)
	Gaziantep	29.5 (53.6)	4.5 (8.4)	-1.5 (-2.7)	-5.7 (-10.4)	4.3 (7.8)	3.1 (5.6)	-0.3 (-0.5)	-1.5 (-2.7)
	İzmir	28.0 (50.9)	5.9 (10.7)	-0.9 (-1.6)	-7.2 (-13.1)	4.2 (7.6)	3.5 (6.4)	-0.2 (-0.4)	-1.5 (-2.7)
	Kars	26.8 (48.7)	3.3 (6.0)	-5.7 (-10.4)	-8.4 (-15.3)	3.3 (6)	4.1 (7.5)	-0.6 (-1.1)	-2 (-3.6)
	Muğla	28.5 (51.8)	5.7 (10.4)	-1.1 (-2.0)	-7.9 (-14.4)	4.2 (7.6)	3.1 (5.6)	-0.3 (-0.5)	-1.3 (-2.4)
Van	26.3 (47.8)	5.1 (9.3)	-2.0 (-3.6)	-3 (-5.5)	4.3 (7.8)	3.4 (6.2)	-0.3 (-0.5)	-1 (-1.8)	
Zone 2	Bursa	24.9 (45.3)	4.4 (8.0)	-2.0 (-3.6)	-7.2 (-13.1)	3.1 (5.6)	3 (5.5)	-0.3 (-0.5)	-2.1 (-3.8)
	Çanakkale	26.1 (47.5)	9.5 (17.3)	-1.1 (-2.0)	-7.1 (-12.9)	3.3 (6)	3.1 (5.6)	-0.2 (-0.4)	-1.5 (-2.7)
	Edirne	25.3 (47.5)	7.6 (13.8)	-0.9 (-1.6)	-6.4 (-11.6)	2.8 (5.1)	2.7 (4.9)	-0.2 (-0.4)	-1.6 (-2.9)
	İstanbul	24.7 (44.9)	6.2 (11.3)	-1.5 (-2.7)	-5.4 (-9.8)	2.7 (4.9)	2.5 (4.5)	-0.2 (-0.4)	-1.3 (-2.4)
	Samsun	23.1 (42.0)	3.4 (6.2)	-1.1 (-2.0)	-6.8 (-12.4)	3.3 (6)	3.1 (5.6)	-0.3 (-0.5)	-2 (-3.6)
	Trabzon	24.1 (43.8)	6.1 (11.1)	-1.0 (-1.8)	-4.7 (-8.5)	2.9 (5.3)	2.7 (4.9)	-0.1 (-0.2)	-1.8 (-3.3)

Since the given values are the extreme values for each city; while recommending the design gradient value, the average of the maximum temperature values of each zone would be appropriate. According to given analysis results; a  $27.3^\circ\text{C}$  positive temperature difference for Zone 1 and  $24.6^\circ\text{C}$  for Zone 2 is obtained for  $T_1$  as the averages of the corresponding analyzed locations. Zone maximum extreme  $T_1$  values are  $29.5 \Delta^\circ\text{C}$  (Gaziantep) and  $25.3 \Delta^\circ\text{C}$  (Edirne) for Zone 1 and Zone 2 respectively. Average of the maximum of the gradient values 10cm below the surface,  $T_2$  are 5.0 and  $6.2 \Delta^\circ\text{C}$  for Zone 1 and 2.

Negative gradient  $T_1$  values are  $-2.3 \Delta ^\circ\text{C}$  and  $-1.3 \Delta ^\circ\text{C}$  on average and have the extreme values for the same city as positive gradient for Zone 1 as  $-6.3 \Delta ^\circ\text{C}$  (Erzurum) and  $-2.0 \Delta ^\circ\text{C}$  for Bursa for Zone 2.

Appraising the results, the usage of  $28 \Delta ^\circ\text{C}$  vertical temperature difference value as  $T_1$  for positive gradient case and  $6 \Delta ^\circ\text{C}$  vertical temperature difference value for negative difference values are selected. The corresponding Zone 2 values are  $25 \Delta ^\circ\text{C}$  and  $5 \Delta ^\circ\text{C}$  for positive and negative gradient cases, respectively. The negative gradient values are equivalent to almost 0.2 of the positive gradient values.

Since the  $T_2$  values are very close to each other for both zones, a common value,  $6 \Delta ^\circ\text{C}$  adequate for positive and  $1 \Delta ^\circ\text{C}$  for negative gradient case. These values can be shown with a table as in Table 4.4 and graphically as in Figure 4.10.

Table 4.4 Recommended Thermal Gradient Values for Positive and Negative Gradients

Zone Name	Positive Gradient		Negative Gradient	
	$T_1$ ( $^\circ\text{C}$ )	$T_2$ ( $^\circ\text{C}$ )	$T_1$ ( $^\circ\text{C}$ )	$T_2$ ( $^\circ\text{C}$ )
Zone 1	28	6	-6	-1
Zone 2	25	6	-5	-1

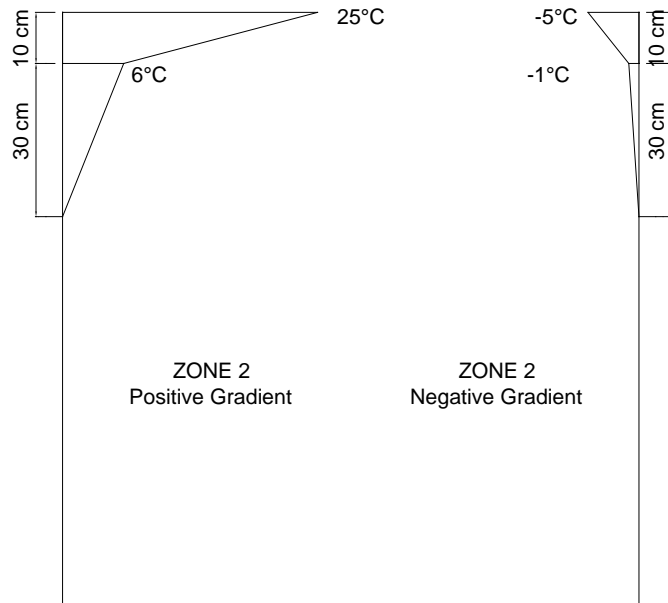
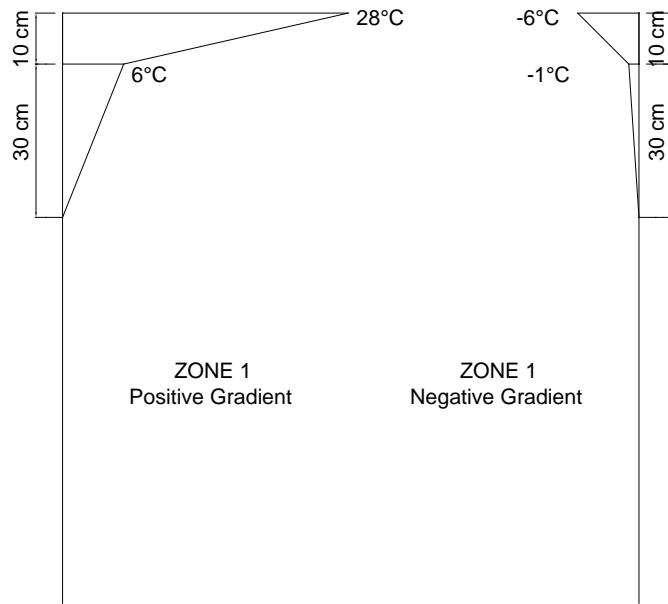


Figure 4.10 Recommended thermal gradient shapes and values for positive and negative gradient

### 4.3. Analysis to Obtain Stresses and Forces and the Results

The aforementioned bridge is modeled in a 3 D finite element analysis program which is specialized for bridge design, namely, LARSA4D and preliminary analysis of the bridge under permanent loads are made (Figure 4.11). Thermal analysis of the superstructure is made by using “Nonlinear Thermal Gradient Tool” of the program. Information about the geometry of the cross section and the material properties are given in the previous chapter. As boundary conditions, expansion bearings are defined in all piers except the fixed pier (P3) like the original example.

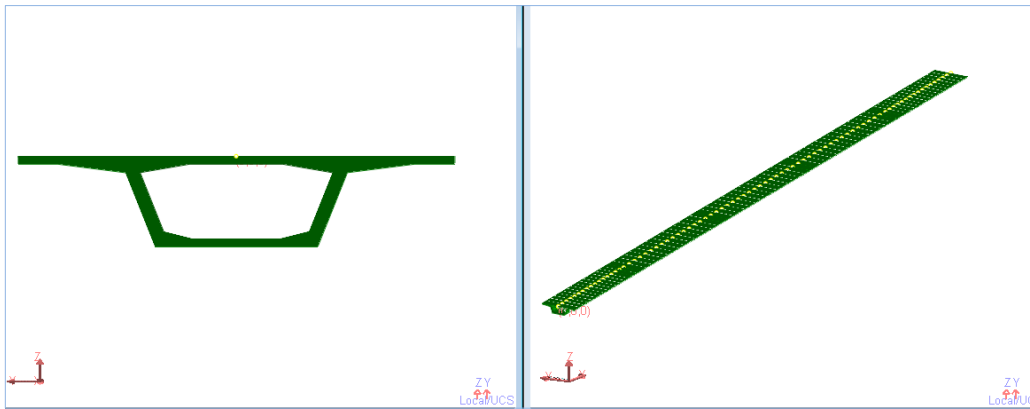


Figure 4.11 3D model of the analyzed bridge, constructed in LARSA 4D

Since the analyzed bridge model is a balanced cantilever segmental type of bridge, the division of the bridge frame model is made accordingly. The segment layout of the bridge and the labels of the segments are given in Figure 4.12

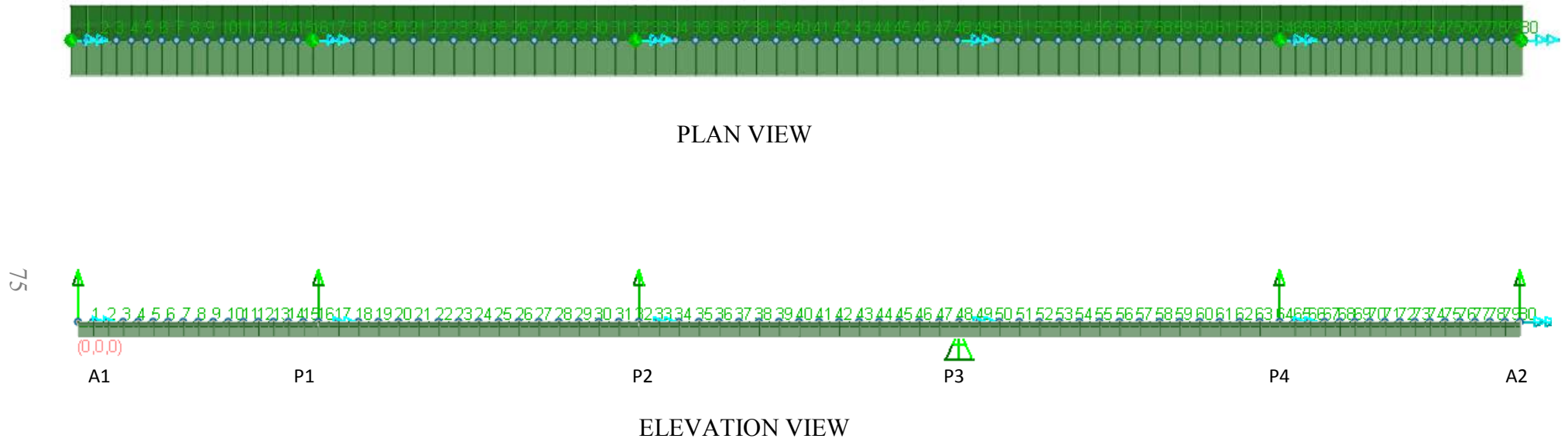


Figure 4.12 Segment labels of the analyzed bridge model, (a) plan view, (b) elevation view

### 4.3.1 Validation of Analysis Model

LRFD Design Example is prepared under AASHTO Zone 3 thermal gradient loading conditions. The concrete grade used in the analysis is C40 concrete and coefficient of thermal expansion is  $1.08 \cdot 10^{-5} \text{ 1/}^\circ\text{C}$ . Geometrical properties of the bridge parts are the same for the LRFD Example and the analyzed bridge in this study. As seen from Figure 4.13, the results are very close to each other. After the confirmation of 3<sup>rd</sup> zone thermal stress and secondary moment (restraining moment) analysis results with the LRFD example and justifying the analysis model; the gradients of proposed solar radiation zones of Turkey are applied to the model to calculate the vertical temperature conduction difference caused moments and stresses for both the positive and negative thermal gradient case.

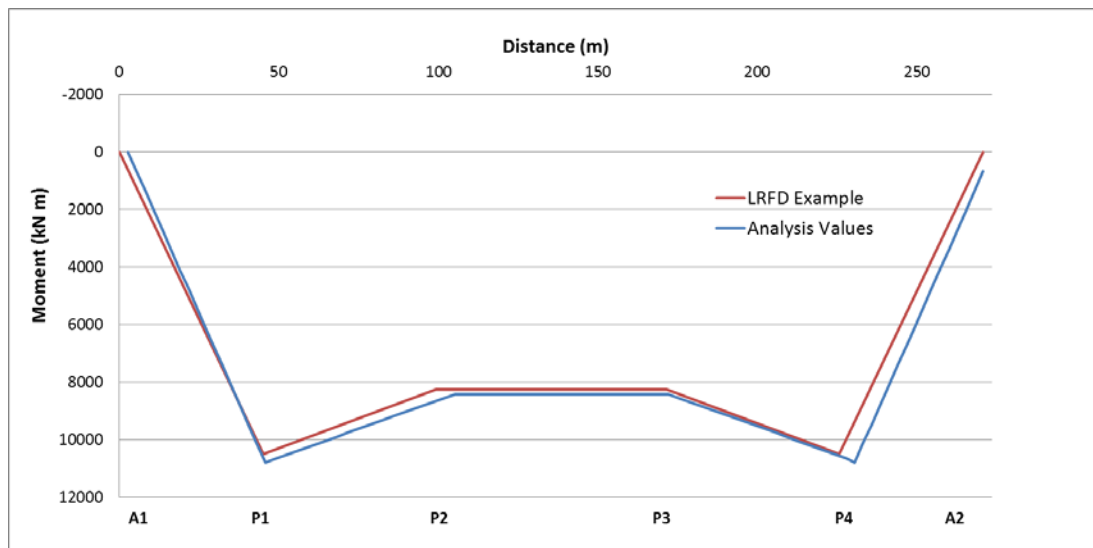


Figure 4.13 Comparison of LRFD Design Example restraining moment values with the analysis values for AASHTO Zone 3 positive gradient condition

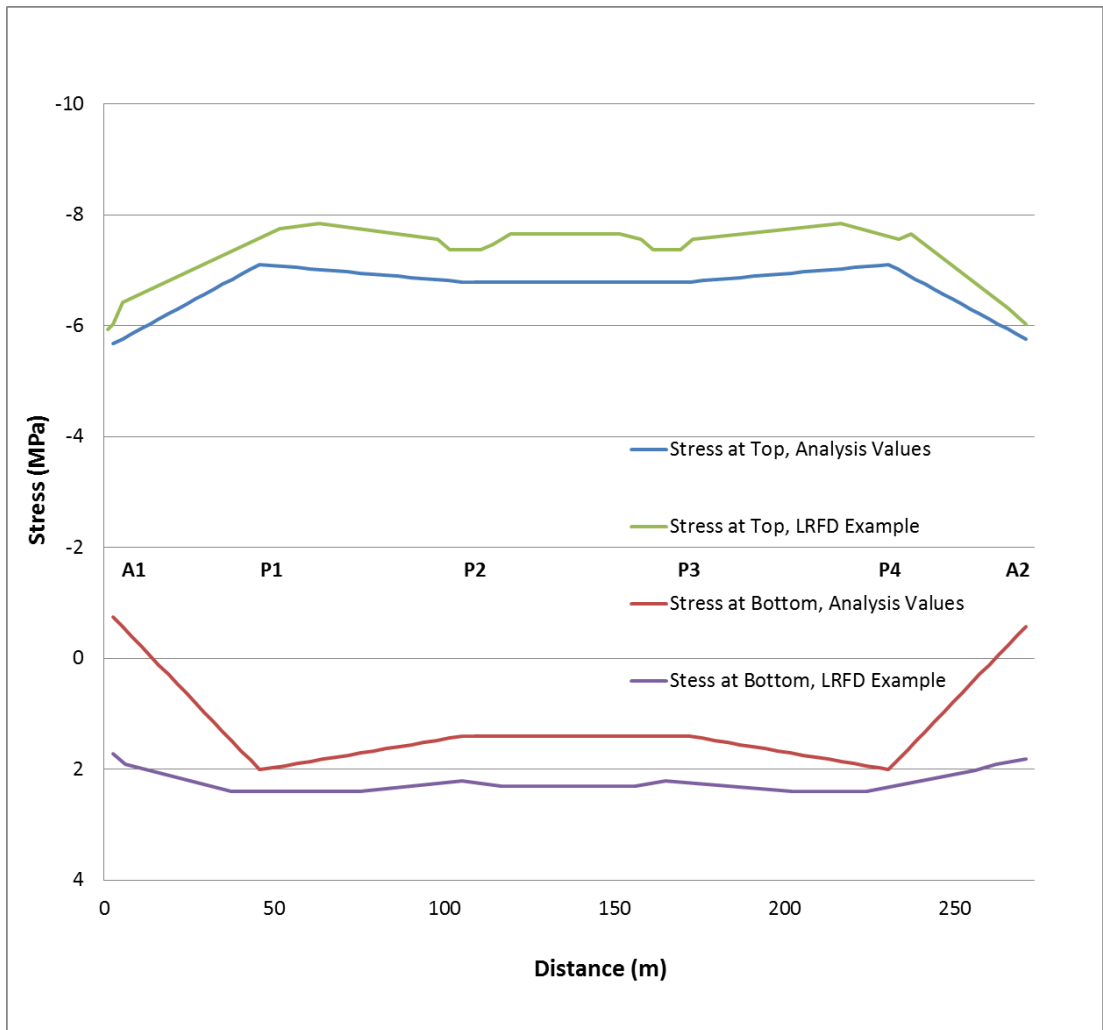


Figure 4.14 Comparison of LRFD Design Example top stress and bottom stress values with the analysis values for AASHTO Zone 3

#### 4.3.2 Moment and Stress Resultants of the Analyzed Bridge Model in this Study

In the following graphs, the temperature gradient caused restraining moment graphs are given for Zone 1 Positive, Zone 1 negative, Zone 2 Positive and Zone 2 Negative case (Figure 4.15, Figure 4.16, Figure 4.17, and Figure 4.18)

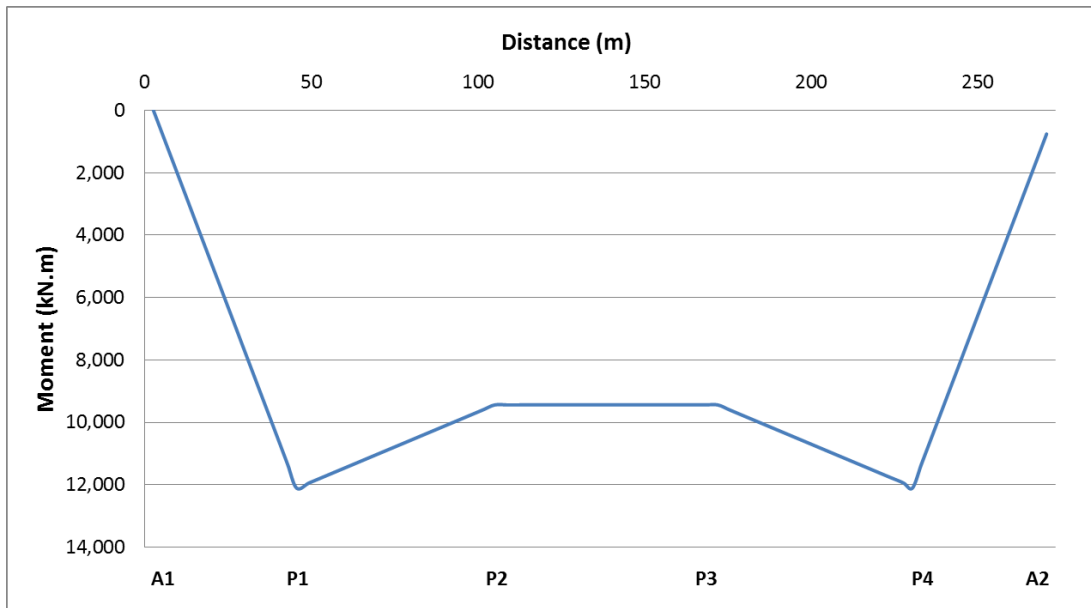


Figure 4.15 Non-linear positive temperature gradient restraining moments for Zone 1

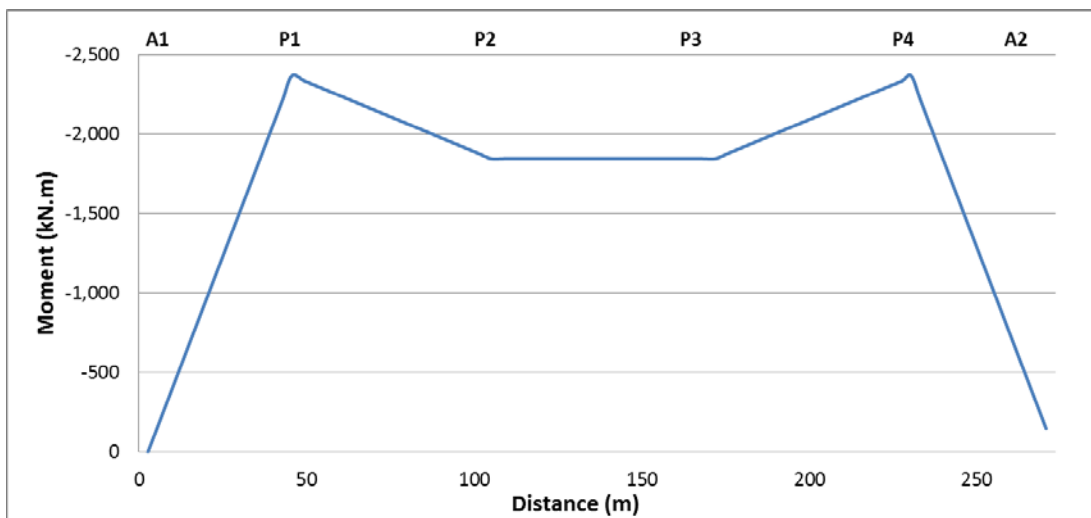


Figure 4.16 Non-linear negative temperature gradient restraining moments for Zone 1

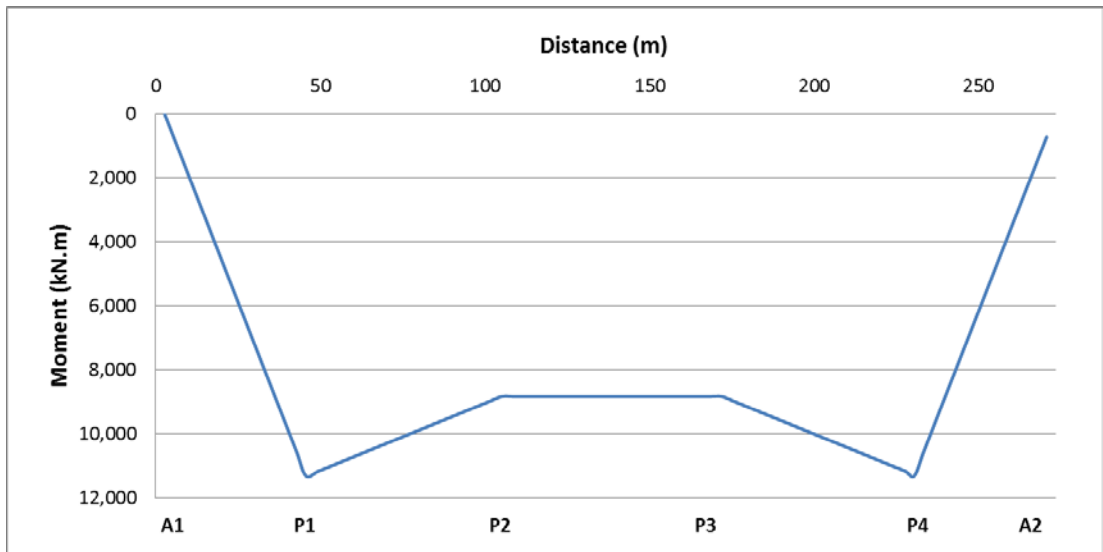


Figure 4.17 Non-linear positive temperature gradient restraining moments for Zone 2

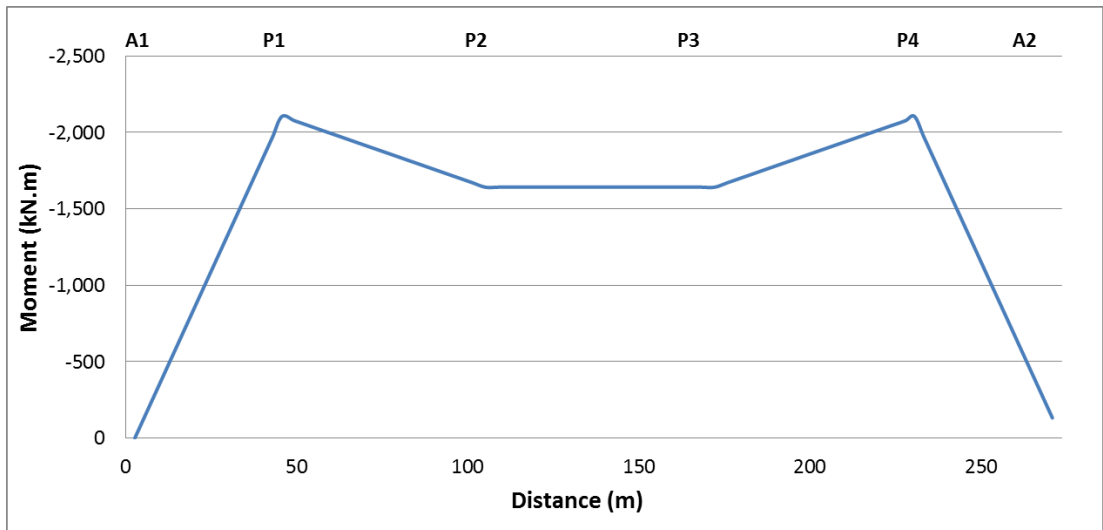


Figure 4.18 Non-linear negative temperature gradient restraining moments for Zone 2

The most critical thermal stress values are developed at the 17<sup>th</sup> and 65<sup>th</sup> segments with similar results (the detailed segment layout was given in Figure 4.12 before). The detailed cross section stresses for recommended Zone 1 positive, Zone 1 negative, Zone 2 positive and Zone 2 are given in the Figures 4.19, 4.20, 4.21, and 4.22 respectively (compression is shown in negative and tension is shown in positive in all graphs).

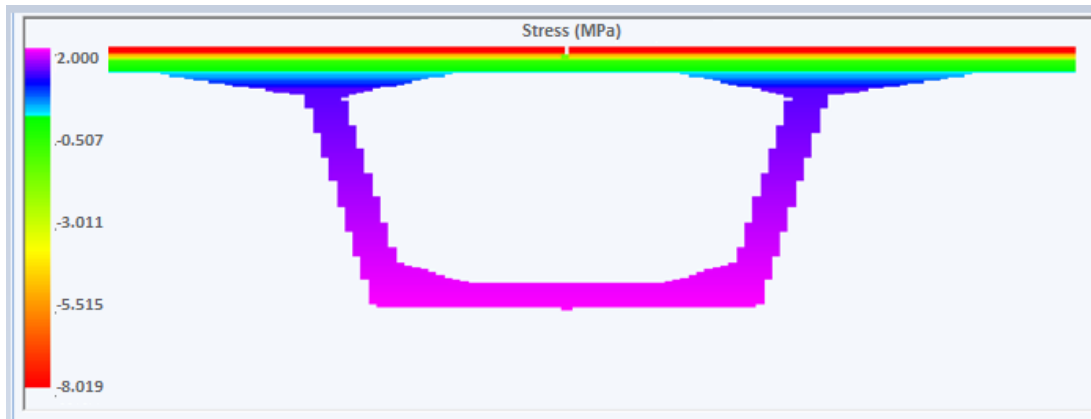


Figure 4.19 Maximum stresses at support under positive gradient for Zone 1

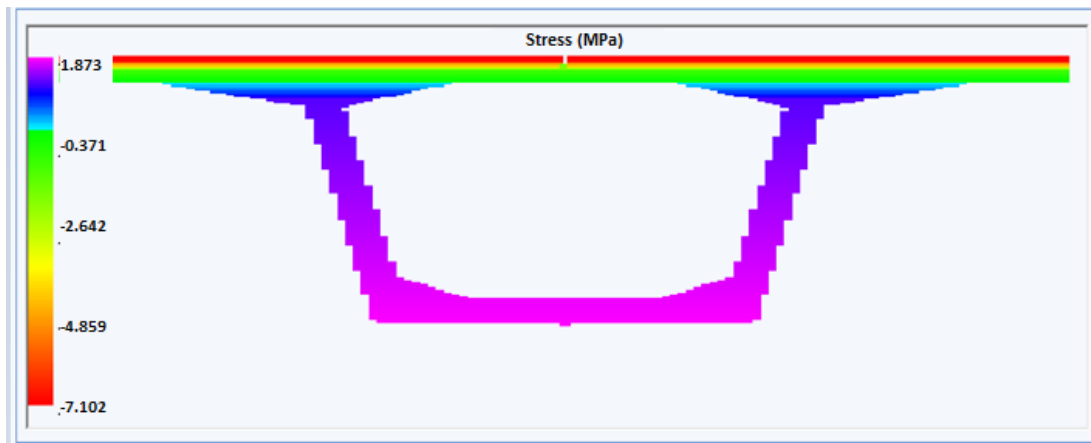


Figure 4.20 Maximum stresses at support under negative gradient for Zone 1

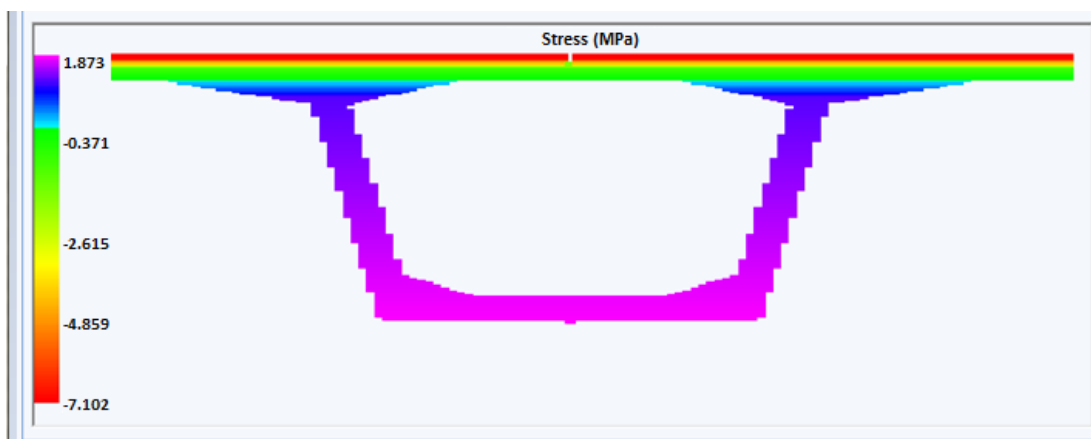


Figure 4.21 Maximum stresses at support under positive gradient for Zone 2

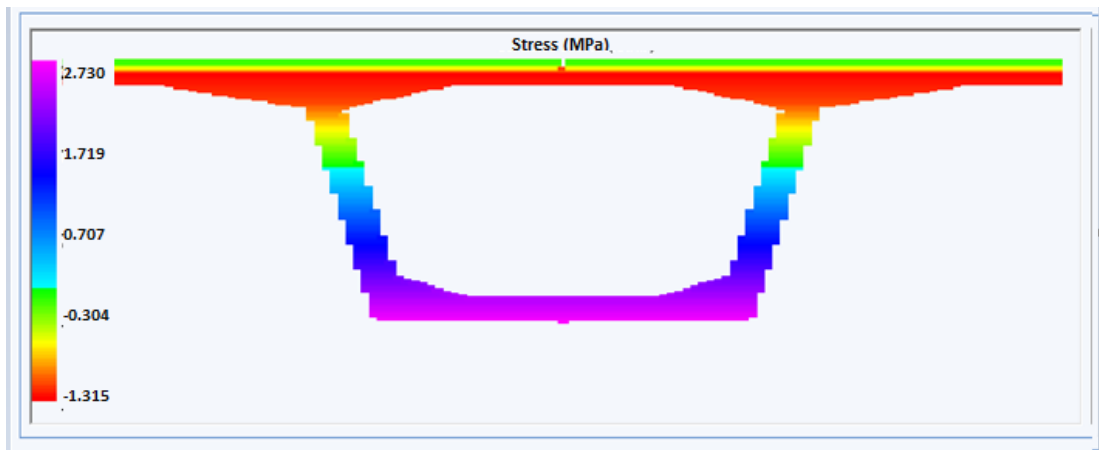


Figure 4.22 Maximum stresses at support under negative gradient for Zone 2

The analysis result for proposed solar radiation zones of Turkey for the interested section with the pre-given material properties are given in the following graphs for the center of top and bottom of the section with compression is shown in negative (Figure 4.23, Figure 4.24, Figure 4.25, and Figure 4.26)

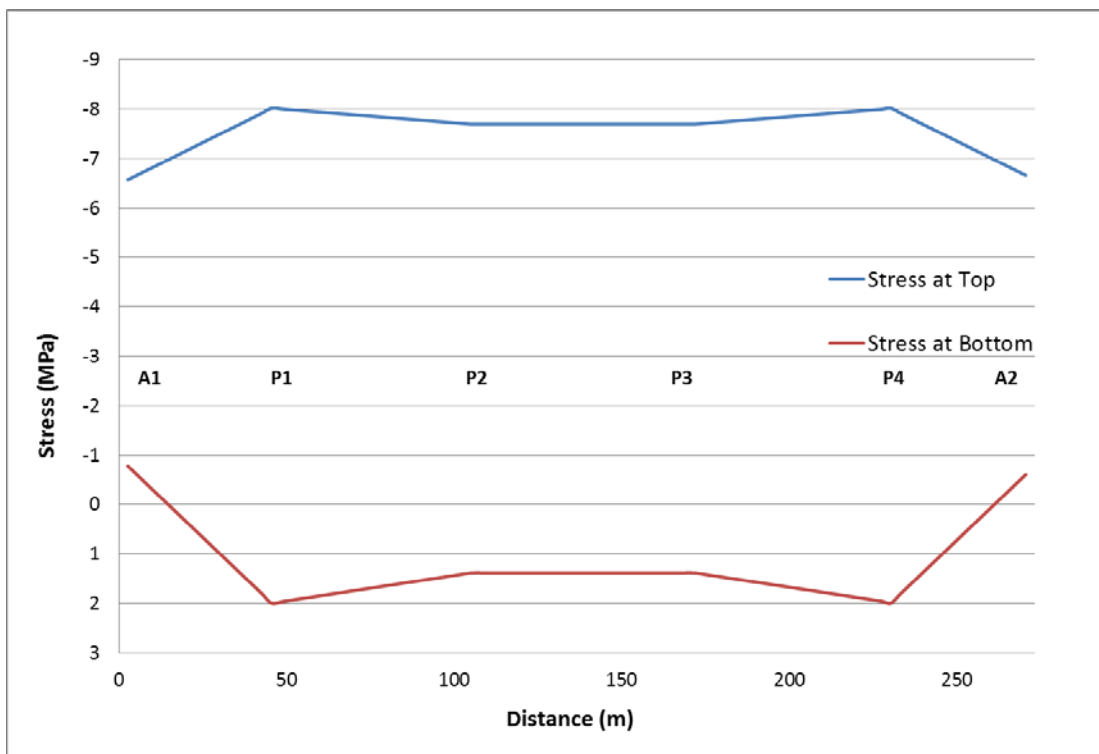


Figure 4.23 Positive thermal gradient total stresses for proposed Zone 1

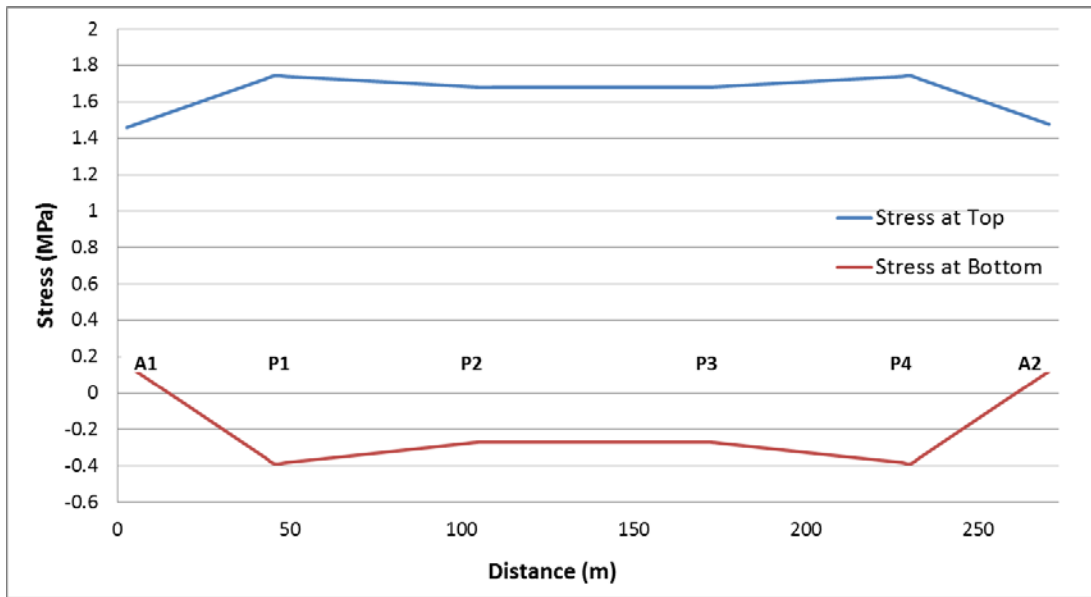


Figure 4.24 Negative thermal gradient total stresses for proposed Zone 1

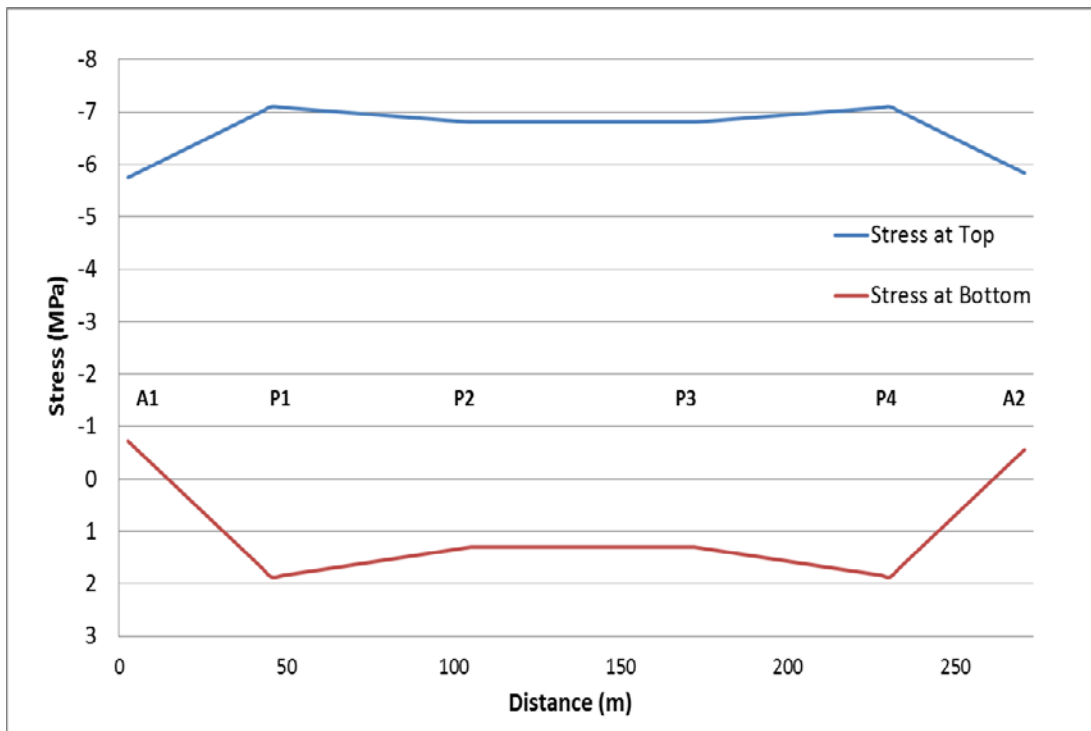


Figure 4.25 Positive thermal gradient total stresses for proposed Zone 2

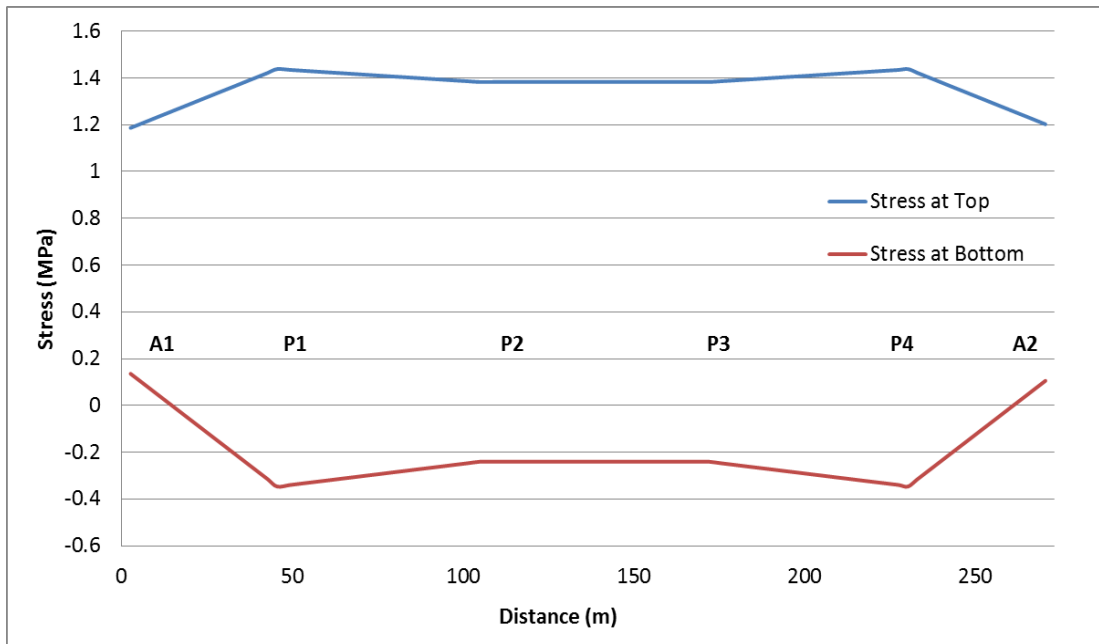


Figure 4.26 Negative thermal gradient total stresses for proposed Zone 2

In addition to C35, the same section is also analyzed for positive thermal gradient for different concrete grades, C40 and C45 which are commonly used in post-tensioned segmental bridges in order to see the effect of material grade to thermal gradient originated stresses. The positive gradient analysis results for different kinds of materials is shown in the following figures (Figure 4.27 and Figure 4.28)

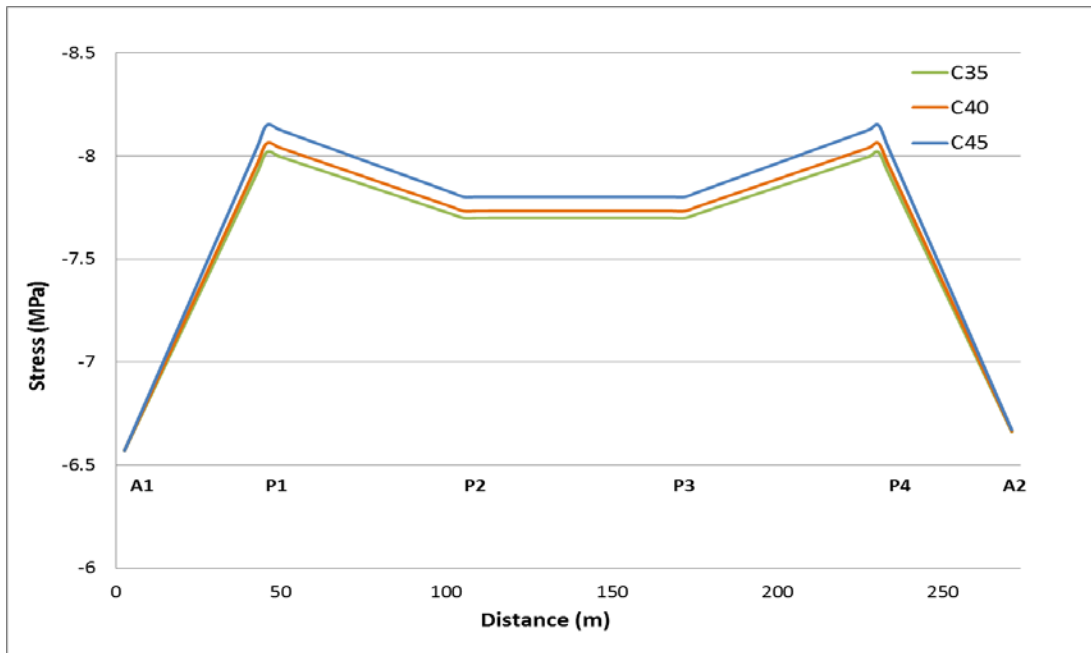


Figure 4.27 Top stress values for different concrete grades caused by positive gradient of Zone 1

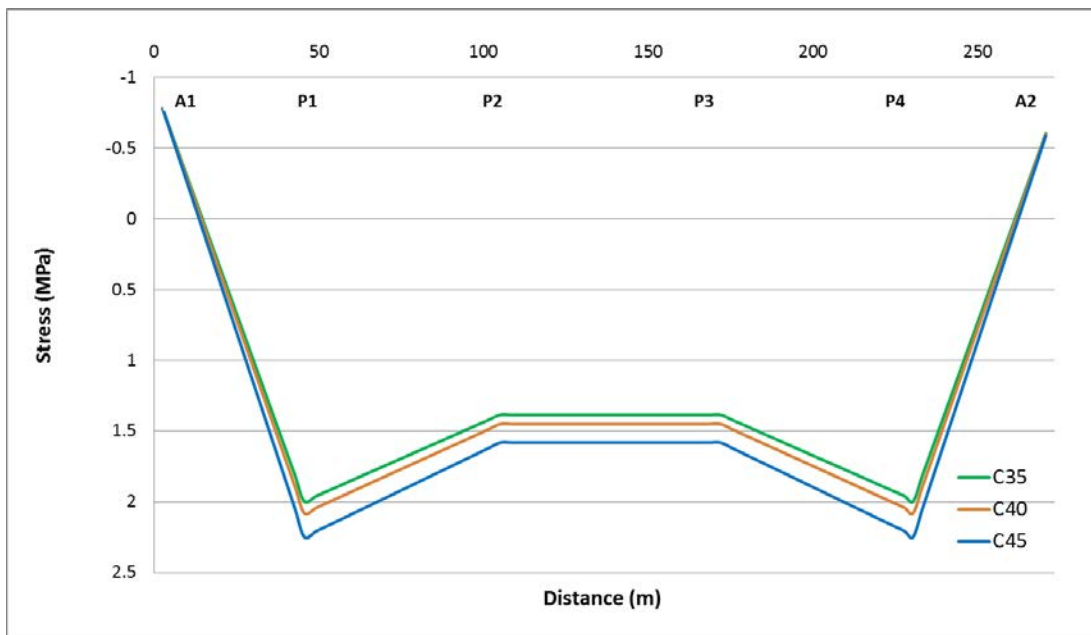


Figure 4.28 Bottom stress values for different concrete grades caused by positive gradient of Zone 1

As can be seen from the above figures, the change in the concrete material grade does not affect the highest stress values much. The stress values get higher as the grade increases since the elasticity modulus is increasing.

As mentioned in the section 3.3.2 , according to AASHTO (2012), the allowable stress limits for concrete is investigated for two time intervals of construction schedule, temporary stresses before the losses due to creep and shrinkage before the appliance of prestress and stresses at service limit state after prestress losses. The maximum compression and tension limits for the analyzed segmental bridge structure with the material used in the analysis, C35 concrete is tabulated in Table 4.5.

Table 4.5 Allowable compression and tension stresses for C35 concrete for thermal gradient analysis of a segmental bridge top section according to AASHTO (2012)

Time Interval	Compressive Stress (MPa)	Tension Stress (MPa)
Before prestress	15.8	3.7
After prestress	15.8	1.5

As seen from Figure 4.19 and Figure 4.21, the highest compressive stresses for the analyzed section are 8.0 and 7.0 MPa for Zone 1 and Zone 2 respectively. The highest negative stress values are 2.0 and 1.9 MPa as can be seen from Figure 4.20 and Figure 4.22. The compressive stress values are all below the allowable compression limits, whereas, the tensile stress limits for C35 are exceeded for Zone 1 negative gradient case and very close to the limit for Zone 2 negative gradient case. The results show that, in addition to the one done for dead and live loads, additional prestressing is necessary to overcome these temperature gradient originated stresses.

#### **4.4. Comparison of the Thermal Gradient Originated Resultant Forces and Stresses with the Resultants of the Other Load Types**

In order to see the role of thermal gradient in the overall design of box girder concrete bridges, and the proportion of it in the total stress and moment development; a comparison of the other load effects is made by applying the other most effective load components on the same analysis model.

The self-weight of the structure is calculated and the other types of dead loads like wearing surfaces, traffic barriers and blisters also included in the design. The live load arrangement is made according to AASHTO LRFD (2012), Section 3.6.1.3.1. In that section, AASHTO recommends the usage of 90 percent of the effect of two design trucks spaced a minimum of 15.24 m between the leading truck axle of one truck and the rear axle of the other truck, combined with 90 percent of the effect of the design lane load for negative moment between points of contra flexure under a uniform load on all spans, and reaction at interior piers only. The distance between the axles of each truck shall be taken as 4.26m. The two design trucks shall be placed in adjacent spans to produce maximum force effects. Axles that do not contribute to the extreme force effect under consideration shall be neglected.

H<sub>30</sub>S<sub>24</sub> truck load and lane load which are the live loads that are commonly used in bridge design in Turkish practice and HL93 truck load of AASHTO specifications are selected for the analysis. Moreover, AYK45 truck load which satisfies target reliability index 3 of KAMAG 1007 P project, (Koç, 2013) is also applied to the model. The resultant positive and negative moment values (Figure 4.29) and stress values are given for each truck mid span and supports for both maximum compression stress and tension stress conditions are given in Figures 4.29, 4.30 and 4.31 respectively.

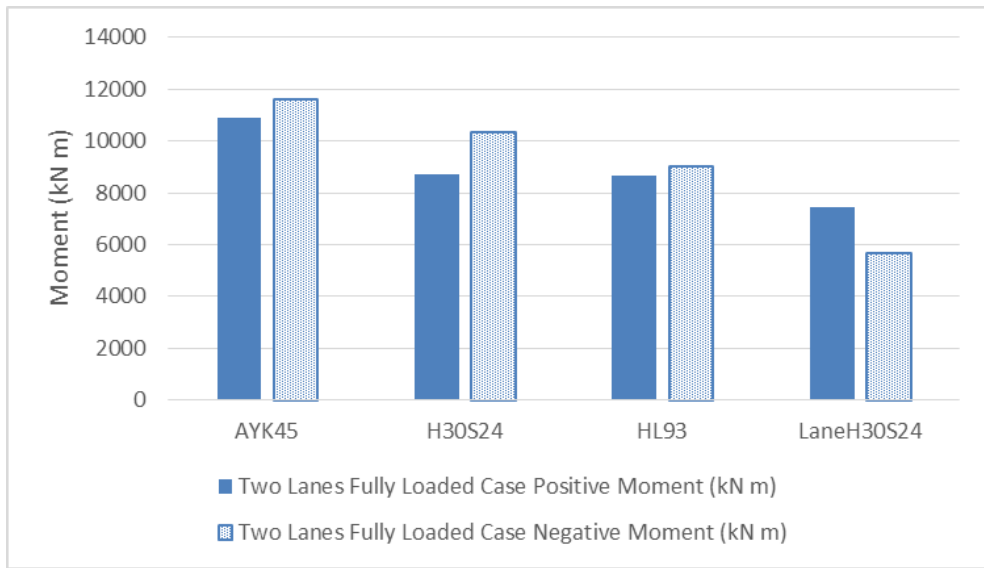


Figure 4.29 Positive and negative moment values for various truck loads

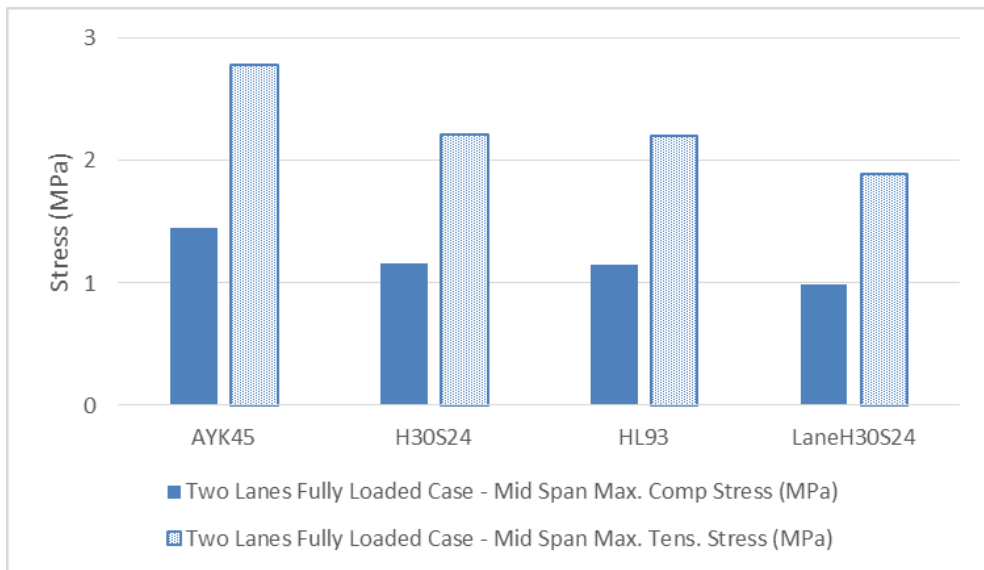


Figure 4.30 Maximum and minimum truck stresses for mid-span

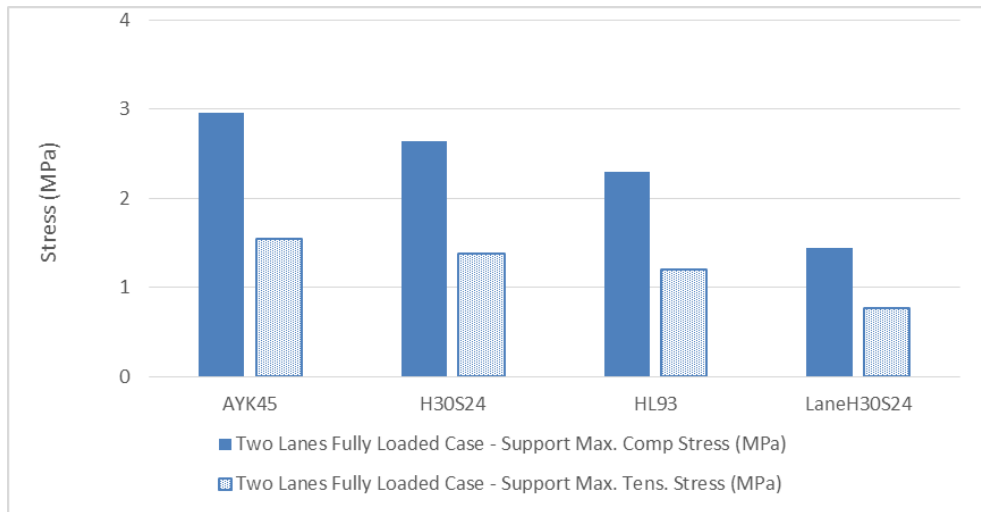


Figure 4.31 Maximum and minimum truck stresses for support

After the calculation of dead loads, superimposed dead loads and impact included live load stresses, the comparison is made with thermal gradient stresses for both Zone 1 and Zone 2 calculated for mid-span and support critical arrangements. Moreover, the total stresses on the bridge are also given for relevant load combinations. The tabulation of the Zone 1 maximum compression and tension stresses for mid-span, Zone 1 maximum compression and tension stresses for support, Zone 2 maximum compression and tension stresses for mid-span, Zone 2 maximum compression and tension stresses for support are given in respectively in Figures 4.32, 4.33, 4.34 and 4.35.

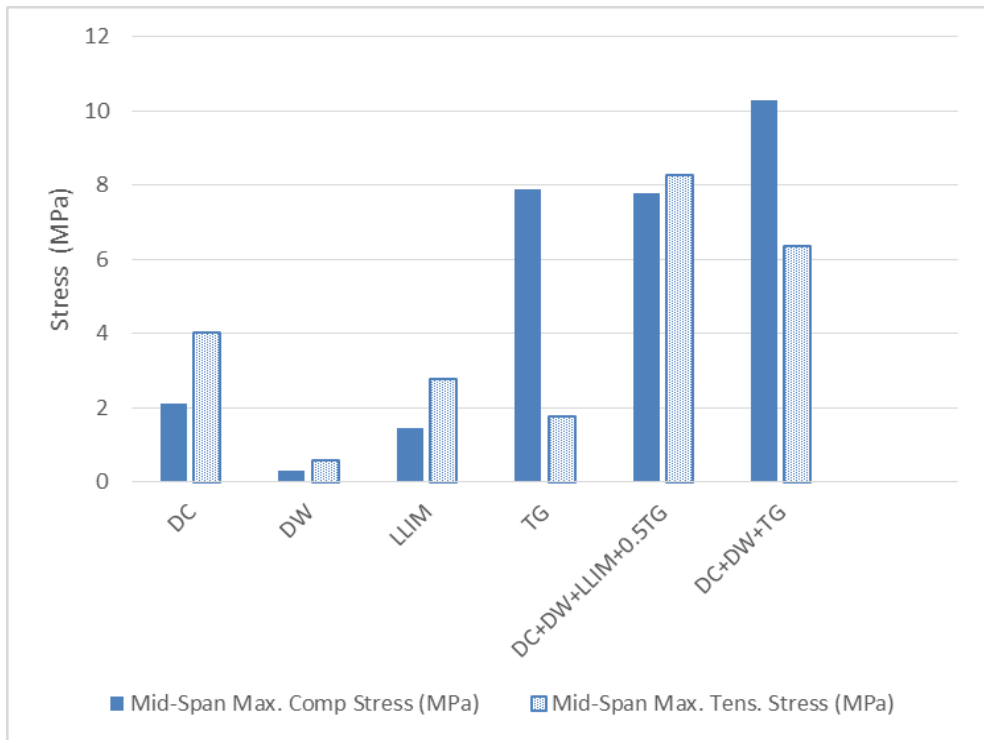


Figure 4.32 Zone 1 maximum compression and tension stresses for mid-span

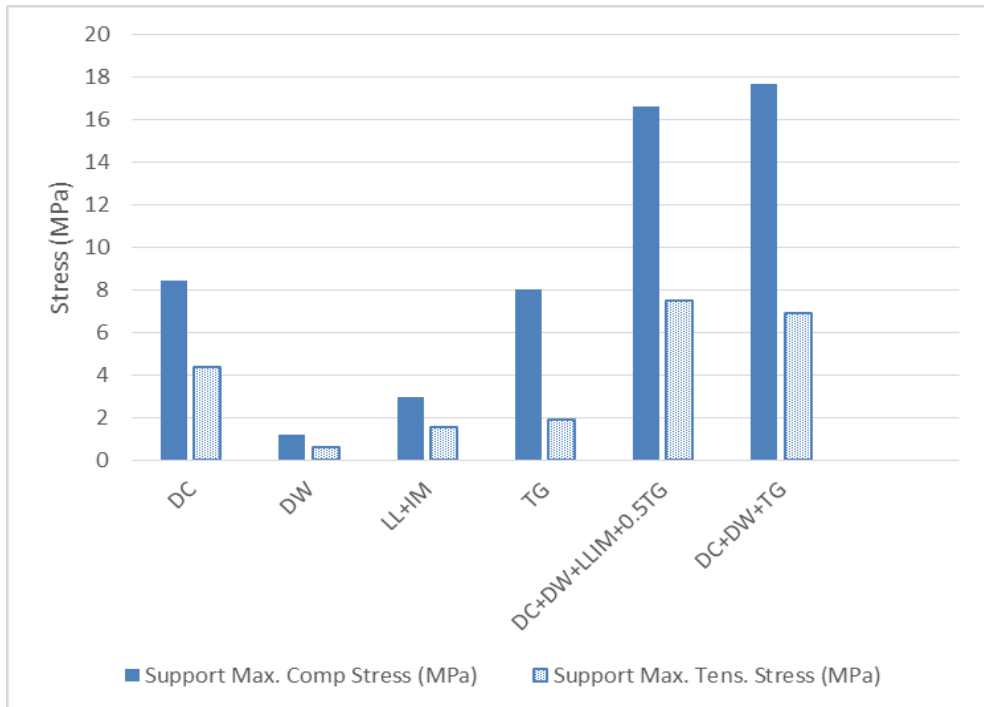


Figure 4.33 Zone 1 maximum compression and tension stresses for support

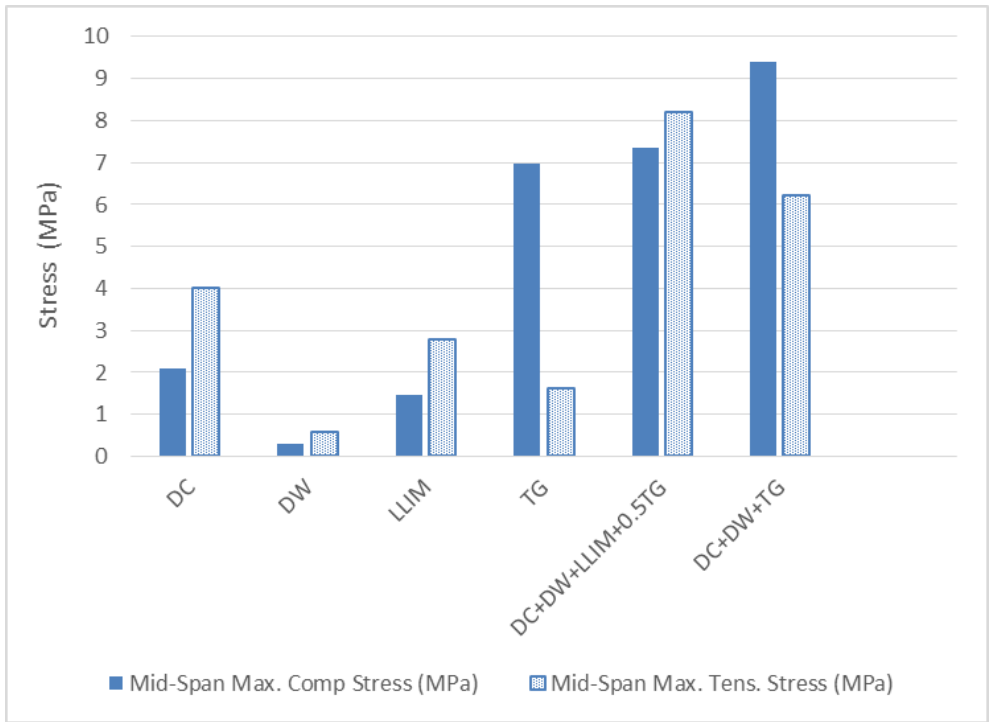


Figure 4.34 Zone 2 maximum compression and tension stresses for mid-span

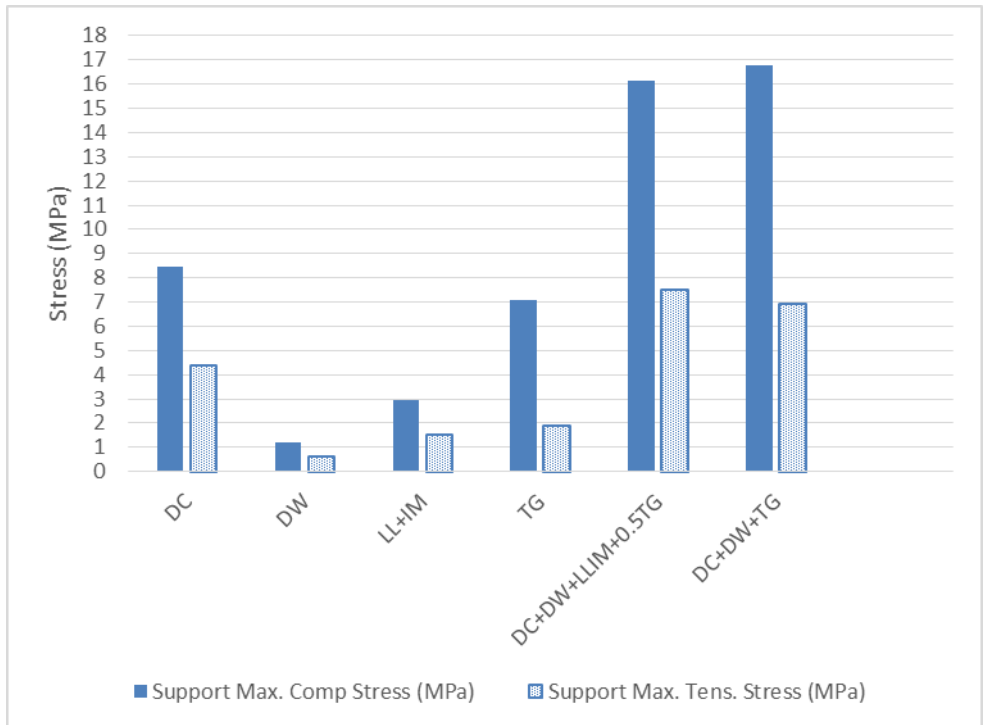


Figure 4.35 Zone 2 maximum compression and tension stresses for support

As it can be seen from the charts, thermal gradient stresses are very considerable comparing the resultant stresses of other main load parameters like dead load, superimposed dead loads and impact included live load. In order to see the proportion of thermal gradient stresses on the load combinations, Figures 4.36, 4.37, 4.38, and 4.39 are given.

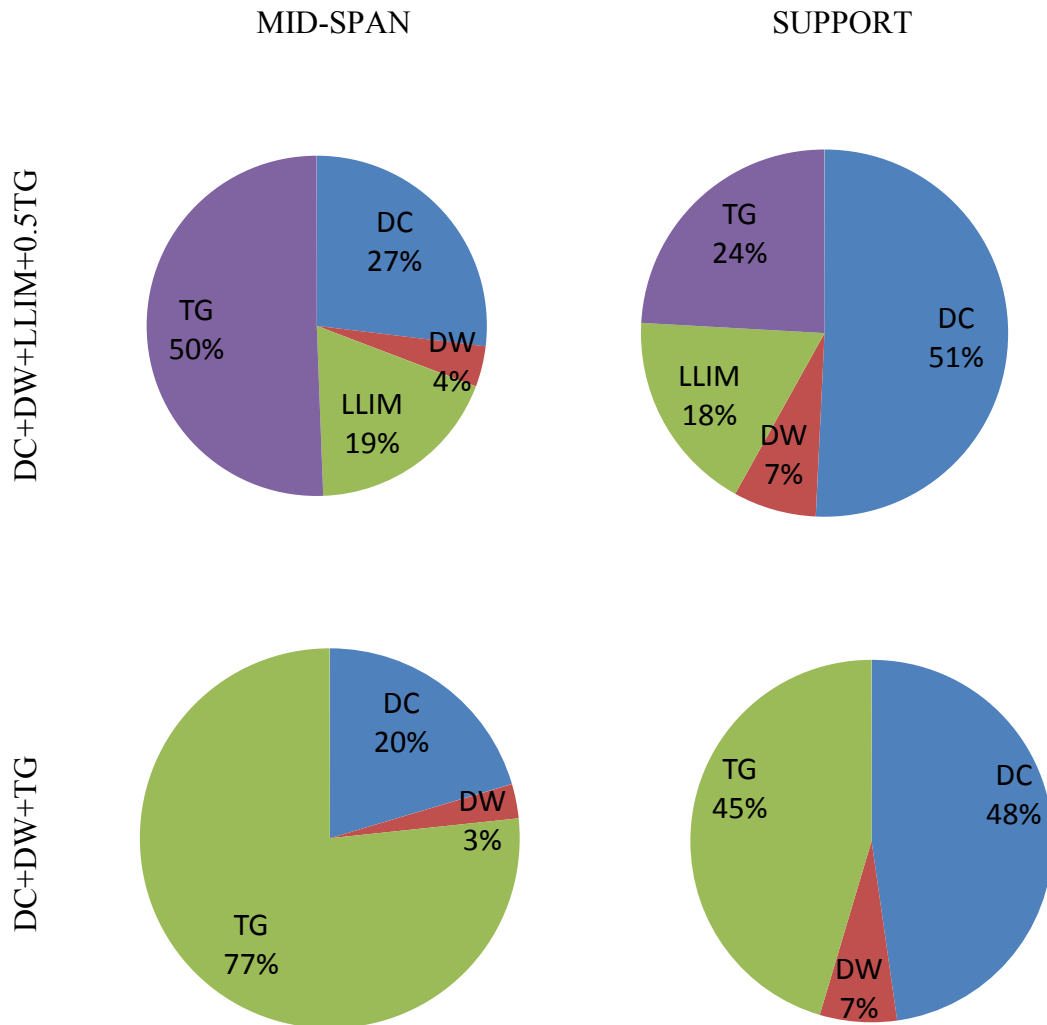


Figure 4.36 Compression stress proportions on the thermal gradient case included load combinations for Zone 1

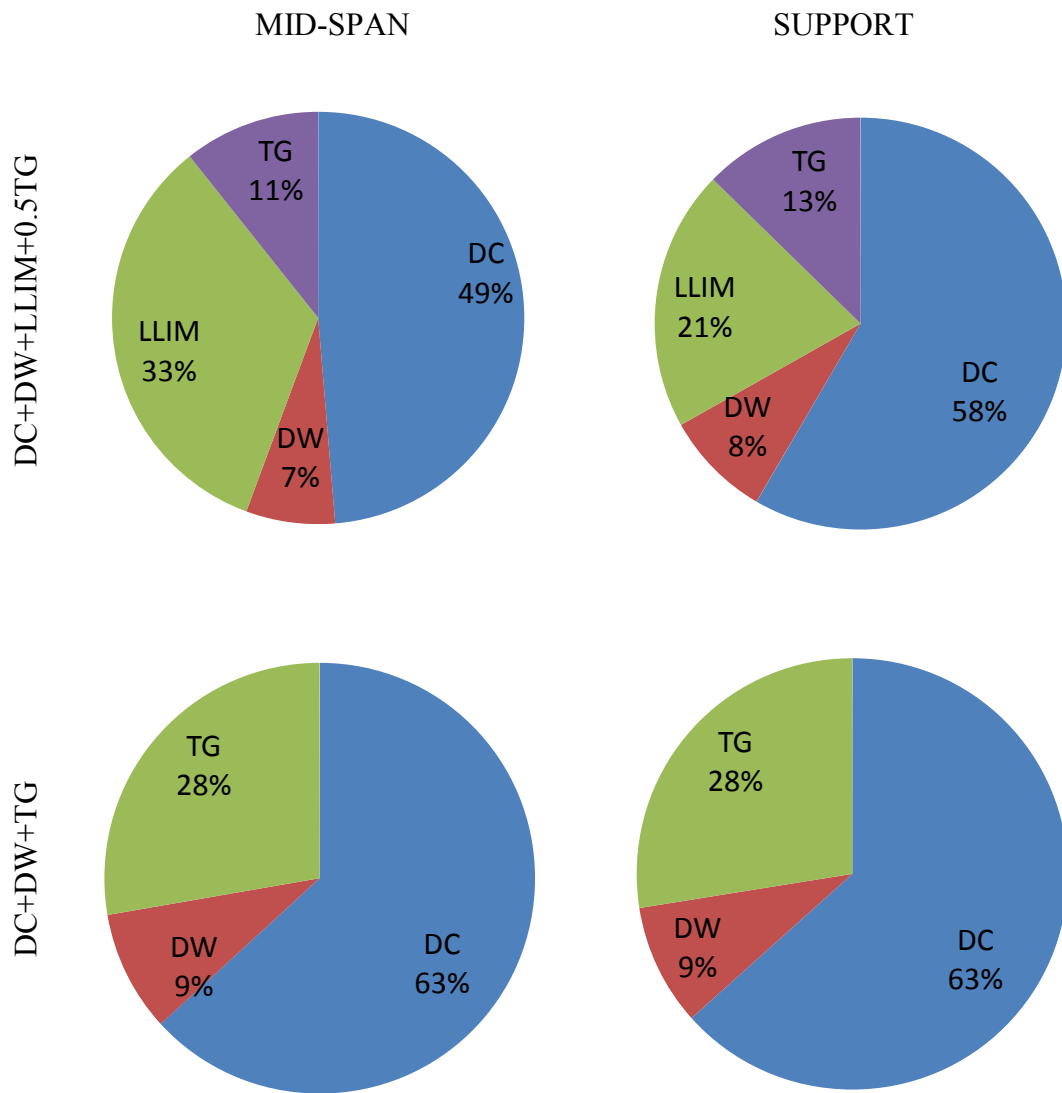


Figure 4.37 Tension stress proportions on the thermal gradient case included load combinations for Zone 1

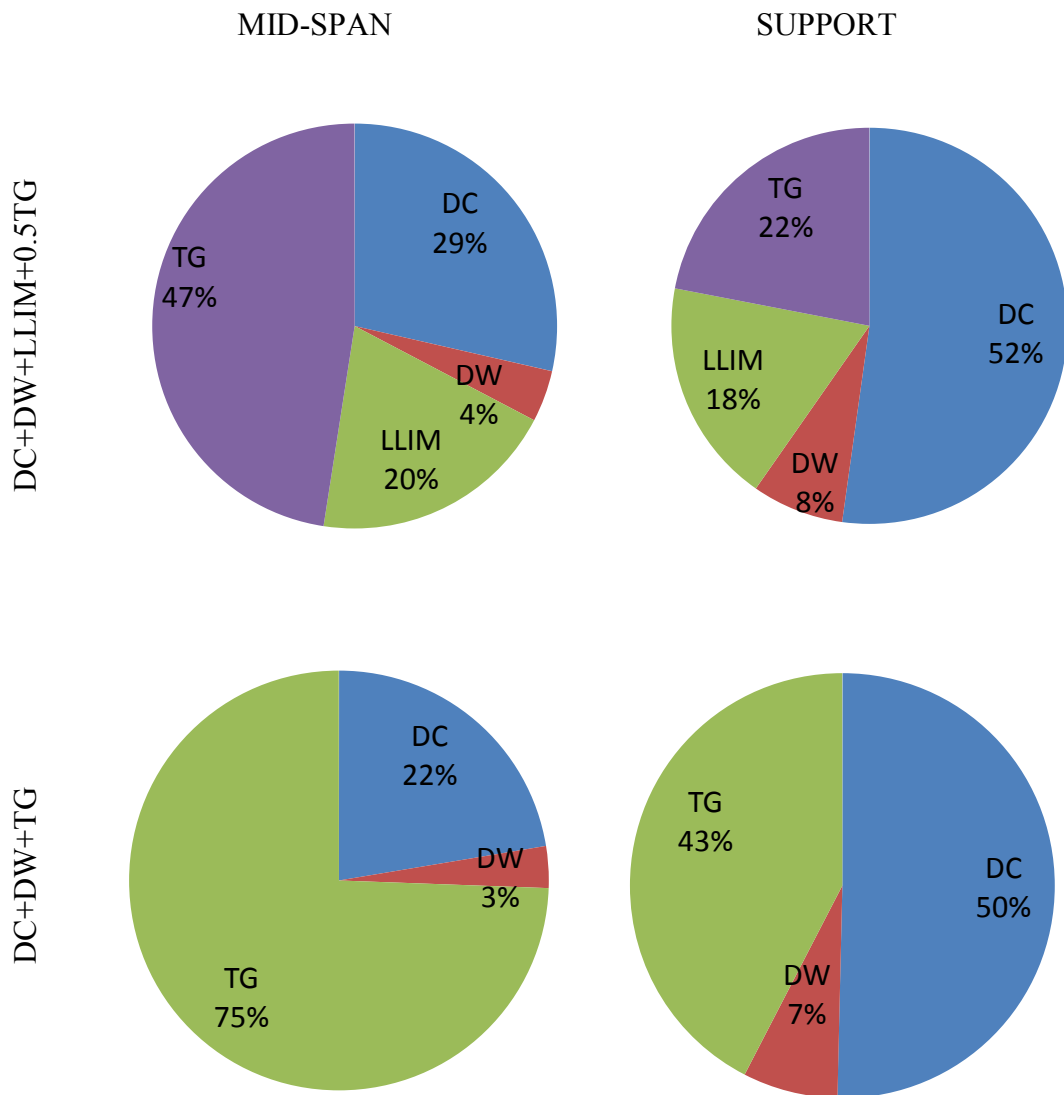


Figure 4.38 Compression stress proportions on the thermal gradient case included load combinations for Zone 2

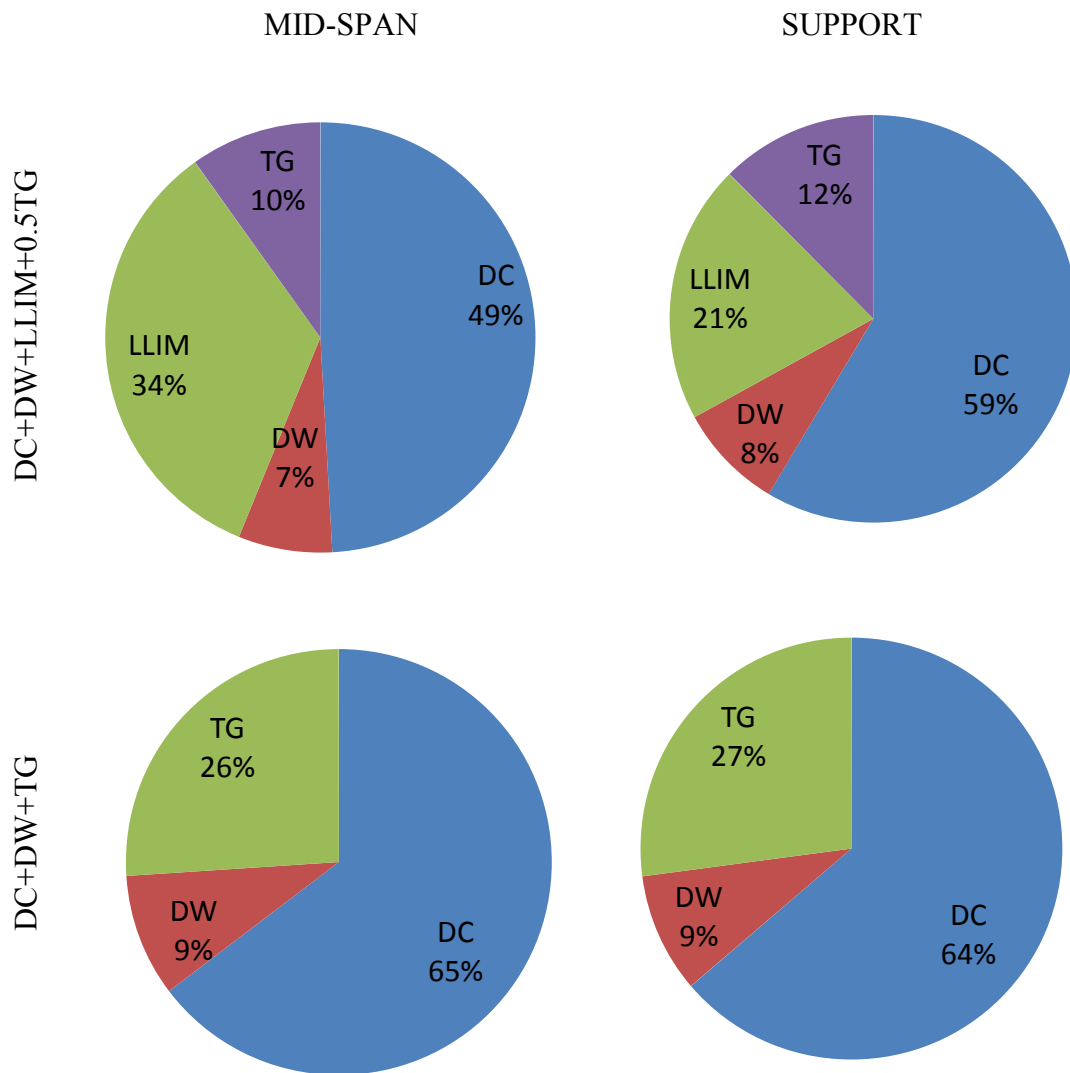


Figure 4.39 Tension stress proportions on the thermal gradient case included load combinations for Zone 2

The most remarkable findings of these charts is that, thermal gradient stresses has 50% effect on DC+DW+LL<sub>IM</sub>+0.5TG combination and 77% effect on DC+DW+TG combination, for Zone 1 maximum compression stresses for mid-span. The corresponding results for Zone 2 are 47% and 75% for live load including and not including load combinations, respectively.

Taking into consideration both span and support tensile stress results, for live load including load combination; for both Zone 1 and Zone 2; thermal gradient has 10~13% role, whereas, for non-live load including load combination, that ratio is 26~28%.

As seen from the above charts, thermal gradient has an important role on especially span stresses for compression stress condition. Gradient results are more critical for mid-spans than the supports for compressive stresses. For live load including load combination, thermal gradient results nearly doubles the live load effects.

Also for the combination that does not involve live load; thermal gradient load is far by the most influencing load parameter for compressive case. For tensile stress case, mid-span and support results are very close to each other



## CHAPTER 5

### CONCLUSIONS AND FUTURE WORK

In this study, a solar radiation map for Turkey is constructed and design gradient shape is recommended for especially box girder bridge design. The corresponding map and the values for temperature gradients are obtained by analyzing the primary influencing data for selected 16 cities of the country from the two proposed solar radiation zones, Zone 1 and Zone 2 for Turkey.

Main findings and conclusions of this study are as follows:

- Two different zones have been identified for Turkey to be used in thermal gradient loading of concrete box bridges after detailed investigation of local solar changes at different parts of the country.
- Correctness of analytical bridge model has been achieved through example bridge results based on AASHTO 3<sup>rd</sup> Zone.
- At each proposed zone, investigation of thermal gradient induced stresses for concrete box girder bridges resulted in comparable stresses at different parts of the same zone based on local solar variations.
- The analyze result value to determine positive gradient  $T_1$  value for Zone 2 is the same as the AASHTO recommendation, and the proposed value for Zone 1 is slightly below the AASHTO value. Therefore; independent solar radiation zones for Turkey is suggested and, usage of  $28 \Delta^\circ\text{C}$  for Zone 1 and  $25 \Delta^\circ\text{C}$  for Zone 2 for design of bridges for thermal gradient is recommended.
- It is seen that the temperature difference 10 cm below the top surface, namely  $T_2$  values can be taken as  $6 \Delta^\circ\text{C}$  for both of the zones.

- After 40cm from the top of the section, the temperature values throughout the depth does not change flagrantly that means the temperature gradient is zero after 40 cm.
- Since the negative gradient values after the analysis is obtained are quite smaller than AASHTO recommendations; it will be convenient to use -0.30 times of the positive gradient value for the bridges which have decks of which top surfaces has asphalt topping less 5cm, and -0.20 times of positive gradient for the decks which have higher insulating materials as current AASHTO LRFD Code recommends.
- In this study it is verified that nonlinear temperature distribution developed through the depth of box girder type bridges can cause bending moments as high as the ones generated by dead and live loads. Moreover, in terms of stresses, the obtained values are so high; that, especially for negative gradient condition, the high tensile forces imposes the requirement of additional prestressing in order to satisfy tensile stress limitation requirements and avoid cracking of the section.

For future investigations, the following studies may be done to improve the subject:

- The proposed thermal gradients may be applied on different bridges having different types of box girder bridges. This difference may be in the depth of girder, span width and other dimensional properties. Also box girder bridges having more than one cell may be analyzed.
- A substantial number of segmental box girder bridges have segments whose girder depth is increasing from mid-span to the supports. In some bridges this difference is more than two times. Therefore, a bridge with a varying superstructure depth should also be investigated.

- A bridge analysis with not only temperature gradient loading, but also other kinds of load cases like earthquake and wind resultant forces may also be implemented to compare the effects for other important load factors governing the bridge design.
- Transverse temperature stresses may also be investigated to find out the temperature difference between the different webs of the girder and a transverse temperature gradient may be suggested.



## REFERENCES

Aksoy, B. (1997a). Estimated Monthly Average Global Radiation for Turkey and Its Comparison with Observation. *Renewable Energy*, 10, 625–633.

Aksoy, B. (2011). Solar Radiation over Turkey and Its Analysis. *International Journal Of Remote Sensing*, 32(21), 6261-6272.

Albostan, U. (2013). Implementation of Coupled Thermal and Structural Analysis Methods for Reinforced Concrete Structures (Master Thesis, Middle East Technical University)

American Association of State Highway and Transportation Officials (AASHTO). (1989a). *Guide Specifications for Design and Construction of Segmental Bridges*, Washington, DC.

American Association of State Highway and Transportation Officials (AASHTO). (1989b). *Guide Specifications: Thermal Effects in Concrete Bridge Superstructures*, Washington, DC.

American Association of State Highway and Transportation Officials (AASHTO). (1989c). *Standard Specifications for Highway Bridges*, Washington, D.C.

American Association of State Highway and Transportation Officials (AASHTO). (1994b). *Interim Specifications for the Guide Specifications for Design and Construction of Segmental Bridges*, Washington, DC.

American Association of State Highway and Transportation Officials (AASHTO). (1998a). *LRFD Bridge Design Specifications*, Washington, D.C.

American Association of State Highway and Transportation Officials (AASHTO). (1999). *Guide Specifications for Design and Construction of Segmental Bridges*, Washington, DC.

American Association of State Highway and Transportation Officials (AASHTO). (2002). *Standard Specifications for Highway Bridges*, Washington, D.C.

American Association of State Highway and Transportation Officials (AASHTO). (2012). *LRFD Bridge Design Specifications*, Washington, D.C.

American Society of Heating, Refrigerating and Air-Conditioning Engineers (ASHRAE). (2001). *ASHRAE Handbook*, Atlanta.

Branco, F. A., & Mendes, P. A. (1993). Thermal Actions for Concrete Bridge Design. *Journal of Structural Engineering*, 119(8), 2313-2331.

British Standards Institution (BSI). (1979). *Steel, Concrete and Composite Bridges: Part 5: Code of Practice for Design of Composite Bridges*. BS 5400, London.

Cooke, N., Priestly, M. J. N., & Thurston, S. J. (1984). Analysis and Design of Partially Prestressed Concrete Bridges under Thermal Loading. *Prestressed Concrete Institute Journal*, 16(6), 338.

Elbadry, M. M., & Ghali, A. (1983). Temperature Variations in Concrete Bridges. *Journal of Structural Engineering*, 109(10), 2355-2374.

European Committee for Standardization (CEN). (2003). *Eurocode 1: Actions on Structures Part 1-5: General Actions-Thermal Actions*. The European Standard BS EN 1991-1-5:2003, Brussels.

German Institute for Standardization (DIN). (1967). *Strassen and Wegbrucken (Street and Road Bridges)*. DIN 1072, Berlin and Koln.

Hamilton, H. R., Consolazio, G. R. (2009) Validation of Stresses Caused by Thermal Gradients in Segmental Concrete Construction. Final Report, UF Project No. 00030906. University of Florida Department of Civil and Coastal Engineering.

Hoffman, P.C., McClure, R.M., and West, H.H. (1980) Temperature Studies for an Experimental Bridge, Research Project 75-3 Interim Report, Pennsylvania State University.

Honório J.D. (2007). *Conceptual Design of Long-Span Cantilever Constructed Concrete Bridges* (Master Thesis, Royal Institute of Technology (KTH), Sweden).

Imbsen, R. A., Vandershaf, D. E., Schamber, R. A., and Nutt, R. V. (1985) *Thermal Effects in Concrete Bridge Superstructures*. NCHRP Program Report 276, Transportation Research Board, Washington D.C., 63-67.

Koç, A. F. (2013). *Calibration of Turkish LRFD Bridge Design Method for Slab on Steel Plate Girders*. (Master Thesis, Middle East Technical University).

Lee, J. H. (2011). Investigation of Extreme Environmental Conditions and Design Thermal Gradients During Construction for Prestressed Concrete Bridge Girders. *Journal of Bridge Engineering*, 17(3), 547-556.

Lee, J. H., & Kalkan, I. (2012). Analysis of Thermal Environmental Effects on Precast, Prestressed Concrete Bridge Girders: Temperature Differentials and Thermal Deformations. *Advances in Structural Engineering*, 15(3), 447-460.

Leonhardt, F., Kolbe, G., Peter, J. (1965) Temperaturunterschiede Gefährden Spannbetonbrilcke (Temperature Differences Endanger Prestressed Concrete Bridges), *Beton und Stahlbetonbau*, 60 (7): 231-244.

Lingamgunta, C., & Veziroglu, T. N. (2004). A Universal Relationship for Estimating Clear Sky Insolation. *Energy Conversion and Management*, 45(1), 27-52.

National Aeronautics and Space Administration (NASA). Surface Meteorology and Solar Energy: Data subset., <http://eosweb.larc.nasa.gov>., last visited in January 2014.

National Climatic Data Center, National Oceanic and Atmospheric Administration (NOAA). Hourly/Sub-Hourly Observational Data., [gis.ncdc.noaa.gov/map/viewer](http://gis.ncdc.noaa.gov/map/viewer), last visited on January 2014.

Post-Tensioning Institute (PTI) and Precast/Prestressed Concrete Institute. (1997). *Precast Segmental Box Girder Bridge Manual*, Arizona.

Potgieter, I. C., & Gamble, W. L. (1983). Response of Highway Bridges to Nonlinear Temperature Distributions. University of Illinois Engineering Experiment Station. College of Engineering. University of Illinois at Urbana-Champaign.

Priestley, M. N. (1978). Design of Concrete Bridges for Temperature Gradients. *ACI Journal Proceedings*, 75(5), 209-217.

Roberts, C. L., Breen, J. E., and Kreger, M. E. (1993). Measurement based revisions for segmental bridge design criteria. Research Report, 1234-3F, Center for Transportation Research, Univ. of Texas at Austin.

Roberts-Wollman, C. L., Breen, J. E., & Cawrse, J. (2002). Measurements of Thermal Gradients and Their Effects on Segmental Concrete Bridge. *Journal of Bridge Engineering*, 7(3), 166-174.

Schlaich, J., & Scheef, H. (1982). *Concrete Box-Girder Bridges (Vol. 1)*. International Association for Bridge and Structural Engineering, Zurich.

Shushkewich, K. W. (1998). Design of Segmental Bridges for Thermal Gradient. *PCI Journal*, 43(4), 120-137.

T.C. Bayındırlık Bakanlığı, Karayolları Genel Müdürlüğü. (1982). *Yol Köprüleri için Teknik Şartname*, Ankara.

The Scientific And Technological Research Council Of Turkey (TUBITAK) (2009-2014) KAMAG 1007, 110G093.

Theryo, T.S. (2005). Precast Balanced Cantilever Bridge Design Using AASHTO LRFD Bridge Design Specifications. American Segmental Bridge Institute.

Turkish Standards Institute, TS500 (2000). Requirements for Design and Construction of Reinforced Concrete Structures, Ankara.

Wood, B. A. (1997). Thermal Gradients and Their Effects on Segmental Concrete Box Girder Bridges (Doctoral Dissertation, The University of Texas at Austin).

<http://www.cement.org/for-concrete-books-learning/concrete-technology/concrete-design-production/mass-concrete>, last visited on December 2014.

## APPENDIX A

### NUMERICAL HAND CALCULATION DESIGN EXAMPLE

Thermal stresses are developed because of restraint to expansion and rotation from the restraints coming from the section itself due to the need of section to stay plane and the restraints resulting from the support conditions. Cross section cause stresses that vary in the vertical direction whereas support conditions induce stresses that change longitudinal direction.

Here is an example given for calculating the primary compressive thermal stresses developed due to the positive gradient for the mid-span section in LRFD Design Example (Figure 4.1). The total section depth is constant along the whole length of the bridge. The only variable, the section bottom flange depth is changing from 23 cm to 46 cm from mid-span sections to the supports. Calculations are made for mid-span sections since as Shushkewich (1998) indicates,  $T_{top}$  and  $T_{bot}$  values have larger values at midspan and smaller values at the support.

Secondary stresses are than can be calculated by a plane frame computer program using the calculated equivalent temperature gradient values as inputs.

The primary stresses components are the superposition of the thermal stresses  $f(y)$ , axial stresses  $N_p/A$  and the flexural stresses  $M_p y / I$ . Secondary stresses also cause axial stresses  $N_s/A$  and additional moments  $M_s y/I$ . The total stress is the sum of these components.

The thermal stress component may be considered as a tensile resultant force  $P_R$  applied with eccentricity  $e_{top}$  from the top of girder. This resultant force is can be thought as equal to a primary tensile axial force  $N_p$  and primary bending moment in negative direction,  $M_p$ , applied at  $y_{top}$ , the distance of taken as distance of the neutral axis of the section with respect to the top. (Figure A.1)

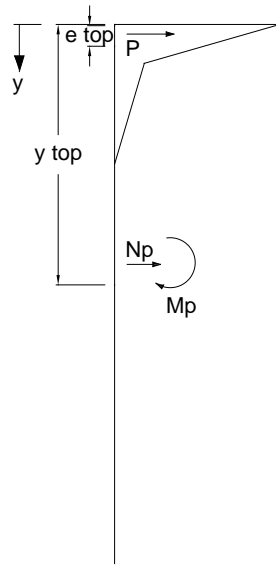


Figure A.1 Equivalent force and stress diagram for positive and negative gradient

Here, an example is given for the example bridge section that the necessary information is given before, with the thermal gradient values suggested for Zone 1.

With the help of the section properties and following formulas the primary force and moment effects can be calculated. In the following figure, the simplified equivalent I-section for the example box girder section and the gradient that will be applied is shown (Figure A.2 and Figure A.3)

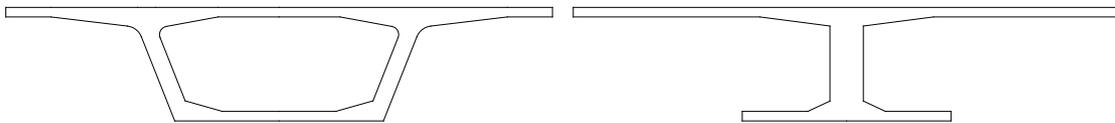


Figure A.2 Equivalent I-section for the example box girder section

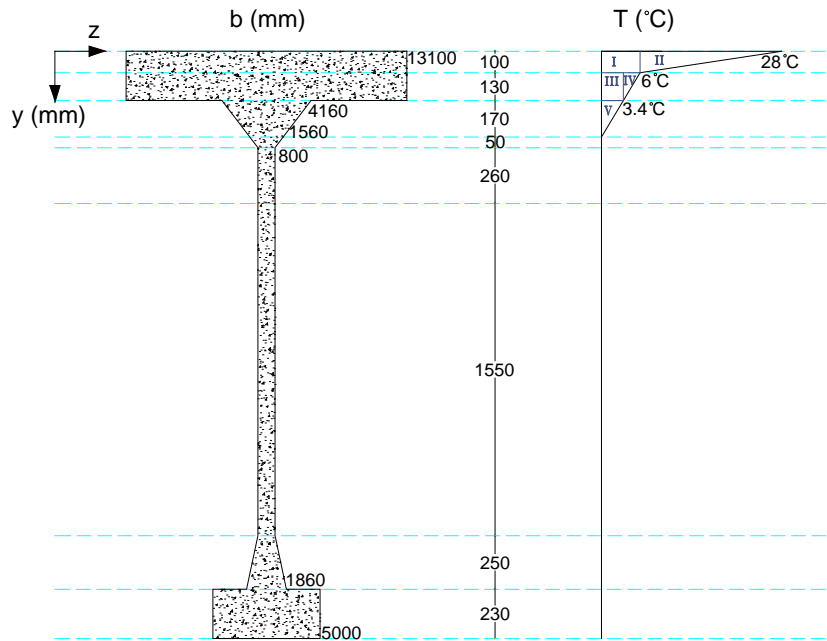


Figure A.3 Equivalent section dimensions and the applied gradient

$$A = 7.0856 \times 10^6 \text{ mm}^2$$

$$I = 6.9597 \times 10^{12} \text{ mm}^4$$

$$y_{\text{top}} = 0.9256 \times 10^3 \text{ mm}$$

$$E = 33000 \text{ MPa (C35)}$$

$$\alpha = 10^{-5} \text{ 1/}^\circ\text{C}$$

$$f(y) = E \alpha TG(y) \tag{A.1}$$

$$P = E \alpha \sum_y TG(y)b(y) dy \tag{A.2}$$

$$M = E \alpha \sum_y TG(y)b(y) y dy \tag{A.3}$$

If the section top stresses are calculated resulted from the positive and negative gradient for the topmost fibers of the section for Zone 1, with Equation (A.1),

$$f(\text{top})_p = E \alpha TG(\text{top}) = 33000 * 0.00001 * 28 = 9.24 \text{ MPa}$$

$$f(\text{top})_n = E \alpha TG(\text{top}) = 33000 * 0.00001 * 6 = 1.98 \text{ MPa}$$

Then, resultant axial force P and bending moment M can be calculated by dividing the section into subsections and summing the results as given in the Table A.A.1 and Table A.A.2.

Table A.A.1 Positive Temperature Gradient Primary Force Calculations for Zone 1

Section	E (MPa)	$\alpha$ (1/°C)	TG (°C)	b (mm)	t (mm)	P (kN)	y (mm)	M (kN m)
I	33000	0.00001	6	13100	100	2594	50	130
II	33000	0.0000100	11	13100	100	4755	33	157
III	33000	0.0000100	3.4	13100	130	1911	165	315
IV	33000	0.0000100	1.3	13100	130	731	143	105
V	33000	0.0000100	1.7	2860	170	273	287	78
Total						<b>10264</b>		<b>785</b>

Table A.A.2 Negative Temperature Gradient Primary Force Calculations for Zone 1

Section	E (MPa)	$\alpha$ (1/°C)	TG (°C)	b (mm)	t (mm)	P (kN)	y (mm)	M (kN m)
I	33000	0.00001	-1	13100	100	-432	50	-22
II	33000	0.00001	-3.5	13100	100	-1513	33	-50
III	33000	0.00001	-0.6	13100	130	-337	165	-56
IV	33000	0.00001	-0.8	13100	130	-450	143	-64
V	33000	0.00001	-0.3	2860	170	-48	287	-14
Total						<b>-2780</b>		<b>-206</b>

$$e_{top} = M/P \quad (A.4)$$

Using (A.4)  $e_{top}$  is calculated as 76.5 mm from the top for the positive gradient.

The resultant axial force and the distance of this force to the top of the section,  $e_{top}$  due to thermal component can be assumed as constant for segmental box girder concrete bridges since the dimensions of the upper parts of the girder are usually constant and the thermal gradient applied acts with its highest values near the top of the section.

As seen in the table  $P=10264$  kN and  $M= 785$  kNm is found from the calculations. From Equation (A.4),  $e_{top}$  is calculated as 76mm from the top of the girder. After finding the axial force, bending moment about the top, and the eccentricity; equivalent primary tensile axial force and moment to the compressive thermal stress component can be determined for the whole cross section with the following equations:

$$N_p = P \quad (A.5)$$

$$M_p = P (y_{top} - e_{top}) \quad (A.6)$$

where

$y$ =distance from the center of gravity of the cross-section to the top

$A$ = area of the section

$I$ = moment of inertia of the section about the neutral axis

$TG(y)$  = temperature at depth  $y$

$b(y)$  = section width at depth  $y$

$E$  and  $\alpha$  are the modulus of elasticity and coefficient of thermal expansion of the structure material, respectively.

After finding these primary effects, secondary effects can be calculated by applying one of the following three inputs to a finite element analysis program.

- i. Axial force  $N_p$  and bending moment  $M_p$  calculated by the Equations (A.5) and (A.6).
- ii. Equivalent uniform temperature  $T_{unif}$  and linear gradient  $T_{grad}$

$$T_{unif} = N_p / (E \alpha A) \quad (A.7)$$

$$T_{grad} = M_p / (E \alpha I) \quad (A.8)$$

where  $A$  is the area of the section and  $I$  is the moment of inertia

- iii. Section top and bottom temperatures  $T_{top}$  and  $T_{bot}$

$$T_{top} = T_{unif} + T_{grad} y_{top} \quad (A.9)$$

$$T_{bot} = T_{unif} - T_{grad} y_{bot} \quad (A.10)$$

where  $y_{top}$  and  $y_{bot}$  are the distances from the top and bottom of the section and the neutral axis.

From the above equations  $N_p$  is equal to  $P$ , which is 167310kN and  $M_p$  is found as 14700 kNm.  $T_{unif}$ ,  $T_{grad}$ ,  $T_{top}$  and  $T_{bot}$  are found as 4.4°C, 3.8 °C/mm, 7.9 °C and -2.3 °C, respectively. Then, using the necessary ones as inputs, according to the capabilities of the secondary axial force and bending moment can be determined by a plane frame computer program.

Here the corresponding values are given for the whole zones including the suggested zones for Turkey and zones for the USA stated by the AASHTO calculated for the section given above with the predefined material properties (Table A.A.3 and Table A. A.4).

Table A.A.3 Necessary Positive Temperature Gradient, Primary and Secondary Axial Load and Temperature Values to Calculate Secondary Thermal Effects

Zone Name	T <sub>1</sub> (°C)	T <sub>2</sub> (°C)	Pp (kN)	Mp (kNm)	Tunif (°C)	Tgrad (m-1)	Ttop (°C)	Tbot (°C)
Turkey Recommended Zone 1	28	6	10264	8715	4.4	3.8	7.9	-2.3
Turkey Recommended Zone 2	25	6	9616	8137	4.1	3.5	7.4	-2.2
the USA Zone 1	30	8	11887	10032	5.1	4.4	9.1	-2.7
the USA Zone 2	25	7	10172	8580	4.4	3.7	7.8	-2.3
the USA Zone 3	23	6	9086	7664	3.9	3.3	7.0	-2.0
the USA Zone 4	21	5	8052	6812	3.4	3.0	6.2	-1.8

Table A. A.4 Necessary Negative Temperature Gradient, Primary and Secondary Axial Load and Temperature Values to Calculate Secondary Thermal Effects

Zone Name	T <sub>1</sub> (°C)	T <sub>2</sub> (°C)	Pp (kN)	Mp (kNm)	Tunif (°C)	Tgrad (m-1)	Ttop (°C)	Tbot (°C)
Turkey Recommended Zone 1	-6	-1	-2780	-2453	-1.3	-0.1	-1.4	-1.2
Turkey Recommended Zone 2	-5	-1	-2564	-2254	-1.2	-0.1	-1.3	-1.1
the USA Zone 1	-6	-2	-4171	-3638	-2.0	-0.2	-2.1	-1.9
the USA Zone 2	-5	-1	-2564	-2254	-1.2	-0.1	-1.3	-1.1
the USA Zone 3	-5	-1	-2564	-2254	-1.2	-0.1	-1.3	-1.1
the USA Zone 4	-4	-1	-2348	-2054	-1.1	-0.1	-1.2	-1.0

It is worthwhile to note that; the values calculated as T<sub>top</sub> and T<sub>bottom</sub> are also get from outputs of Larsa4D analysis and the same results are achieved.



## APPENDIX B

### THE TEMPERATURE AND SOLAR RADIATION DATA FOR THE ANALYZED CITIES

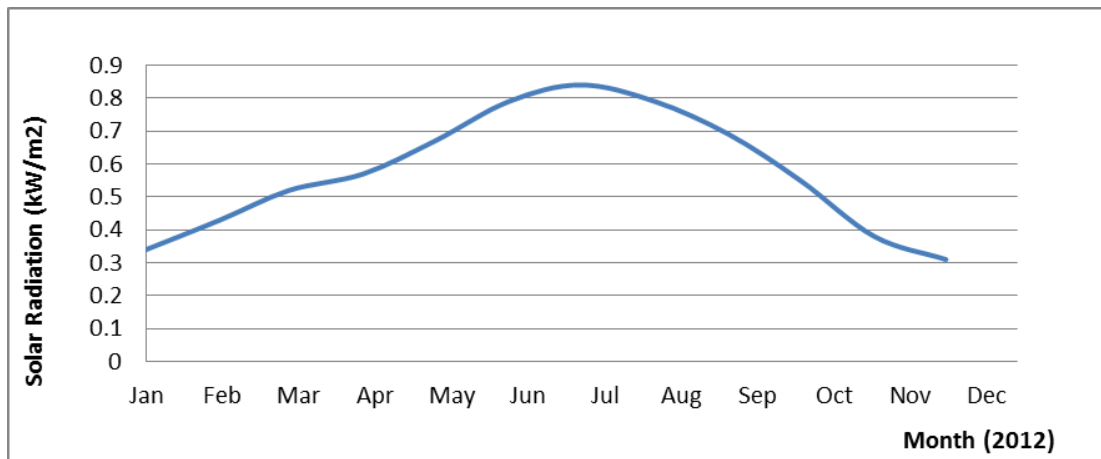


Figure B.1 Solar radiation data for Adana between Jan.2012-Dec.2012

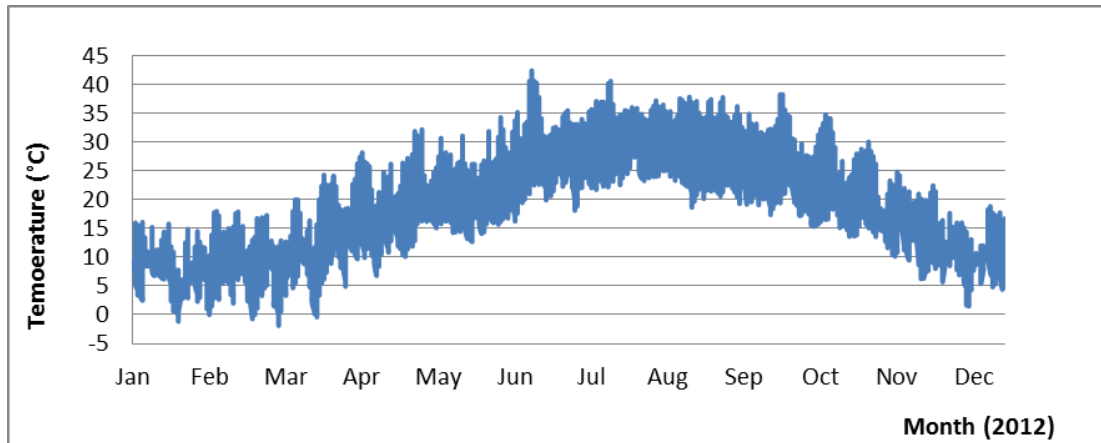


Figure B.2 Temperature data for Adana between Jan.2012-Dec.2012

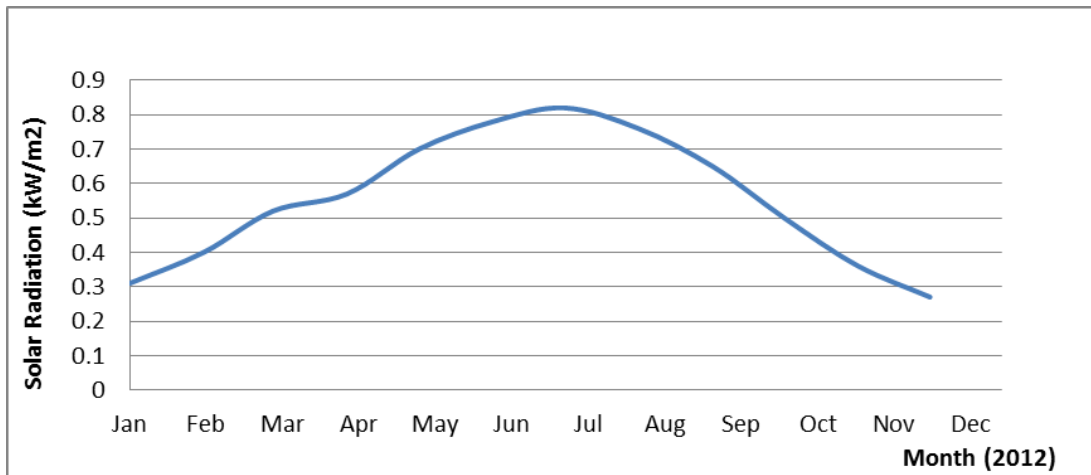


Figure B.3 Solar radiation data for Ankara between Jan.2012-Dec.2012

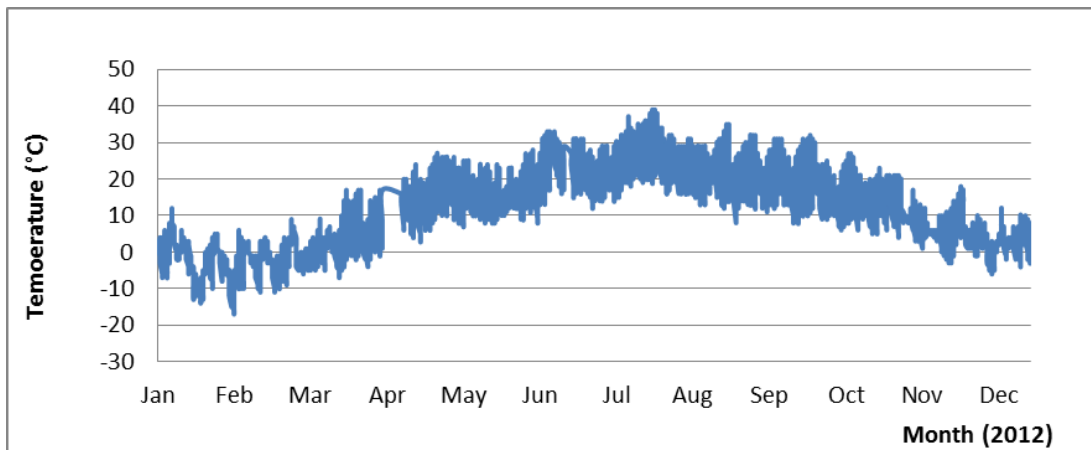


Figure B.4 Temperature data for Ankara between Jan.2012-Dec.2012

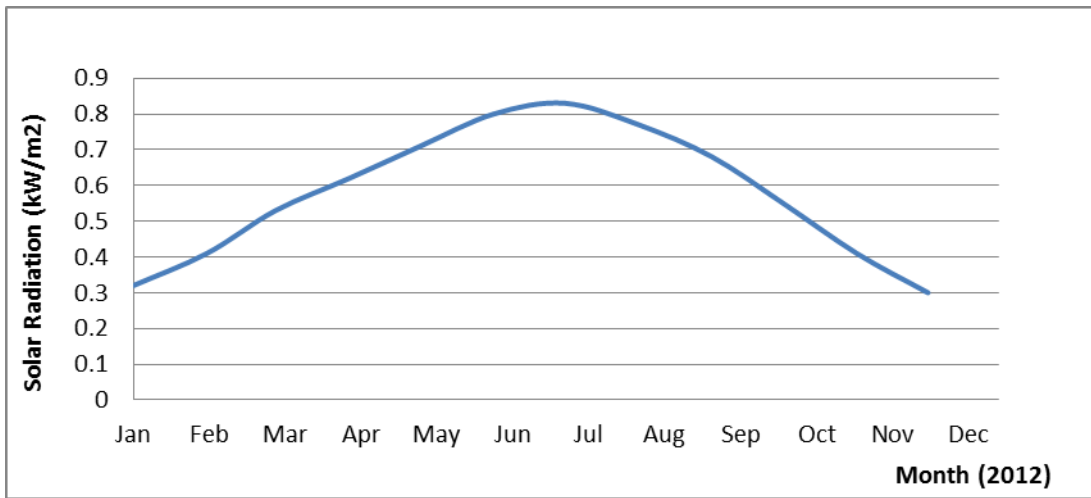


Figure B.5 Solar radiation data for Antalya between Jan.2012-Dec.2012

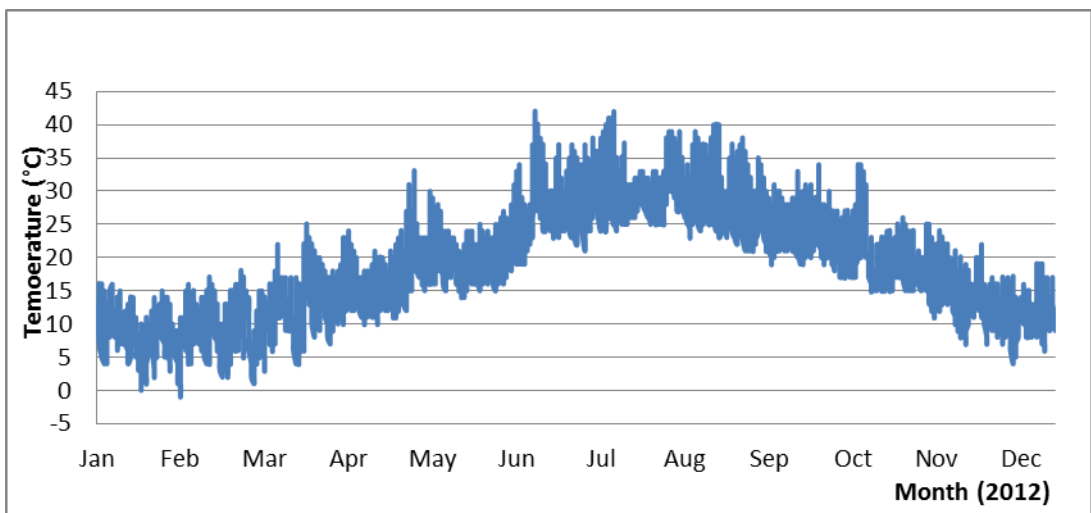


Figure B.6 Temperature data for Antalya between Jan.2012-Dec.2012

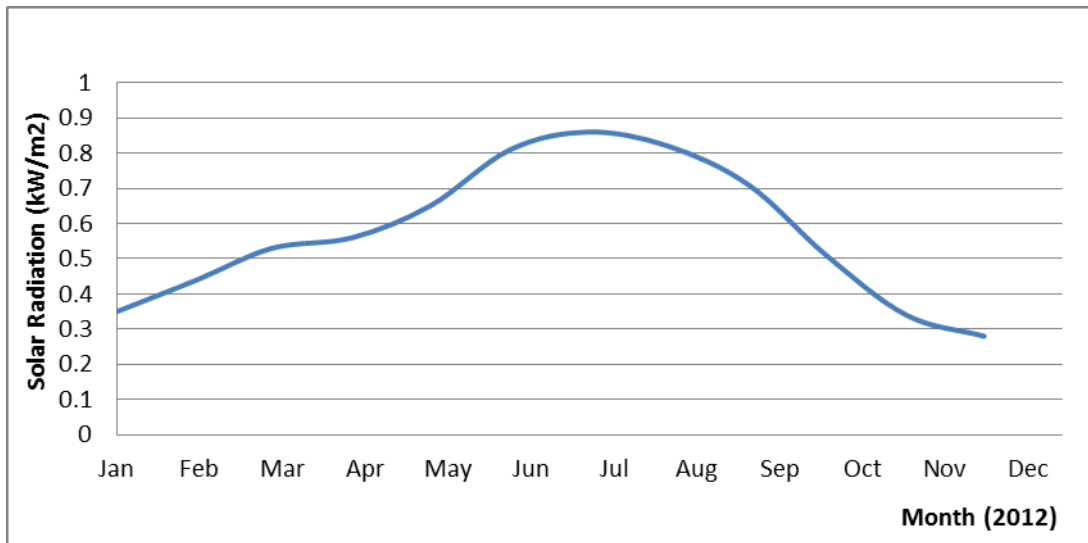


Figure B.7 Solar radiation data for Bingöl between Jan.2012-Dec.2012

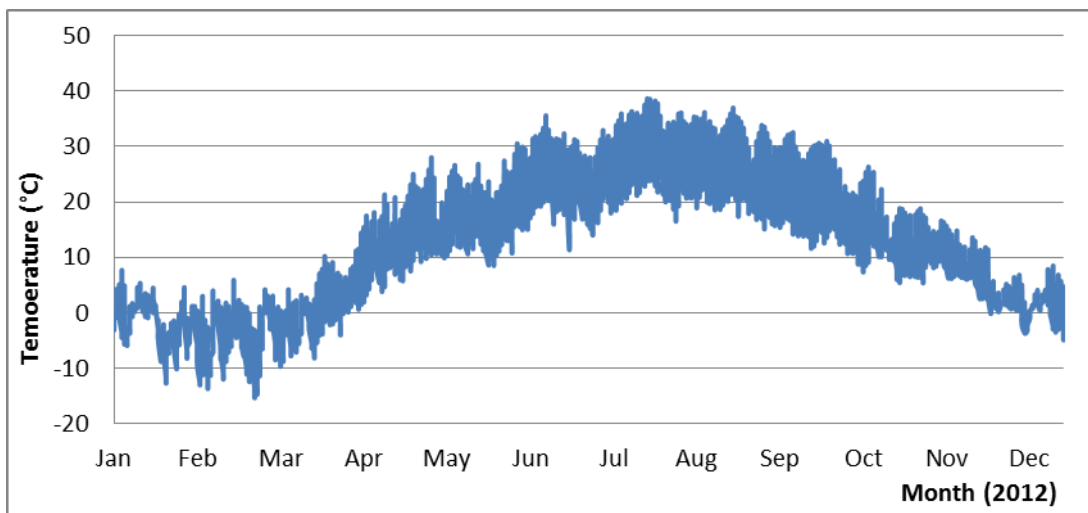


Figure B.8 Temperature data for Bingöl between Jan.2012-Dec.2012

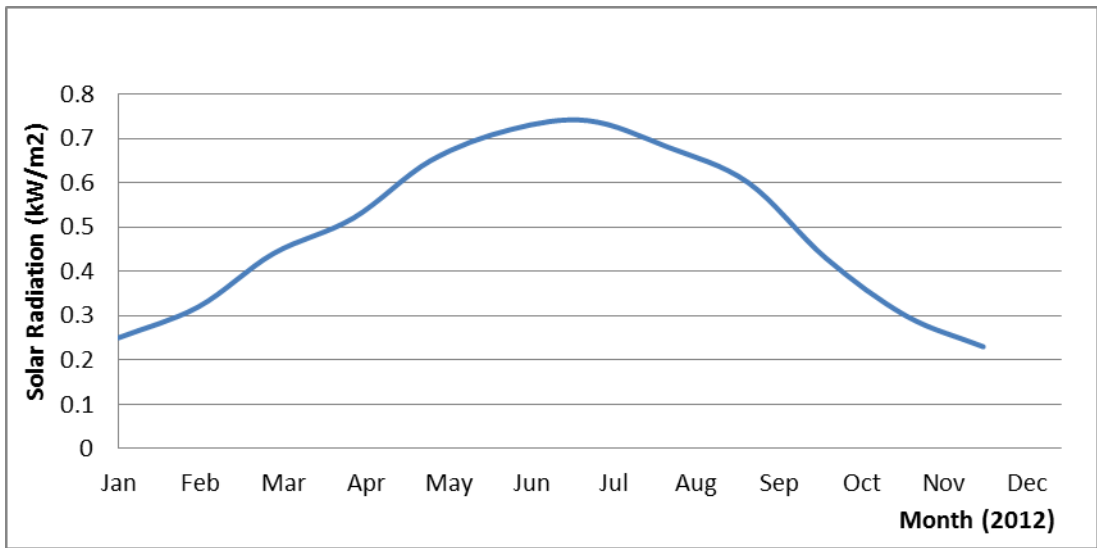


Figure B.9 Solar radiation data for Bursa between Jan.2012-Dec.2012

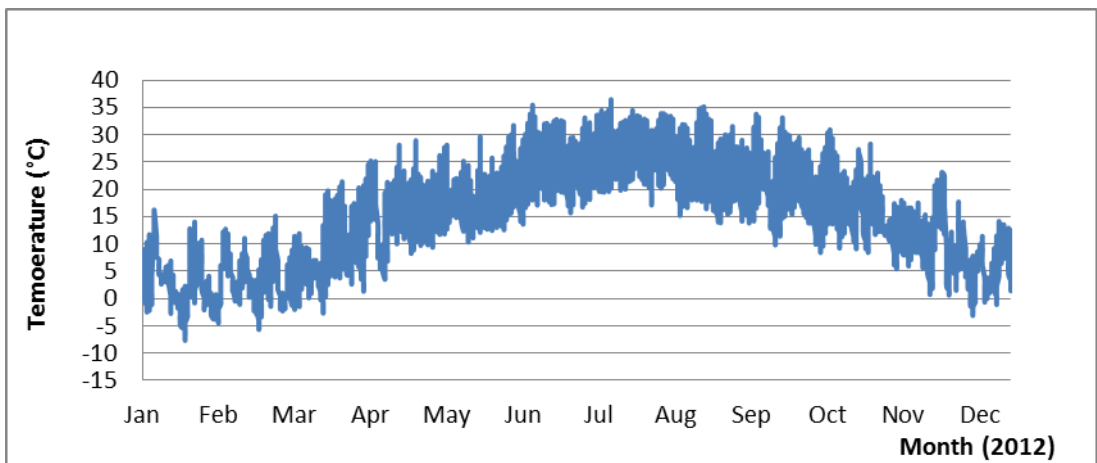


Figure B.10 Temperature data for Bursa between Jan.2012-Dec.2012

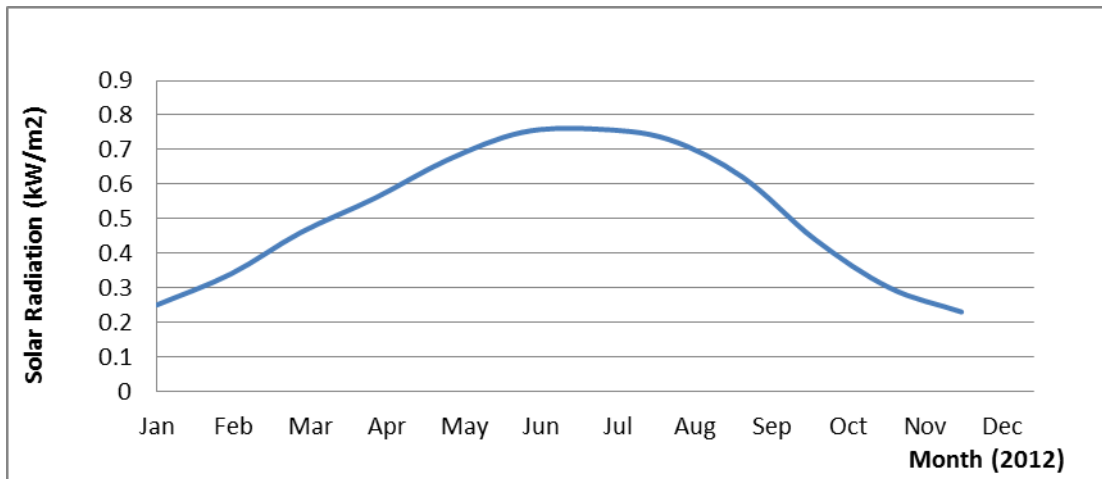


Figure B.11 Solar radiation data for Çanakkale between Jan.2012-Dec.2012

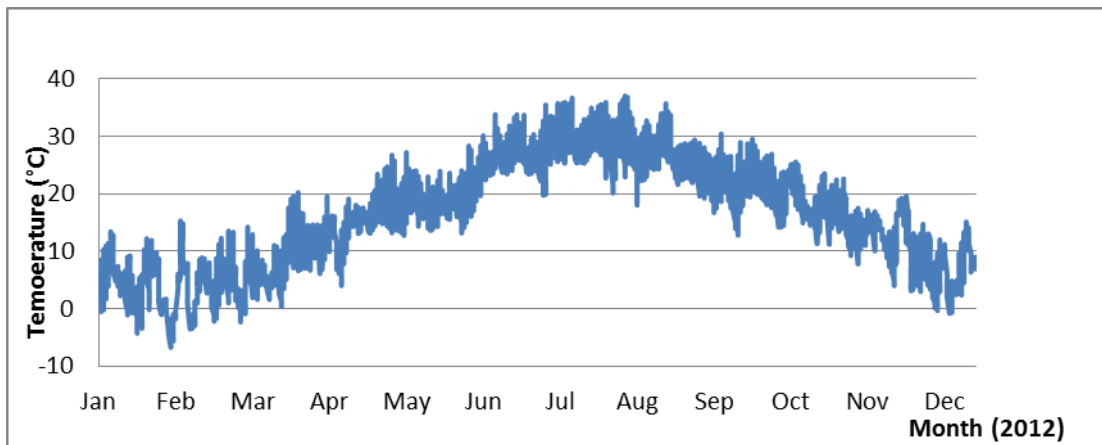


Figure B.12 Temperature data for Çanakkale between Jan.2012-Dec.2012

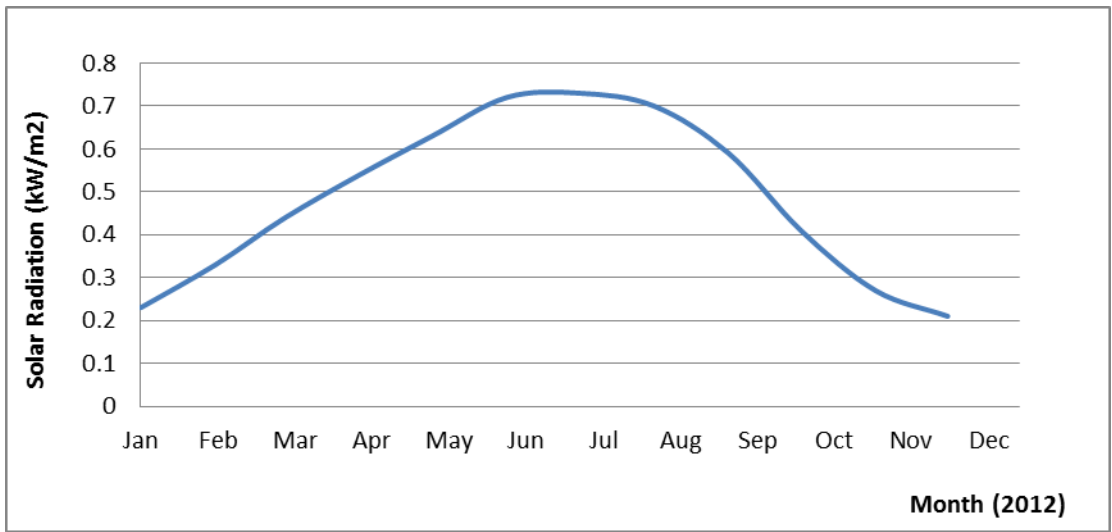


Figure B.13 Solar radiation data for Edirne between Jan.2012-Dec.2012

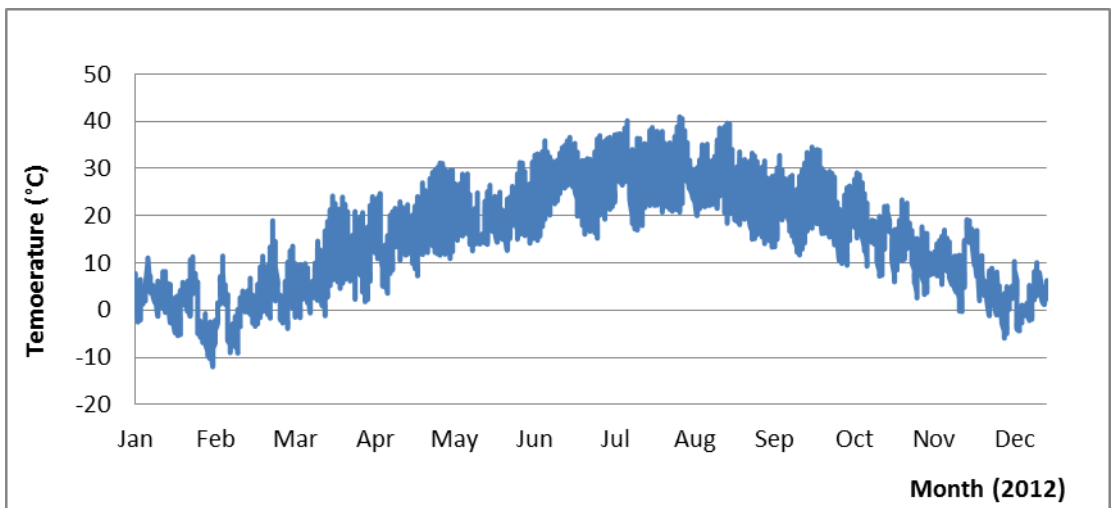


Figure B.14 Temperature data for Edirne between Jan.2012-Dec.2012

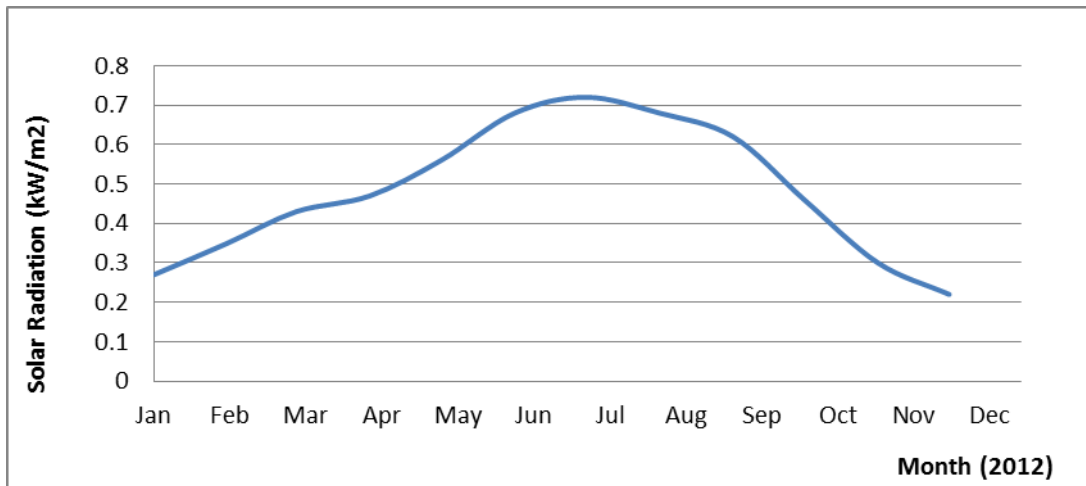


Figure B.15 Solar radiation data for Erzurum between Jan.2012-Dec.2012

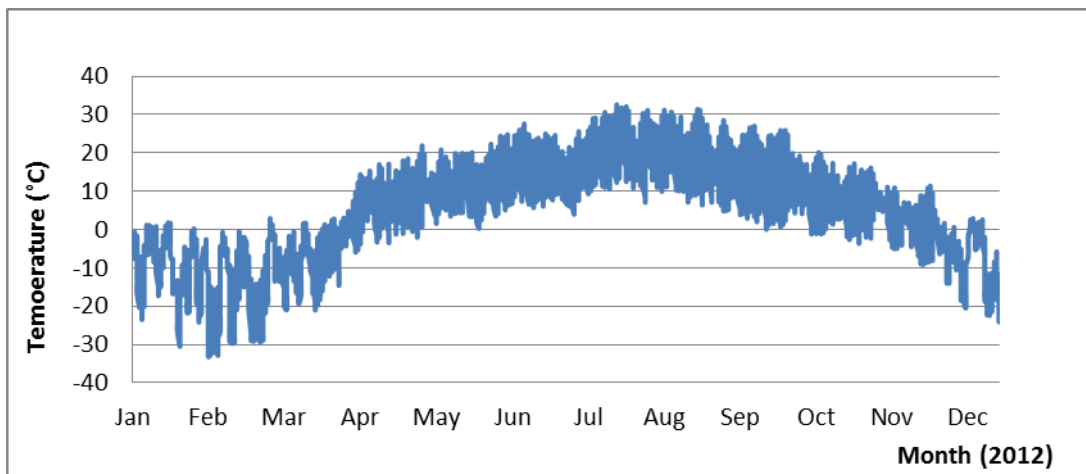


Figure B.16 Temperature data for Erzurum between Jan.2012-Dec.2012

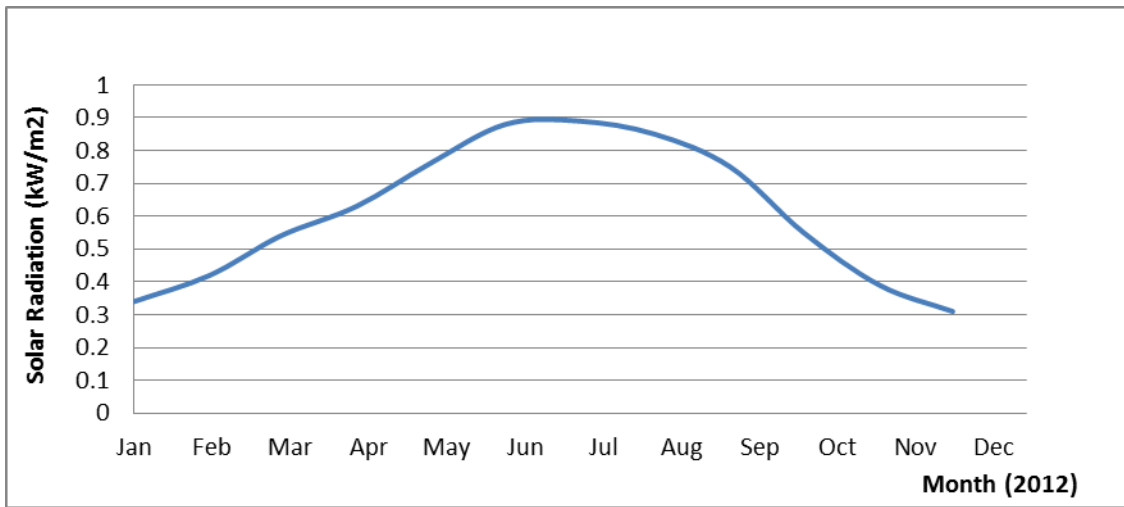


Figure B.17 Solar radiation data for Gaziantep between Jan.2012-Dec.2012

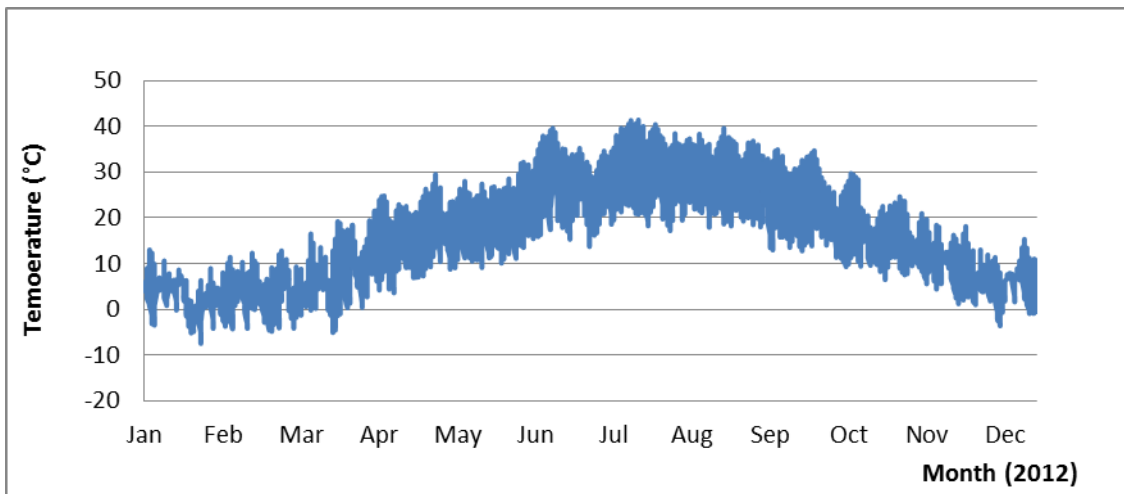


Figure B.18 Temperature data for Gaziantep between Jan.2012-Dec.2012

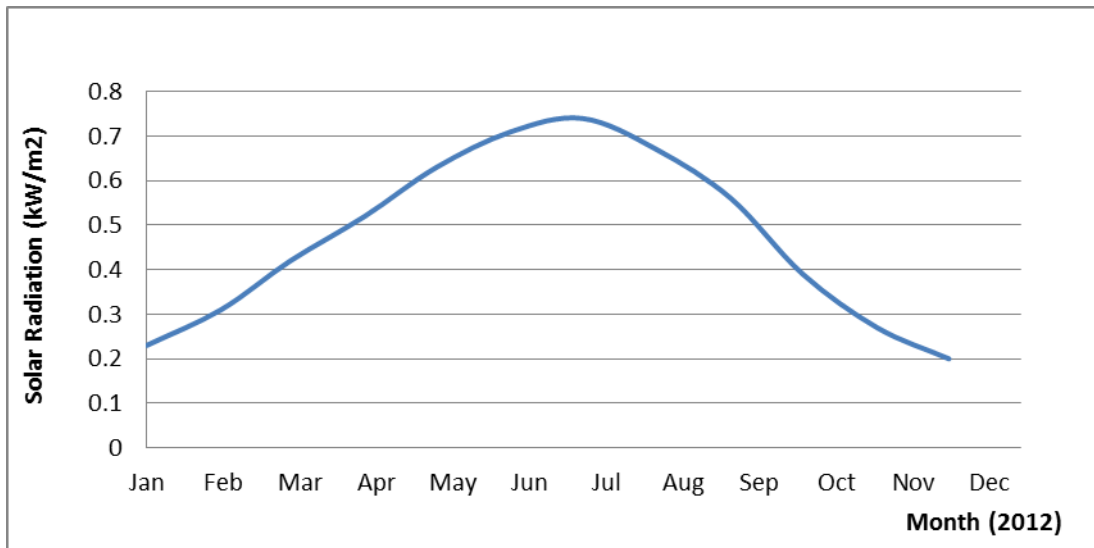


Figure B.19 Solar radiation data for İstanbul between Jan.2012-Dec.2012

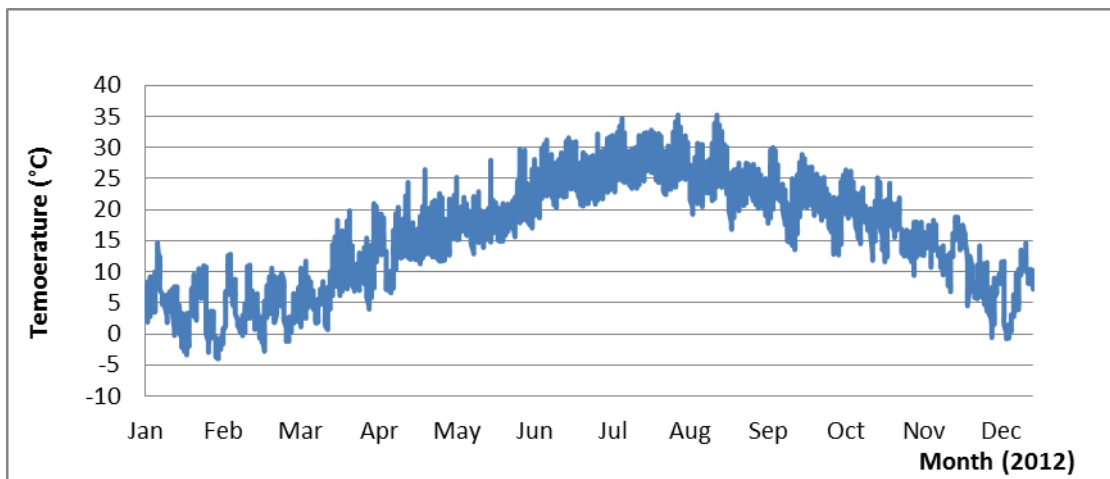


Figure B.20 Temperature data for İstanbul between Jan.2012-Dec.2012

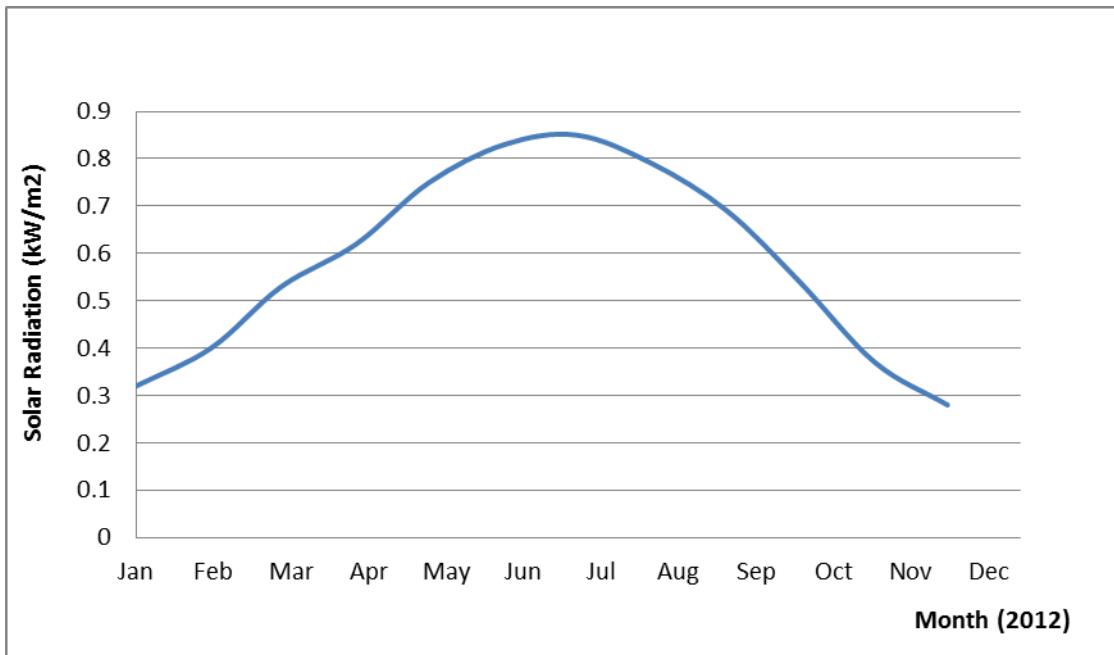


Figure B.21 Solar radiation data for İzmir between Jan.2012-Dec.2012

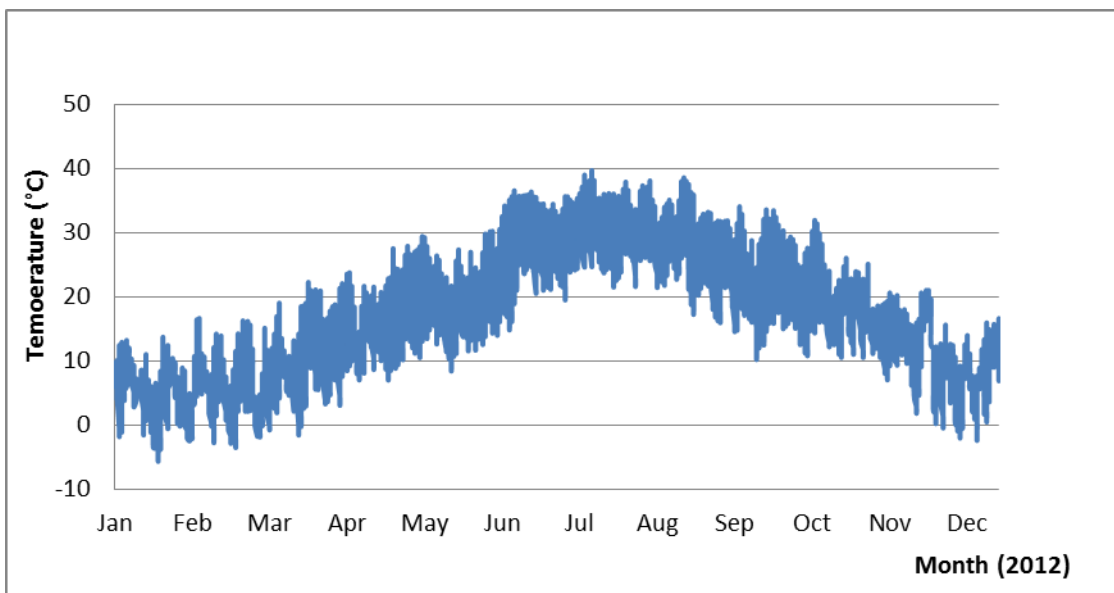


Figure B.22 Temperature data for İzmir between Jan.2012-Dec.2012

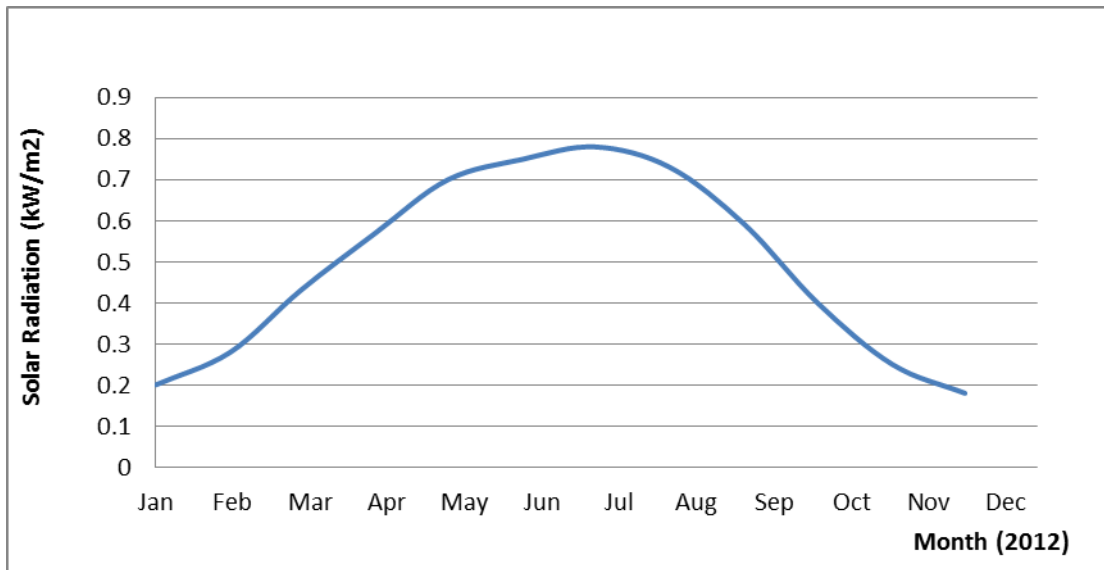


Figure B.23 Solar radiation data for Kars between Jan.2012-Dec.2012

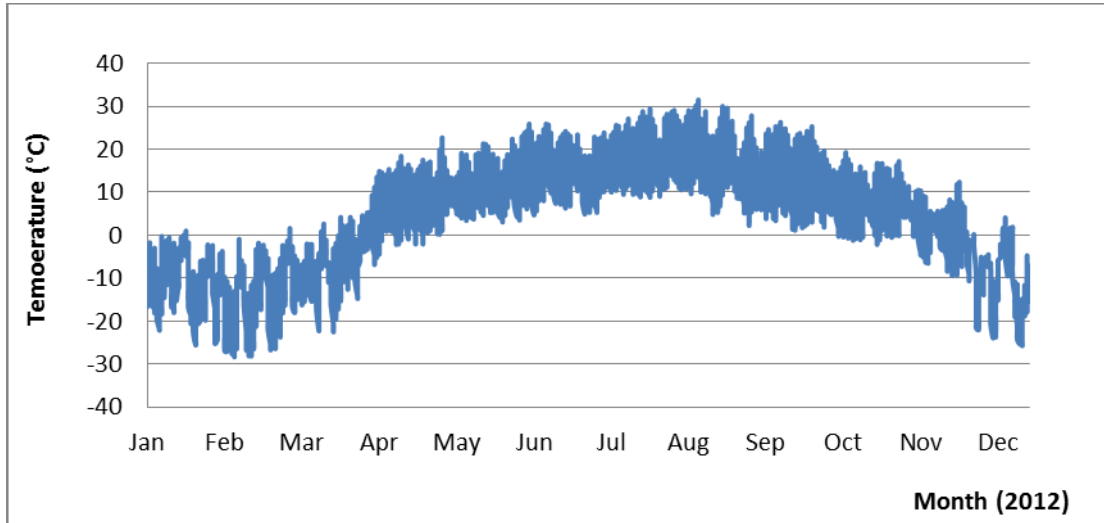


Figure B.24 Temperature data for Kars between Jan.2012-Dec.2012

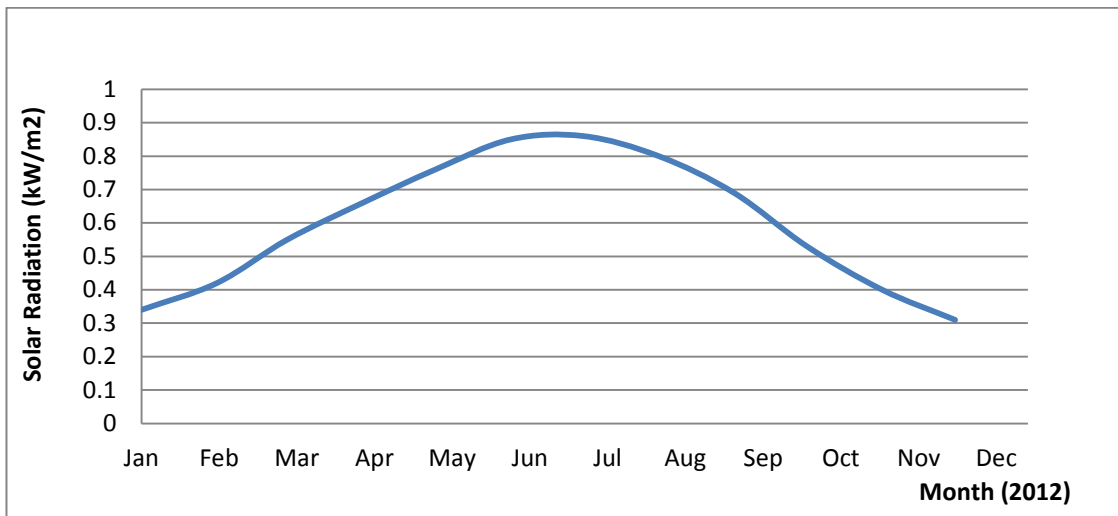


Figure B.25 Solar radiation data for Muğla between Jan.2012-Dec.2012

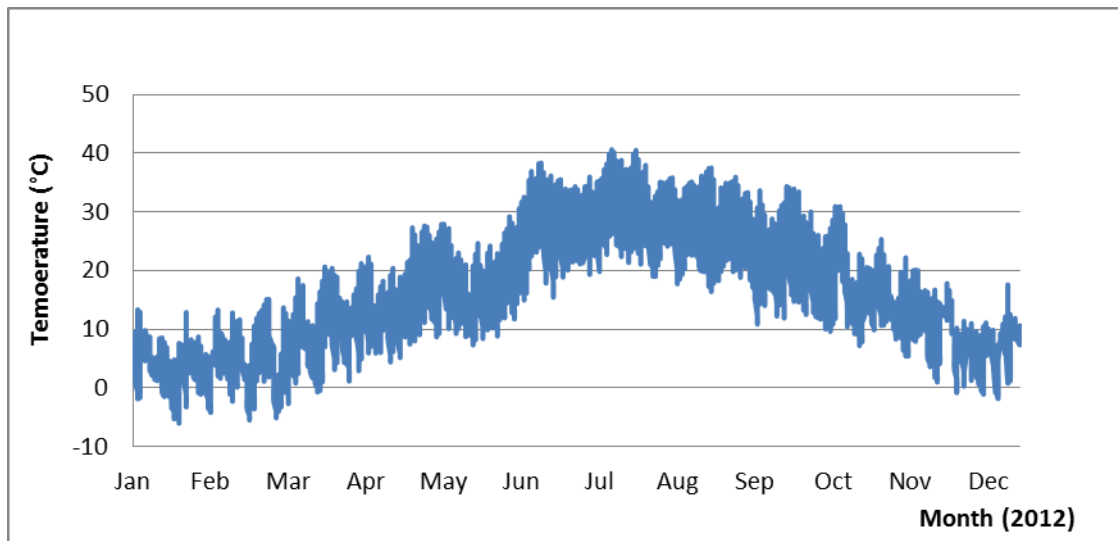


Figure B.26 Temperature data for Muğla between Jan.2012-Dec.2012

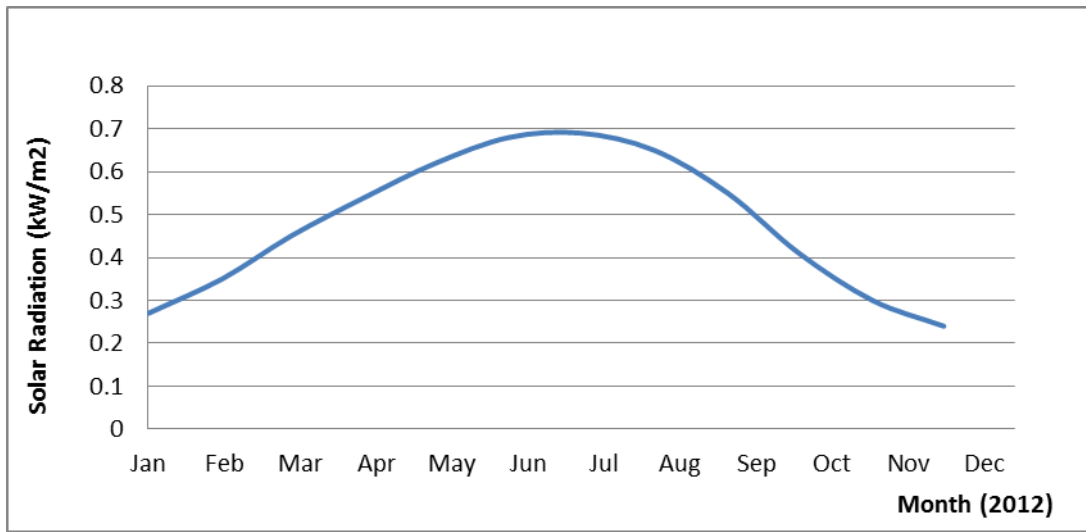


Figure B.27 Solar radiation data for Samsun between Jan.2012-Dec.2012

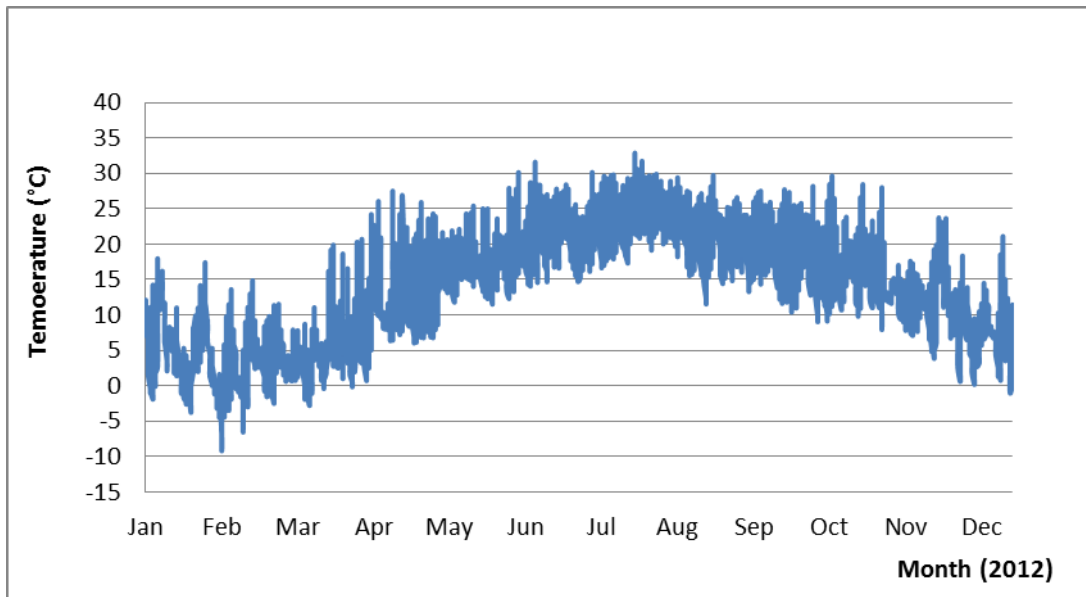


Figure B.28 Temperature data for Samsun between Jan.2012-Dec.2012

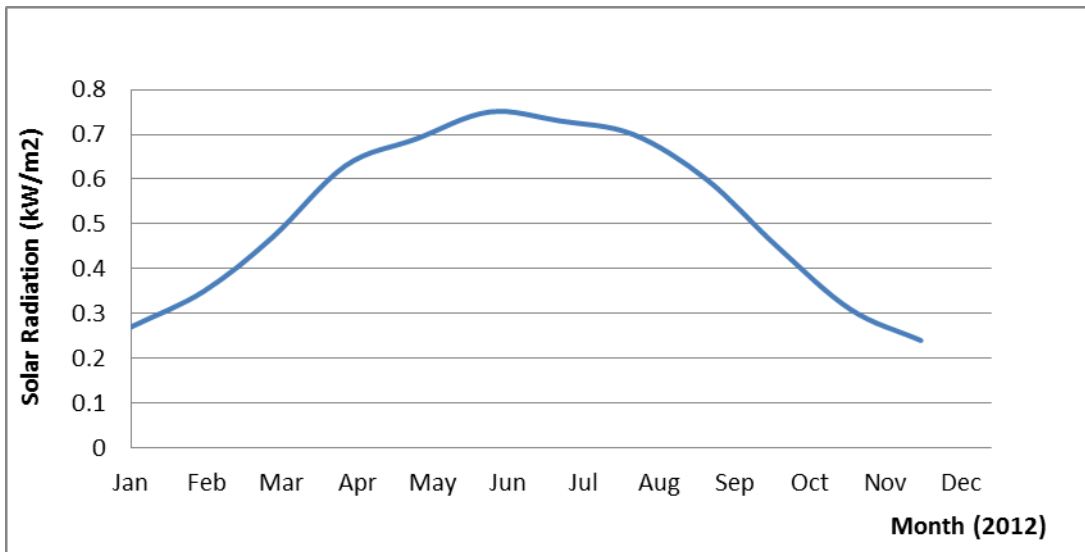


Figure B.29 Solar radiation data for Trabzon between Jan.2012-Dec.2012

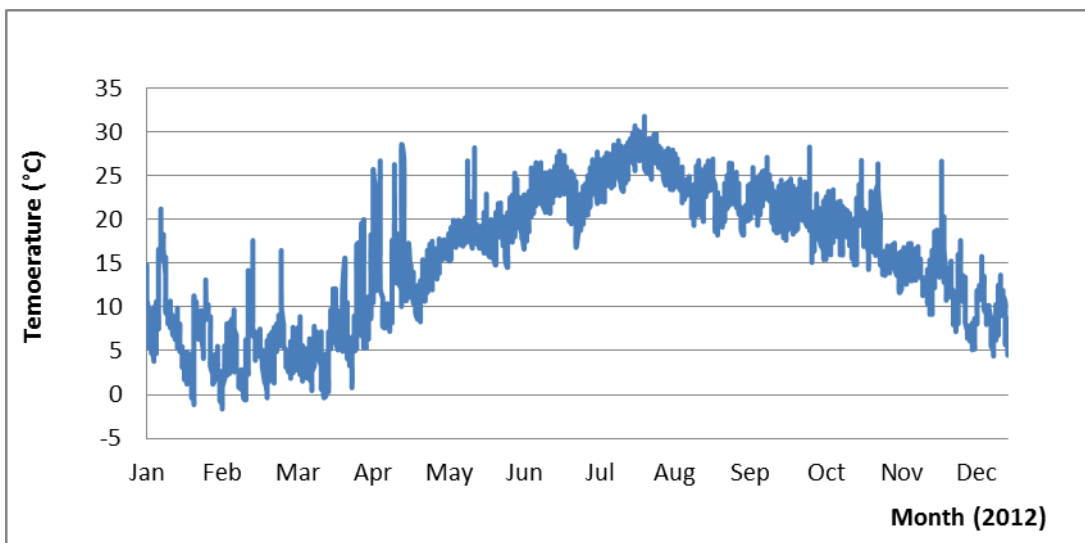


Figure B.30 Temperature data for Trabzon between Jan.2012-Dec.2012

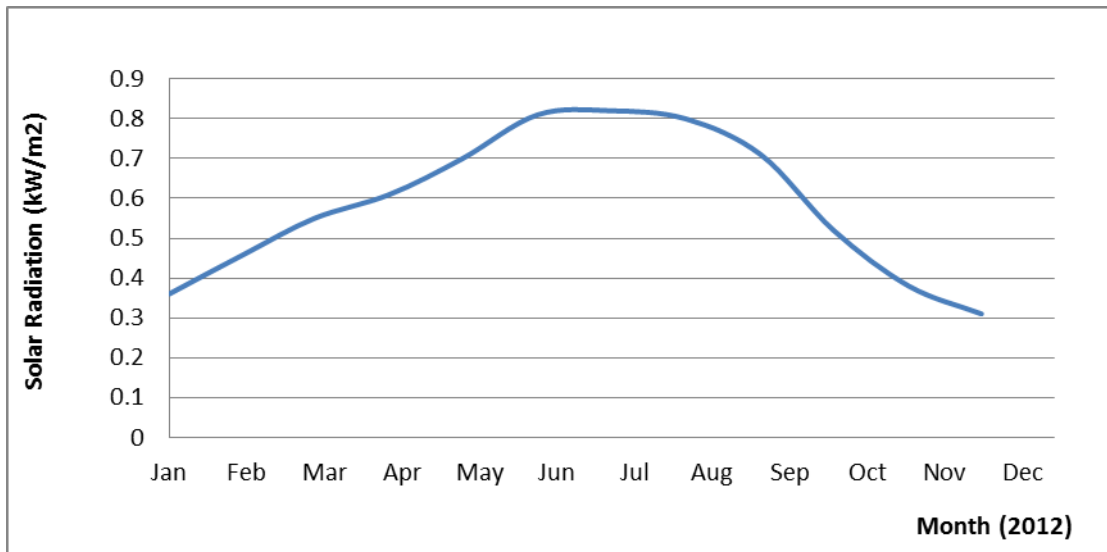


Figure B.31 Solar radiation data for Van between Jan.2012-Dec.2012

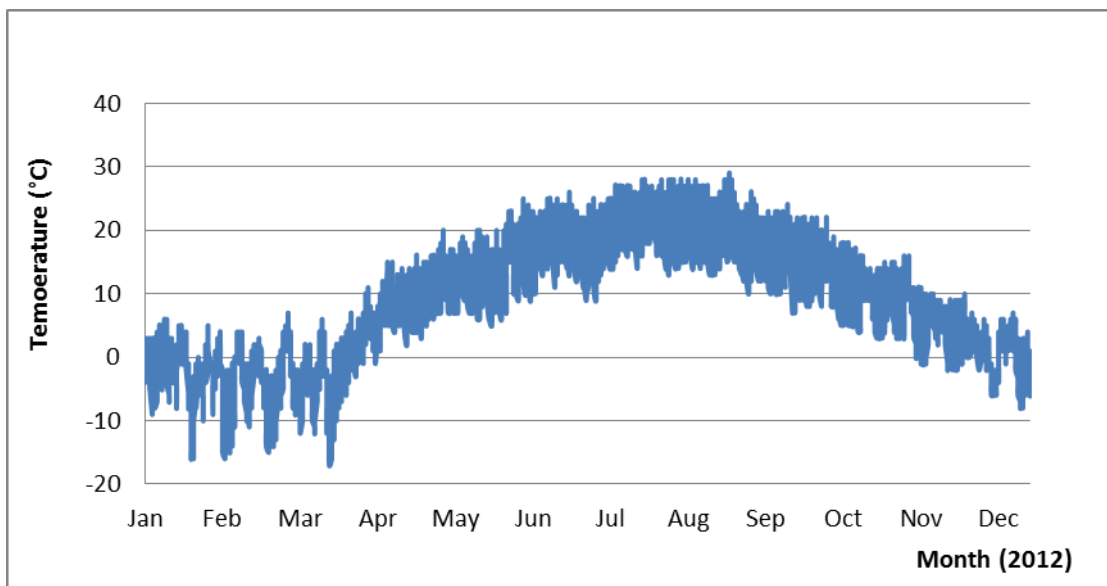


Figure B.32 Temperature data for Van between Jan.2012-Dec.2012